

https://dspace.org/

Kinetics of the ligand substitution reactions of Co (III) corrinoids and model macrocyclic compounds

Bradley, J C

2016-08-18
http://hdl.handle.net/10539/20894

Downloaded from a DSpace repository. https://dspace.org/

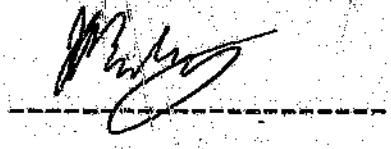
Submitted for MSc(Chemistry)
December 1992

KINETICS OF THE LIGAND SUBSTITUTION REACTIONS OF Co(III) CORRINOIDS AND MODEL MACROCYCLIC COMPOUNDS

Submitted by : Miss J.C.Bradley
Supervisor : Dr H.M.Marques

DECLARATION

I declare that the work presented in this thesis was carried out exclusively by myself, under the supervision of Dr H.M.Marques.



Miss J.C.Bradley
86-00118/R

ACKNOWLEDGEMENTS

I would like to thank my supervisor, Dr H.M.Marques, for his support and advice throughout this project. I am especially grateful to Prof K.L.Brown, Head of the Department of Chemistry at Mississippi State University, for providing samples of aquocyanocobinamide and diaquocobinamide and particularly for providing details of his unpublished synthetic method for producing diaquocobinamide. Finally, I would also like to thank my father, Prof J.D.Bradley, for his advice and patience in proofreading this thesis.

ABSTRACT

Diaquocobinamide (DAC) was prepared from cyanocobalamin (vitamin B_{12}) via the intermediate aquocyanocobinamide (Factor B). Brown's method for the conversion of Factor B to DAC, involving the reduction of Co(III) using zinc wool under a circulating inert atmosphere, followed by treatment with 1 mol dm^{-3} HCl, was used.[29] At best a 93% yield, based on HPLC peak integration, was recorded. DAC samples were kept frozen under an inert atmosphere in the dark to prevent the formation of stable yellow corrinoids. Thermodynamic parameters for the conversion of DAC to aquohydroxocobinamide (AHC) (ΔH° = 44 kJ mol^{-1}, ΔS° = -35 J $K^{-1}mol^{-1}$), and of AHC to dihydroxocobinamide (DHC) (ΔH° = 37 kJ mol^{-1}, ΔS° = -59 J $K^{-1}mol^{-1}$), were determined by in-cell spectrophotometric titrations. The value of pK_{a1} at 25°C calculated from these parameters compares well with available literature values[3,5], but the value of pK_{a2} does not. Experimental error in the pH measurement during the titrations for the second equilibrium are expected to be responsible for the inconsistent results. Binding constants of AHC (pH 12.00) with five ligand : cyanide, azide, pyridine, N-methylimidazole, and 3-amino-1-propanol were determined by in-cell spectrophotometric titrations at 25°C. Comparison of the calculated unconditional binding constants with available data on DAC, aquocobalamin (vitamin B_{12a}) and Factor B (*i.e.* the *trans*-ligands H_2O, 5,6-dimethylbenzimidazole (dmbzim), and CN^-) confirmed the *trans* labilising order, H_2O < dmbzim < OH^- < CN^-.[1,14] The dependence of the observed rate constant (k'_{obs}) for the reaction of DAC/AHC/DHC with HN_3/N_3^- on pH was studied over the pH range 3 - 12 at 25°C using stopped flow spectroscopy. DHC was shown to be substitutionaly inert. An equation derived to describe the relationship between the second order rate constant and pH was shown to fit the high pH data well, but not the low pH data. An explanation for this behaviour could not be found. The k'_{obs} for the substitution of water in vitamin B_{12a} by pyridine, and of

water in AHC (pH 12.00) by cyanide, azide, N-methylimidazole, and pyridine, showed saturating behaviour at higher ligand concentrations (± 0.4 mol dm^{-3}). The reaction of AHC with the ligand 3-amino-1-propanol did not show saturating behaviour over the ligand concentration range investigated (up to 1.0 mol dm^3). Saturation kinetics were shown to be useful in distinguishing between a dissociative (D) and an interchange dissociative (I_D) mechanism of substitution. The dependence of the saturating rate constants (k_{sat}), and the activation parameters thereof, on the nature of the different ligands investigated, confirmed that an I_D mechanism was operable in both cases. Synthesis of the corrin model macrocycle, 6,14-diphenyl-1,4,8,12-tetraazacyclopentadeca-4,6,12,14-teraene (Ph_2[15]tetraenatoN_4)[10,11] was successful. Inclusion of the cobalt atom however, produced an unstable corrin species, which made this model compound unsuitable for subsequent kinetic work.

TABLE OF CONTENTS

1 INTRODUCTION 1 - 19

1.1 Structure of the corrinoids 2 - 4
1.2 Functions of the corrinoids 4 - 7
1.3 The model compound approach 8 - 9
1.4 *Cis*- and *trans*-effects 9 - 18
Nomenclature 11
Trans-effects 11 - 14
Cis-effects 14 - 18
1.5 Aims of the project 19

2 SYNTHESIS OF DIAQUOCOBINAMIDE 20 - 38

2.1 Synthesis of aquocyanocobinamide (Factor B) 21 - 26
Conversion of vitamin B_{12} to dicyanocobinamide 21 - 22
Conversion of dicyanocobinamide to Factor B 23 - 26
2.2 Synthesis of DAC 27 - 31
2.3 Optimisation of the conditions used in the synthesis of DAC from Factor B 32 - 36
Investigation of an alternative reducing agent 32 - 33
Investigation of an optimum reduction time 34
Investigation of an optimum acid concentration 35
Investigation of an optimum time for exposure to the acid 36
2.4 Comparison of Brown's synthetic technique with other literature methods 37

3 THE ACID DISSOCIATION CONSTANTS OF COORDINATED WATER IN DIAQUOCOBINAMIDE 39 - 50

3.1 Experimental procedures 40 - 42
3.2 Results 42
3.3 Analysis and interpretation of data 43 - 48
3.4 Discussion 49 - 50

4 BINDING CONSTANTS OF AQUOHYDROXOCOBINAMILE WITH FIVE SELECTED LIGANDS 51 - 70

4.1 Experimental procedures 52 - 53
4.2 Results 53 - 55
4.3 Analysis and interpretation of data 56 - 65
4.4 Discussion 66 - 69
4.5 Conclusions 70

5 pH PROFILE OF THE KINETICS OF THE REACTION OF DAC WITH AZIDE 71 - 79

5.1 Experimental procedures 71 - 72
5.2 Results 72 - 73
5.3 Discussion 73 - 79
5.4 Conclusions 79

6 THE USE OF SATURATION KINETICS TO DISTINGUISH BETWEEN AN I_D AND A D MECHANISM OF LIGAND SUBSTITUTION : TEST CASE USING AQUOCOBALAMIN 80 - 101

6.1 Experimental procedures 85 - 86
6.2 Results 86 - 97
6.3 Discussion 97 - 100
6.4 Conclusions 101

7 SATURATION KINETICS TO DISTINGUISH BETWEEN AN I_D AND A D MECHANISM FOR THE SUBSTITUTION OF THE AXIAL WATER MOLECULE IN AQUOHYDROXOCOBINAMIDE BY FIVE LIGANDS 102 - 125

7.1 Experimental procedures 102 - 103
7.2 Results 103 - 115
7.3 Discussion 115 - 123
7.4 Conclusions 123 - 125

8 SYNTHESIS OF MODEL COMPOUNDS 126 - 140

8.1 Synthesis of Co(III) 6,14-diphenyl-1,4,8,12-tetraazacyclopentadeca-4,6,12,14-tetraene, $[Co(Ph_2[15]tetraenatoN_4)]^+$ 129 - 138

Synthesis of 4-phenyl-1,2-dithiole-3-thio 131 - 132
Synthesis of 4-phenyl-1,2-dithiolium hydrogen sulphate 132 - 134
Synthesis of N,N'-bis(2-thioformyl-2-phehyl-vinyl)trimethylenediamine, $H_2[SHPhHtn]$ 134 - 135
Synthesis of 6,14-diphenyl-1,4,8,12-tetraaza-cyclopentadeca-4,6,12,14-tetraene, $Ph_2[15]tetraenatoN_4$ 136 - 137
Insertion of the cobalt(II) metal ion, $Co(Ph_2[15]tetraenatoN_4)$ 138

8.2 Synthesis of Co(III) 6,14-diphenyl-1,4,8,12-tetraazacyclopentadeca-4,6,8,10,12,14-hexaene, Co(Ph_2[15]hexaaenatoN_4) 138
8.3 Discussion 139 - 140
8.4 Conclusions 140

9 CONCLUSIONS 141 - 144

10 REFERENCES 145 - 147

11 APPENDIX : SUPPLEMENTARY DATA FOR MAIN TEXT 148 - 183

11.1 Supplementary data for chapter 3 148 - 151
11.2 Supplementary data for chapter 4 152 - 156
11.3 Supplementary data for chapter 5 157 - 158
11.4 Supplementary data for chapter 6 159 - 162
11.5 Supplementary data for chapter 7 163 - 179
11.5.1 Cyanide 163 - 166
11.5.2 Azide 167 - 169
11.5.3 Pyridine 170 - 173
11.5.4 N-methylimidazol 174 - 175
11.5.5 3-amino-1-propanol 176 - 179
11.6 Supplementary data for chapter 8 180 - 183

12 APPENDIX : DERIVATIONS OF EQUATIONS USED IN MAIN TEXT 184 - 211

12.1 Chapter 3 184 - 188
Derivation of equations 3.3.1 and 3.3.2 184 - 186
Derivation of equations 3.3.3, 3.3.4, and 3.3.5 186 - 188

12.2 Chapter 4 189 - 194
Derivation of equation 4.3.1 189 - 190
Derivation of equation 4.3.2 190 - 192
Derivation of equation 4.3.3 192 - 194
Derivation of equation 4.3.4 194
12.3 Chapter 5 195 - 198
Derivation of equation 5.3.1 195 - 198
12.4 Chapters 6 and 7 199 - 211
Derivation of equation 6.3 199 - 203
Derivation of equation 6.4 204 - 205
Derivation of equation 6.7 205 - 208
Derivation of equation 6.8 209 - 210
Derivation of equation 6.2.2 210
Derivation of equation 6.2.3 210
Derivation of equation 6.2.4 210 - 211
Derivation of equation 6.2.5 211

13 APPENDIX : DETAILS ON EXPERIMENTAL MEASUREMENTS 212

13.1 pH Determination 212
13.2 UV/VIS Spectrophotometer 212
13.3 High performance liquid chromatography 212
13.4 Stopped flow spectrophotometry 212

LIST OF NON-STANDARD ABBREVIATIONS AND TRIVIAL NAMES IN TEXT

AHC	aquohydroxocobinamide
[14]aneN$_4$	1,4,8,11-tetraazacyclotetradecane
[15]aneN$_4$	1,4,8,12-tetraazacyclopentadecane
DAC	diaquocobinamide
DDQ	2,3-dichloro-5,6-dicyano-p-benzoquinone
DHC	dihydroxocobinamide
[14]dieneN$_4$	1,4,8,11-tetraazacyclotetradeca-1,3-diene
DIM	1,4,8,11-tetraaza-2,3-dimethylcyclotetradeca-1,3-diene
dmbzim	5,6-dimethylbenzimidazole
DMF	dimethylformamide
DMG	dimethylglyoximate
HPLC	high performance liquid chromatography
H$_2$[SHPhHtn]	N,N'-bis(2-thioformyl-2-phenylvinyl)trimethylenediamine
Ph$_2$[15]hexaenatoN$_4$	6,14-diphenyl-1,4,8,12-tetraazacyclopentadeca-4,6,8,10,12,14-hexene
Ph$_2$[15]tetraenatoN$_4$	6,14-diphenyl-1,4,8,12-tetraazacyclopentadeca-4,6,12,14-tetraene
SYC	stable yellow corrinoids
TCPP^{6-}	tetracarboxyphenylporphinato
[14]tetraeneN$_4$	1,4,8,11-tetraazacyclotetradeca-1,3,8,10-tetraene
TIM	1,4,8,11-tetraaza-2,3,9,10-tetramethylcyclotetradeca-1,3,8,10-tetraene
TMpyP^{2+}	tetrakis(4-N-methylpyridyl)porphine
Vitamin B$_{12}$	aquocobalamin
Vitamin B$_{12a}$	cyanocobalamin

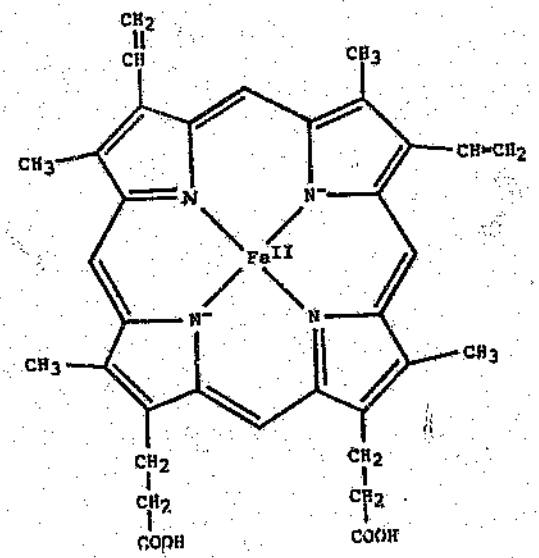
1 INTRODUCTION

Protein molecules containing metal complexes of highly unsaturated ligand ring systems are involved in a variety of essential biological functions. Figure 1.1 indicates the two classes of these naturally occurring unsaturated ligand ring systems, the porphyrins and the corrins. Porphyrins are ubiquitous in nature, playing varied and important roles in both the animal and plant kingdoms. Iron porphyrins are essential for the oxygen-carrying and storage functions of haemoglobin and myoglobin, and the electron transport functions of the cytochromes. In the plant kingdom, magnesium porphyrins are required for the light-capturing function of the chlorophylls. Corrins, in contrast, are restricted to the animal kingdom. Cobalt corrins are found in vitamin B_{12}, a vitamin required to catalyse reactions involving,

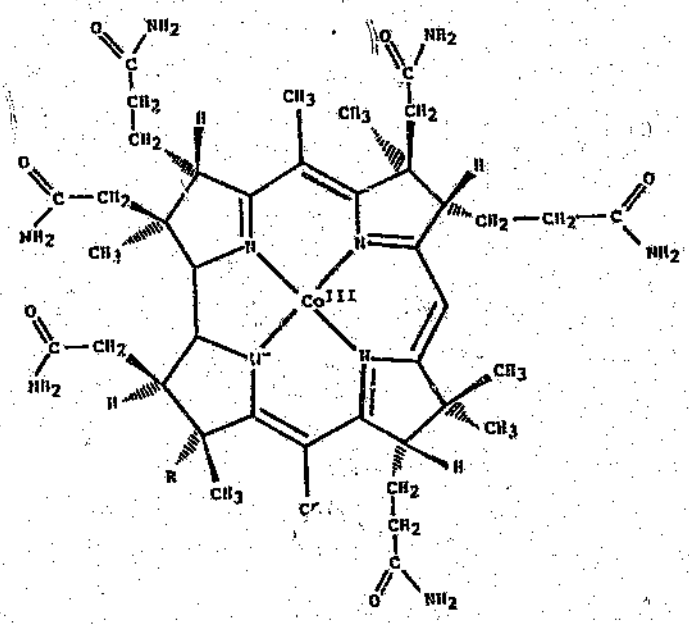
(1) the transfer of a methyl group,
(2) the transfer of a hydride.

Figure 1.1 Structure of (a) the porphyrin ring (*e.g.* haemoglobin) and (b) the corrin ring (*e.g.* vitamin B_{12}).

(a)



(b)



Vitamin B_{12} has elicited scientific interest from numerous disciplines since its isolation in 1948 in the form of dark red crystals of cyanocobalamin. Coordination chemists became active in vitamin B_{12} research in 1961 following Lenhert and Hodgkin's demonstration by X-ray analysis that the coenzyme form of vitamin B_{12} contained a cobalt-carbon bond and was thus the first known naturally occuring organo-metallic compound.[1] Pratt identifies two areas of chemistry in which our understanding has developed from an understanding of the coordination chemistry of vitamin B_{12},[1]

(1) organometallic compounds containing σ-bonded carbanion ligands (in contrast to π-bonded ligands such as CO, olefins, acetylenes *etc.*),
(2) the nature of the metal-ligand bond and *cis*- and *trans*-effects.

It is in this second area that the work described in this thesis is relevant.

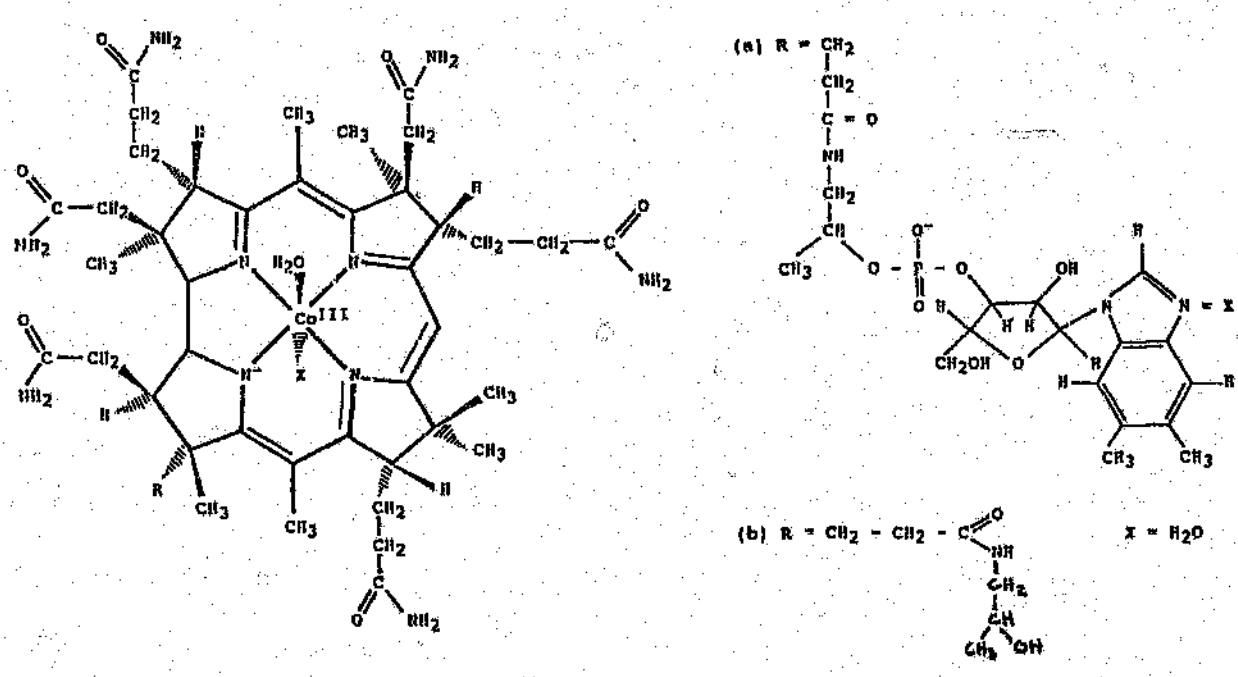
1.1 STRUCTURE OF THE CORRINOIDS

The class of molecules known as the cobalt corrinoids, the best known member being vitamin B_{12} (cyanocobalamin), have a cobalt atom coordinated to the four nearly coplanar nitrogen atoms of a corrin ring in common. X-ray analysis has indicated that the corrin ring is buckled and very flexible, a different conformation being found for each corrin structure determined.[2] The corrin ring is asymmetric, with all acetamide side chains projecting towards one side of the ring (upper or β face) and all propionamide side-chains towards the lower side or α face.[1] The corrin ring binds the cobalt(III) atom in one plane, leaving two axial positions available for binding to other ligands.

Differences within the corrin class arise concerning the valency and coordination number of the cobalt atom, the number and identity of the axial ligands, the identity of the side chains and any functional groups on the corrin ring, and substitution or protonation/deprotonation reactions on the corrin ring itself. More often than not the corrin complexes display octahedral symmetry, with the central cobalt atom in the +3 oxidation state. Within the corrinoid class, further sub-groupings have emerged. The cobinamides, illustrated in figure 1.1.1, are distinguished from the cobalamins, for example, by the absence of a nucleotide side chain which projects down and terminates in a 5,6-dimethylbenzimidazole base, usually coordinated to the cobalt atom. The base always coordinates to the lower face of the corrin.[1]

If aquocobalamin (vitamin B_{12a}) can be considered to be the parent cobalamin, then diaquocobinamide (DAC) is considered to be the parent cobinamide. Comparatively little work has been done on DAC, largely due to difficulties associated with its synthesis.[3]

Figure 1.1.1 Molecular structure of (a) vitamin B_{12a}, the parent cobalamin, and (b) diaquocobinamide (DAC), the parent cobinamide.



Stereoisomers are not produced in the ligand substitution reactions of cobalamins because only one axial site is available for substitution. The same cannot however be said for the cobinamides. Firth *et al.* reported isomerisation in aquocyanocobinamide and aquocyanocobyric acid. Here the two isomers were present in approximately equal concentrations at equilibrium and had very similar spectra.[4] Isomerisation required the presence of free CN^- and was postulated to proceed through the intermediate formation of dicyano species. No stereoisomers are known for the organocobinamides. Here the axial ligand cannot exist free in solution, and hence isomerisation cannot occur.[2]

One would expect all corrinoids with two different axial ligands, both of which could exist free in solution, to exhibit isomerism. Firth's aquocyano isomers could be separated chromatographically and thus the rate of interconversion between the two isomers was relatively slow.[2] For ligands with lower binding constants isomerisation would be expected to proceed more rapidly since the proportion of unbound ligand would be greater than in the CN^- case. This would make it difficult to establish the existence of two separate isomers chromatographically.

1.2 FUNCTIONS OF THE CORRINOIDS

The two classes of reactions catalysed by vitamin B_{12} were described above. In both cases the catalyst is the complex (or holo-enzyme) formed from a corrinoid (the coenzyme) together with a protein (the apoenzyme).[1] The complete corrinoids (the cobalamins, the cobinamides being classed as incomplete corrinoids) have been the subject of some interest for many years in connection with the elucidation of their function as coenzymes. Comparisons between cobalamins and cobinamides are

useful in evaluating the role of the axially coordinated benzimidazole moiety in the reactions of cobalamins.[5] In addition, in enzyme-bound cobalamin, the coordinate linkage between the cobalt atom and the 5,6-dimethylbenzimidazole moiety is broken and thus it is postulated that the enzyme-bound cobalamin should react like a cobinamide rather than a cobalamin.[6]

Most of the features of the ligand substitution reactions shown by the corrinoids find parallels amongst the reactions of other cobalt(III) complexes, *viz.* the inertness of the hydroxo- compared to the aquo-complex, the strong labilizing effect of S-bonded SO_3^{2-} and alkyl groups, the reaction with HN_3 as well as N_3^-, the removal of coordinated SO_3^{2-} by H^+ and of CH_3^- by $HgCl_2$ and a dissociative reaction mechanism.[1] There is however a striking difference in the general rates of reaction. Compared to most other cobalt(III) complexes, the highly unsaturated porphyrin and corrin macrocyclic (N_4) ligands have been shown to enhance the rate of ligand substitution at the metal atom by many orders of magnitude. No cases where the nature of both the axial ligands and the incoming ligand for the ligand substitution reactions of corrins, bis(dimethylglyoximato) ($(DMG)_2$), $(NH_3)_4$ *etc.*, remained the same could be found in the literature, and hence the *cis*-effects of these N_4-macrocycles cannot be compared directly. Labilising trends can nevertheless be observed. Table 1.2.1 below gives the second order observed rate constants for the substitution of H_2O by SCN^- and N_3^- for various Co(III)-N_4 complexes.

Figure 1.2.1 Molecular structure of Co(III)nitroaquobis(dimethylglyoximato).

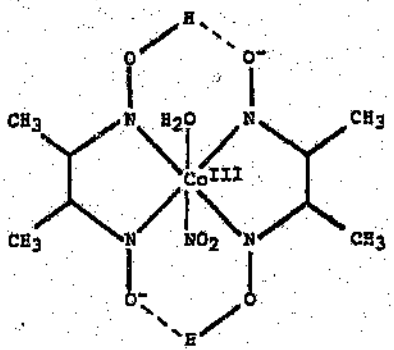


Table 1.2.1 Second order observed rate constants for the substitution of H_2O by SCN^- and N_3^- for various Co(III)-N_4 complexes measured under similar conditions (pH~7)[7]

trans-[Co.L_4.X.H_2O] + Z ⇌ *trans*-[Co.L_4.X.Z] + H_2O

N_4 Ligand	Z	k_{II}^{obs} / M^{-1} s^{-1}
aquocobalamin	SCN^-	5.0 X 10^3
	N_3^-	7.9 X 10^2
haematoporphyrin	SCN^-	1.9 X 10^3
	N_3^-	1.4 X 10^2
nitroaquobis(dimethylglyoximato)	SCN^-	5.8 X 10^{-4}
	N_3^-	5.7 X 10^{-4}
$(NH_3)_5$	N_3^-	2.1 X 10^{-5}

The primary influence of the porphyrin and corrin ligands is a profound labilization of the axial bonds. This labilization was proposed to be a consequence of the four Co(III)-imine bonds in the two macrocycles.[1] Differences in rates between the haematoporphyrin and the cobalamin are attributed to the different labilizing effects of the *trans* ligands (aquocobalamin has a benzimidazole group, whereas the haematoporphyrin has an axially coordinated water molecule here).[22] DMG, indicated in figure 1.2.1, was initially believed to be an effective model for the naturally occuring corrinoids. The geometry and charge of the porphyrin, corrin, and DMG are similar, yet DMG reacts 10^6 times slower. Co(III) bis(DMG) complexes have four Co(III)-imine bonds, believed to be a vital component of the corrin and porphyrin lability, but the extensive conjugation seen in these natural macrocycles is absent. The structural and electronic characteristics of the

corrin and porphyrin rings must account for the lability of the porphyrin and corrin axial positions and hence must be the key to their suitability for their biological functions.

A frequently occurring feature of the discussion of the chemistry of corrin and porphyrin complexes is the contention that the electronic interaction between the Co atom and the highly unsaturated ligand systems is sufficiently extensive as to render the Co(III) oxidation state formalism inappropriate.[7,20] Application of crystal field theory to corrinoids, assuming pseudo D_{4h} symmetry, indicates that the six valence electrons of low-spin Co(III) will occupy the low energy d_{xz}, d_{yz} and d_{xy} orbitals. Considerable kinetic inertness is associated with this electronic arrangement. It has been proposed that a π electron charge transfer from the unsaturated corrin ring to the Co(III) produces a low spin pseudo Co(II) metal ion. Applying the same rules of crystal field theory indicates that the extra electron will now occupy a high energy d_{z^2} orbital. Occupation of this orbital could then be responsible for the observed axial ligand labilisation exhibited by the corrin and porphyrin ligands.

Support for this theory comes from comparisons between the rates of ligand substitution reactions of chromium(III) and cobalt(III) porphyrins. The rate of substitution of water ligands of chromium-porphyrin complexes are about 10^3 - 10^4 times faster than "normal" chromium complexes. In an analogous case using cobalt-porphyrins, the substitution rates were seen to be about 10^6 times faster. Cr(III) is known to be harder to reduce than Co(III) because it is a d^3 ion, whereas Co(III) is a d^6 ion. A π electron charge transfer from the unsaturated corrin ring to the Co(III) would then occur more readily than to the Cr(III) and hence the Cr(III) porphyrin would be less labile than the Co(III) porphyrin.[21]

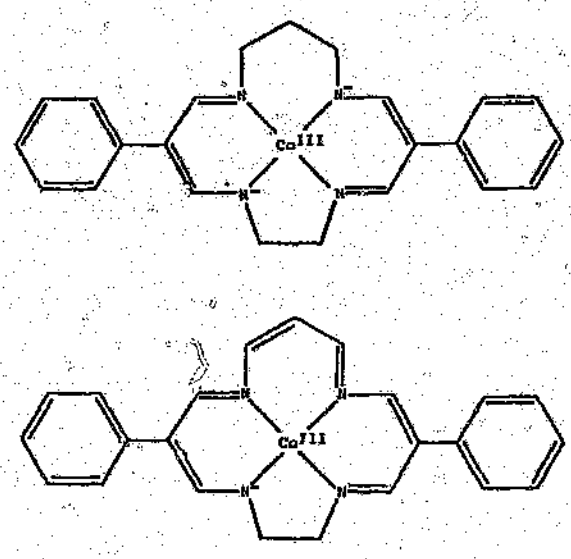
1.3 THE MODEL COMPOUND APPROACH

The understanding of a protein's mode of action, though valuable, is not easily obtainable because of the very complexity of these living systems. The "model system" approach was thus devised in the hope that the knowledge obtained from the simpler systems could be extrapolated to give an understanding of the natural reactions in real systems. Most of the vitamin B_{12} model compounds are cobalt(III) complexes containing various macrocyclic quadridentate amine ligands.

In 1963 it was observed that bis(dimethylglyoximato)cobalt complexes showed reactivity patterns similar to those shown by the cobalt corrins. In view of their similarity to the cobalamins, and for convenience, complexes of this type were named "cobaloximes".[8] However, as indicated above, the promise of this model was not fulfilled when the rates of its reactions were compared to those of the cobalamins.

Recent successes in the synthesis of a great many macrocyclic amine ligands by metal template reactions has further stimulated research activities in various aspects of these model compounds.[9] Tang *et al.* have developed a synthetic route to the formation of some promising new corrin model compounds.[10,11] These compounds, indicated below in figure 1.3.1, have the 1,4,8,12-tetraazacyclopentadecane ([15]aneN_4) macrocyclic structure found in the corrin ring. No work on the substitution kinetics of the Co(III) complexes of these macrocycles has been reported so that their effectiveness as models is not yet known. Furthermore, their solubility in water is probably low, though this problem could be addressed by sulfonating the benzene rings.

Figure 1.3.1 Model macrocycles with the [15]aneN$_4$ skeleton in common with the corrin ring.[10,11]



1.4 CIS- AND TRANS-EFFECTS

The change of one or more ligands in a transition metal complex can have a marked effect on the properties of both the central metal cation and the other ligands. Several mechanisms contributing to this phenomenon can be identified, and broadly classified under three headings:[12]

(1) *cis*- and *trans*- effects or "internal" effects i.e. electronic effects transmitted through the central metal cation,

(2) steric effects due to direct contact between the atoms of different ligands,

(3) "external" effects due to changes in the outer coordination sphere.

The sensitivity of the rate of reaction of octahedral complexes to the nature of the "nonparticipating" ligands is often quite marked, either as a *cis*- or *trans*-effect, or often as a non-directional effect that does not greatly depend upon the relative positions of the ligands concerned. The *cis*- and *trans*-isomers of "normal" octahedral Co(III) complexes do not differ enormously in their reactivity.[13] Pratt *et al.* claim that there is similarly no real evidence that ligands in the corrinoid family exert a significant and systematic difference on rates of ligand substitution in the *cis*- & *trans*-positions.[12]

The study of the mutual interactions of ligands in transition metal complexes can be traced back to observations made on the position and relative ease of ligand substitutions in the preparation of square planar platinum(II) complexes. Chernyaev was the first to recognise the existence of a certain pattern of reactivity, namely, that one ligand affected the kinetic lability of another ligand in the *trans*-position and that the ligands could be arranged in an order of increasing *trans*-labilizing power. Since then many additional ligands have been studied and the order of *trans* activation for Pt(II) complexes can now be written CO, CN^-, C_2H_4 > PR_3, H^- > CH_3^-, $SC(NH_2)_2$ > $C_6H_5^-$, NO_2^-, I^-, SCN^- > Br^-, Cl^- > py, NH_3, HO^-, H_2O.[12] Experimental work has since been extended to include,

(1) the study of the effect of ligands on other properties of complexes such as equilibrium constants and infrared spectra,
(2) a search for *cis*-effects,
(3) other metals and valencies.

Evidence from X-ray diffraction, infrared and UV/VIS spectroscopy, and proton magnetic resonance spectra indicate that *cis*- and *trans*-effects are evident in the substitution

reactions of the cobalt corrinoids too. A strong electronic interaction between the conjugated corrin ring, the cobalt ion and the donor atoms of the axial ligands must thus exist. Firth *et al.* divided the *cis*- and *trans*-effects observed in the corrins into three categories,[4]

1) Ground state effects *e.g.* effects on bond angles and lengths, bending and stretching force constants,
2) Thermodynamic effects *i.e.* equilibria,
3) Kinetic effects *e.g.* rates of ligand substitution.

NOMENCLATURE

The experimental approach to the study of *cis*- and *trans*-effects is to compare the relative effect of a series of ligands by following the effect on some property of ligand Y as ligand X is varied. In this thesis the ligand which is used as the "probe" in ground-state effects is labeled Y. In thermodynamic effects we consider the equilibrium between two ligands Y and Z, and where a set of equilibria are compared the common ligand, if any, is labeled Y. Similarly, for kinetic determinations, we consider the substitution of Y by Z. X is the ligand whose effect we are studying and which we are trying to place in a series relative to other ligands.

TRANS-EFFECTS

The phenomenon of the *trans*-effect was first observed in the square planar platinum(II) complexes. This *trans*-labilising order is slightly different from the order found for Co(III) complexes. The two orders differ in the relatively high positions of CN^-, NO_2^- and CO in the Pt(II) series. Subsequent studies indicated that all the octahedral d^6 metal ions (Co(III), Ru(II), Ir(III), and Pt(IV)) show common features which distinguish them from the square planar d^8 Pt(II) ion.

CN^-, NO_2^- and CO have the ability to form metal-to-ligand bonds. In the octahedral d^6 complexes the *trans*-effect is due mainly to their σ-donor strength and is therefore small, whereas in the square planar d^8 complexes both σ-donor and π-acceptor capacities play their part and result in a high *trans*-effect.[12]

A general *trans*-labilising order of ligand atoms in Co(III) octahedral complexes can be written; Cl, O, N, C (in CN^-) < H, S, Se, I, C (in CH_3^- *etc.*), N (in NO_2^-). A specific order of carbon ligands can also be written; $CN^- < HC{\equiv}C^- < CH_2{=}CH^- < CH_3CH_2^-$. These orders indicate that the most important property of the ligand which determines its influence on the rest of the complex is the amount of negative charge donated via the σ bond to the cobalt ion.[12] The order of ligands observed for *cis*- and *trans*-effects in cobalt(III) complexes shows a general similarity to the nephelauxetic series (also determined by the amount of negative charge donated by the ligand to the metal); F < O, N < Cl < C, Br < S, Se, I.

Ground state, thermodynamic and kinetic *trans*-effects in the corrinoids have been correlated.[14] Table 1.4.1 below gives an example of these effects for the substitution of H_2O by CN^- in various corrinoids.

As the axial ligand X becomes more polarisable and places more negative charge on the cobalt ion, so the rate of water ligand substitution at the other axial position increases, the equilibrium binding constant for the Co(III)-CN^- bond decreases, and the Co(III)-CN^- bond stretching frequency decreases (bond length increases).

Table 1.4.1 *Trans*-effect in cobalt(III) corrinoids.[14]

Ligand, X	k_{II}^{obs} a / $dm^3\ mol^{-1}\ s^{-1}$	log K_{CN} b	ν_{CN} c / cm^{-1}
H_2O	$< 10^3$	> 14	2133
Bzm	8.5×10^2	14.1	2132
HO^-	6.8×10^4	> 9	2131
CN^-	2.1×10^5	8.4	2119
CH_3^-	$> 10^8$	2.1	2088
$CH_3CH_2^-$	$> 10^8$	0.6	2082

a second order rate constants for the reaction of X-Co-OH_2 and/or X-Co with CN^- to give X-Co-CN in aqueous solution at 25°C and an ionic strength of 0.2 mol dm^{-3}

b

$$K_{CN} = \frac{[X\text{-}Co\text{-}CN]}{([X\text{-}Co\text{-}OH_2] + [X\text{-}Co])[CN^-]}$$; various conditions

c infrared stretching frequency of coordinated CN^- in KCl discs

Although the vast majority of cobalt(III) complexes are six-coordinate, several groups of five or even four-coordinate complexes are known in which the cobalt atom may be considered as having the formal oxidation state(III). These complexes represent the extreme case where the thermodynamic effects are so great that no ligand, even H_2O, can form a stable bond to the cobalt atom.[12] In table 1.4.1 above, it is shown that equilibrium constants for the substitution of H_2O by other ligands decrease as the Co-OH_2 bond becomes weaker. This trend eventually leads to the formation of 5-coordinate complexes. The labilizing effect of CH_3^- is so strong, for example, that 5-coordinate alkyl complexes of cobalt(III) may be formed and

isolated.[15] As the amount of negative charge donated by the ligands to the cobalt atom increases, so the preferred coordination number of the complex drops from six to five, *i.e.* the stereochemistry changes from that typical of cobalt(III) to that typical of low-spin cobalt(II).[12]

CIS-EFFECTS

The *cis*-effect observed in the corrinoids can be divided into two categories,

(1) the effect of the axial ligands on the corrin ligand,
(2) the effect of the corrin ligand on the axial ligands.

Electronic spectra have been used to provide information on the *cis*-effect of the axial ligands in the corrinoids. The spectra of corrinoids show a remarkable diversity. When one axial ligand is kept constant, as in a series of cobalamins (Y = Bzm), the different spectra can be fitted into a series showing gradually changing features. Table 1.4.2 below shows the dependence of the wavelength of the main cobalamin absorption band on the nature of the second axial ligand.

These axial ligands can be arranged in an order of *cis*-labilisation which is parallel to the order of *trans*-labilisation. *Cis/trans* differentiation is hence not exhibited by these ligands.

Table 1.4.2 The dependence of the cobalamin's main absorption band (γ band) on the nature of the axial ligand, evidence for a *cis*-effect in a series of cobalamins.[12]

Axial ligand	Wavelength / nm
CH_3^-	374
CN^-	360.5
pyridine	360
imidazole	358
HO^-	357
Cl^-	352
H_2O	350

The extensively conjugated π-electron system of the corrin ring is expected to play a major role in the uncharacteristic lability exhibited by the cobalt(III) metal atom. Comparisons of results from amine, diimine, dimethylglyoximate, porphyrin and corrinoid ligands are complicated by questions regarding steric promotion of labilization and variation of the overall charge of the complex. Nevertheless, Pratt was able to arrange the following ligands in an order of increasing ability to labilise the axial Co(III) bonds: $(NH_3)_4$, en_2 < $(DMG)_2$ < corrin.[12]

The apparent *cis*-labilisation of the corrins can be investigated by observing the effect of progressive degrees of unsaturation in model cobalt(III) macrocycles on their lability. For the three macrocycles (shown in figure 1.4.1), 1,4,8,11-tetraazacyclotetradecane ([14]aneN_4), 1,4,8,11-tetraazacyclotetradeca-1,3-diene ([14]dieneN_4) and 1,4,8,11-tetraazacyclotetradeca-1,3,8,10-tetraene ([14]tetraeneN_4), the rate of substitution of two anions by

water has been investigated.[15] Table 1.4.3 indicates that the lability of these macrocycles increases 10^4-fold when a tetraamine is relaced by a sterically similar tetraimine. Similar studies by Poon *et al.* with the ligands [14]aneN$_4$, 1,4,8,11-tetraaza-2,3-dimethylcyclotetradeca-1,3-diene (DIM), and 1,4,8,11-tetraaza-2,3,9,10-tetramethylcyclotetradeca-1,3,8,10-tetraene (TIM) (also shown in figure 1.4.1), yielded similar results, also given in table 1.4.3.[16] The kinetic lability of these complexes increased in the order [14]aneN$_4$ < DIM < TIM (1:400:1640 for Cl^- and 1:44:170 for Br^-).

Figure 1.4.1 Molecular structure of (a) [14]aneN$_4$, (b) [14]dieneN$_4$, (c) [14]tetraeneN$_4$, (d) DIM, (e) TIM, (f) $TMpyP^{2+}$ and (g) $TCPP^{6-}$

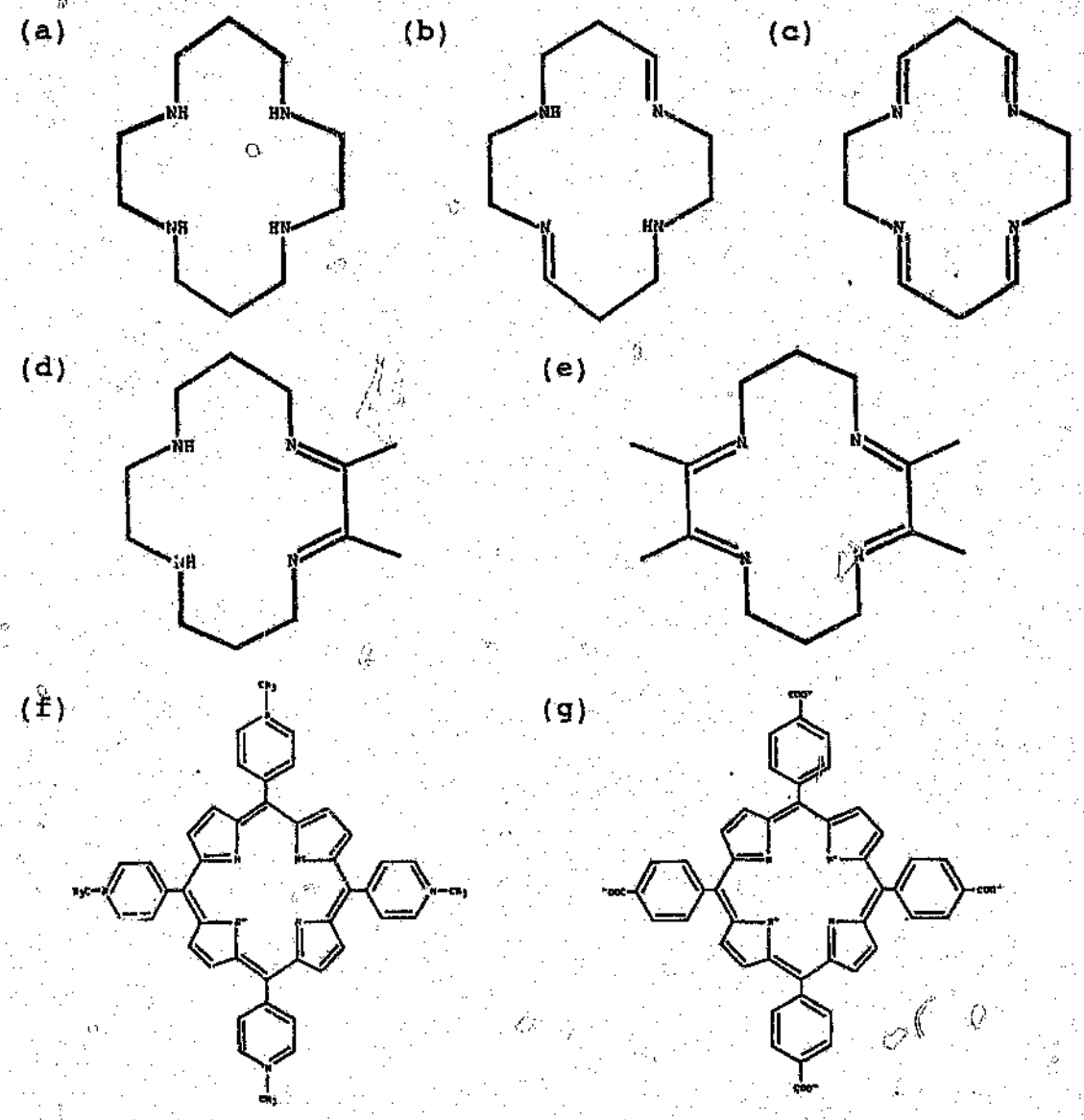


Table 1.4.3 Pseudo first order observed rate constants for the substitution of an anionic axial ligand (Br^- and Cl^-) by H_2O for various N_4-macrocycles.[15,16]

Macrocycle	k_{Br} / s^{-1}	k_{Cl} / s^{-1}
[14]aneN_4	2.2×10^{-5}	1.1×10^{-6}
[14]dieneN_4	7.8×10^{-2}	2.3×10^{-4}
[14]tetraeneN_4	0.12	2.1×10^{-2}
[14]aneN_4	1.3×10^{-8}	1.1×10^{-9}
DIM	5.7×10^{-7}	4.4×10^{-7}
TIM	2.2×10^{-6}	1.8×10^{-6}

Poon's observation that increasing the degree of unsaturation of the macrocyclic ligand increased the lability of the Co(III) centre can be explained. The trend was shown to be a direct consequence of the decreasing enthalpies of activation for the reaction. This is consistent with the view that increasing the degree of electronic delocalisation between an amine macrocycle and the central cobalt(III) ion helps stabilise the five coordinate intermediate of a dissociative mechanism. Polarizability of the central cobalt(III) ion would increase with the increasing extent of electronic delocalization between the metal ion and the encircling unsaturated macrocycle.[16]

The ligand substitution kinetics of the other group of naturally ocurring unsaturated N_4-macrocycles, the porphyrins, supports the theory that the Co(III)-imine bonds in the extensively conjugated ring system are involved in the *cis*-labilisation exhibited by the corrinoids. The availability of water-soluble analogues of naturally occuring porphyrins makes it feasible to carry out detailed kinetic studies of the

substitution reactions at their axial positions. The rate of substitution of H_2O by an incoming ligand for porphyrins with different peripheral charges (shown in figure 1.4.1) are compared in table 1.4.4.[17,18,19] The two reactions investigated were,

$$\text{porphyrin}(H_2O)_2 + L \rightleftharpoons \text{porphyrin}(H_2O)L + H_2O \quad k_1$$
$$\text{porphyrin}(H_2O)L + L \rightleftharpoons \text{porphyrin}L_2 + H_2O \quad k_2$$

Table 1.4.4 Observed rate constants for the substitution of H_2O by C_5H_5N or SCN^- in two porphyrins.[17,18,19]

Observed Rate	$CoTMpyP^{5+}$		$CoTCPP^{3-}$	
Constant / s^{-1}	C_5H_5N	SCN^-	C_5H_5N	SCN^-
k_1	0.7	2.1	$1.4X10^3$	$4.5X10^2$
k_2	2.8	$2.8X10^4$	$2.1X10^3$	$1.8X10^6$

$CoTMpyP^{5+}$ tetrakis(4-N-methylpyridyl)porphinecobalt(III)
$CoTCPP^{3-}$ tetracarboxyphenylporphinatocobaltate(III)

The large amount of electron density placed upon the cobalt(III) by the porphine ligand makes the Co(III) less positive, more like Co(II), and stabilizes a five-coordinate reactive intermediate during the course of the substitution reactions.[18] Negatively charged substituents concentrate electron density at the metal atom, whilst positively charged substituents delocalise electron density. For the pyridine ligand, where Coulombic effects play no role, changing from a positively- to a negatively-charged porphyrin periphery increases the rate of the Co(III)-H_2O bond breaking rate determining step by over 3 orders of magnitude. The major influence of the porphyrin peripheral substituents is thus to modify the degree of electron delocalisation at the porphyrin core which in turn manifests itself in a *cis* effect.

1.5 AIMS OF THIS PROJECT

Although extensive work has been done on the *trans*-effect in cobalamins[1], less has been done with DAC because of inherent difficulties in its synthesis[3] and problems associated with its instability in air.[5] Far less work has been done on the *cis*-effect in corrins because of difficulties in obtaining a series of models with sequentially increasing degrees of unsaturation without the alteration of any other structural features. The present work was intended to,

(1) elaborate on the data supporting a kinetic and thermodynamic *trans*-effect in DAC,

(2) determine the relationship between degree of macrocyclic unsaturation and the *cis*-effect using Tang's model compounds.[10,11] (figure 1.3.1)

Although much work has been done on the mechanism of ligand substitution in aquocobalamin, disagreement still exists as to whether the mechanism is purely dissociative, D[14,22,23,24,25], or interchange dissociative, I_D[23,26,27]. A novel approach to this question, using saturation kinetics is described here. A similar approach was then used to determine the mechanism of ligand substitution in DAC.

2 SYNTHESIS OF DIAQUOCOBINAMIDE (DAC)

Diaquocobinamide was prepared from cyanocobalamin (vitamin B_{12}) via the intermediate aquocyanocobinamide (Factor B). Cobalamins, unlike cobinamides, possess a heterocyclic base capable of coordination to the central cobalt ion (figure 1.1.1). Two methods for the cleavage of the phosphate group, and its accompanying heterocyclic base, are known. Fairly vigorous acid conditions, (*e.g.* concentrated HCl at 65°C for 5 minutes) promotes hydrolysis of the nucleotide side-chain with little or no hydrolysis of the amide side chains.[1] Alternatively, as used in this work, cerium(III) hydroxide can be used as the catalyst for hydrolysis.[30] The hydrolysis product, dicyanocobinamide, is converted to Factor B by acid hydrolysis of one of the Co(III)-CN^- bonds.[2] Cleavage of the second axial CN^- to form DAC is not so simply achieved since this CN^- is very firmly held (a formation constant of log K ~ 14 versus log K ~ 8 for the first CN^-)[1,28].

Two methods for effecting this second CN^- substitution have been reported. Firstly, $NaBH_4$ can be used to reduce Co(III) to Co(I), and a subsequent reaction with CH_3I would then produce methylcobinamide. Photolysis of the cobalt-methyl bond would then lead to the formation of DAC.[3] The second and more popular method involves the direct photolysis of the Co-CN bond in acid. A stream of nitrogen gas is then required to remove the HCN thus formed.[3,28] Complete conversion of Factor B to DAC using this method has, in certain cases, been reported. However, cobalamins and cobinamides are known to be unstable when exposed to light and hence irradiation of Factor B to produce DAC would be expected to result in some photodegradation. Photolysis involves the production of free radicals which, in the presence of air, produce stable yellow corrinoids (degradation products), as shown by an increased optical density of the solution at 455 nm.[3] The

100% conversion of Factor B to DAC thus seems unlikely and an alternative method, not requiring the presence of light, was sought. Prof K.L.Brown kindly supplied us with such a method, involving the reduction of Co(III) using zinc wool.[29]

2.1 SYNTHESIS OF AQUOCYANOCOBINAMIDE (FACTOR B)

All reactions involving corrins were performed in a dark room, since co rins are known to be sensitive to light, decomposing into a variety of unidentified compounds, collectively known as stable yellow corrinoids.[1,3,5,29] It is believed that the stable yellow corrinoids are produced by a reduction of the cobalt followed by an irreversible ring oxidation or some other corrin ring modification.[1] When not in use, synthesis intermediates were stored frozen.

Conversion of Vitamin B_{12} to dicyanocobinamide[30]

The number of molecules of water of crystallization associated with a molecule of vitamin B_{12} in the solid state is not constant, and thus the amount of vitamin in a sample of solid vitamin B_{12} cannot be determined using a simple mass measurement. UV/VIS spectroscopy can, however, be used to determine the effective molecular weight of a sample by measuring the absorbance of the sample at 367 nm after reacting the sample with NaCN (A_{367} dicyanocobinamide = 3.04 X 10^4 dm^3 mol^{-1} cm^{-1})[28].

A solution containing 0,5972 g (0.378 mmol) of vitamin B_{12} (effective molar mass of 1580 g mol^{-1}, true molar mass of 1350 g mol^{-1}) (Roussel), 7.1651 g $Ce(NO_3)_3.6H_2O$ (Aldrich), 0.3863 g NaCN (Merck) and 15 ml 2 mol dm^{-3} NaOH, dissolved in 150 ml water, was refluxed at 145°C for 30 minutes. The pH of the cooled mixture (6.1) was adjusted to 9.0 using 10 mol dm^{-3} NaOH. Cerous hydroxide, present in the reaction mixture as a

precipitate, was removed by centrifugation of the mixture at 9000 rpm for 10 minutes. The precipitate was washed six times with a solution of 50 ml water and 3 ml 30% aqueous ammonia. The washings were combined with the supernatant of the reaction mixture and concentrated down to 150 ml by flash evaporation. The solution was then filtered to remove trace amounts of cerous hydroxide.

HPLC analysis (details in appendix 13.3) of the purple reaction mixture using an analytical 100 mm X 4.6 mm C_{18} reverse phase column with a 5 μm particle size (Brownlee Laboratories) indicated that a 75% conversion of vitamin B_{12} to dicyanocobinamide was achieved. It should be borne in mind that area counts under the HPLC chromatogram peaks are only useful in providing a rough estimate of the concentration of a certain substance in a given sample because the response factor at the monitoring wavelength (here 360 nm) differs for different substances.

The pH of the solution was adjusted to 3.6 using glacial acetic acid. Organic components of the solution were extracted into 10 successive 20 ml portions of 1:1 phenol/chloroform (58.8 g phenol in 50.0 ml chloroform). The purple product (dicyanocobinamide) was completely extracted in the first six extractions, whilst a yellow product, taken to be stable yellow corrinoid species, appeared in the later extractions. The stable yellow components were discarded together with the aqueous phase containing the inorganic salts. Dicyanocobinamide was diluted with 400 ml ether and extracted back into the aqueous phase (400 ml in 10 portions). The aqueous phase, washed twice with 200 ml of ether, was concentrated down to 300 ml by flash evaporation.

Conversion of dicyanocobinamide to Factor B[30]

Cleavage of the first Co-CN bonds was achieved by adding 2 ml 5 mol dm^{-3} acetic acid to the dicyanocobinamide solution, producing HCN and Factor B. The product solution was concentrated down to 5 ml whereupon 25 ml water and a further 2 ml 5 mol dm^{-3} acetic acid was added. Acetic acid and water were removed on a vacuum pump to yield dry Factor B.

A 2.5 cm X 35 cm SP-Sephadex C-25 (Pharmacia Fine Chemicals) cation exchange column was conditioned by passing 400 ml 0.010 mol dm^{-3} NaCl through the column. Chloride ions were then removed by passing 150 ml deionised water through the column, until no more chloride ions were detected ($AgNO_3$). Using water as the eluent, 2 fractions were obtained; the first fraction, seen as a distinct red band, was identified as unreacted Vitamin B_{12} from the first reaction, whilst the second fraction, a purple band, was subsequently shown to be dicyanocobinamide. Changing the eluent to 0.1 mol dm^{-3} $NaCH_3CO_2$ produced a red/orange band subsequently shown to be Factor B. Further elution using 0.1 mol dm^{-3}, and then 0.5 mol dm^{-3} $NaCH_3CO_2$, produced two more fractions, the first, an orange band believed to contain a mixture of Factor B and stable yellow corrinoid species (SYC), and the second, a pale yellow fraction, containing only SYC. Identification of all five fractions was confirmed using UV/VIS spectroscopy and HPLC analysis. The column elution was completed using 2 mol dm^{-3} NaCl. Two more bands were collected, a diffuse pale yellow band containing more SYC, and an amber band containing a mixture of Factor B and stable yellow species.

Figure 2.1.1 below gives the UV/VIS spectrum and HPLC chromatogram of Fraction 3, the fraction believed to contain only Factor B. The small shoulder between 570nm - 600nm on the UV/VIS spectrum suggests a small dicyanocobinamide impurity in

this fraction. Table 2.1.1 gives the elution program used for the HPLC analysis. As explained in the previous chapter, Factor B is present as two isomers. The relative orientation of the corrin side chains and the slight deviation from planarity of the corrin ring result in the corrin molecule having an "upper" and a "lower" face; hence when the two axial ligands are not identical, two geometrical isomers are possible.[28] The chromatogram has the characteristic two peaks produced by the two Factor B isomers, but indicates a further substantial peak with a retention time (RT) of 9.21 minutes. A sample of Factor B, kindly donated by Prof K.L.Brown, was similarly analysed by HPLC and seen to give the same 3 peaks. Using the same elution program, but changing the buffer pH from 7.4 to 3.0, produces a chromatogram of Factor B with only the expected two isomer peaks evident. This indicates, as suggested by the UV/VIS spectrum, that the extra peak was produced by dicyanocobinamide, and that at low pH one axial CN^- is released as HCN.

UV/VIS spectroscopic quantification of the corrinoid species in the various fractions, indicated in Table 2.1.2 was achieved by conversion of the relevant corrinoid species to dicyanocobinamide by addition of NaCN. (A_{367} dicyanocobinamide $= 3.04 \times 10^4$ dm^3 mol^{-1} cm^{-1}).[28] Comparison of the amount of Factor B determined using UV/VIS spectroscopy (74%) and HPLC peak integrations (75%) shows that the use of HPLC peak areas as a measure of the concentration of a corrinoid species is adequate for rough measurements.

Figure 7.1.1 (a) UV/VIS spectrum, (b) HPLC chromatogram (pH 7.4) and, (c) HPLC chromatogram (pH 3.0) of the fraction obtained from the cation exchange column which was identified as Factor B (Fraction 3).

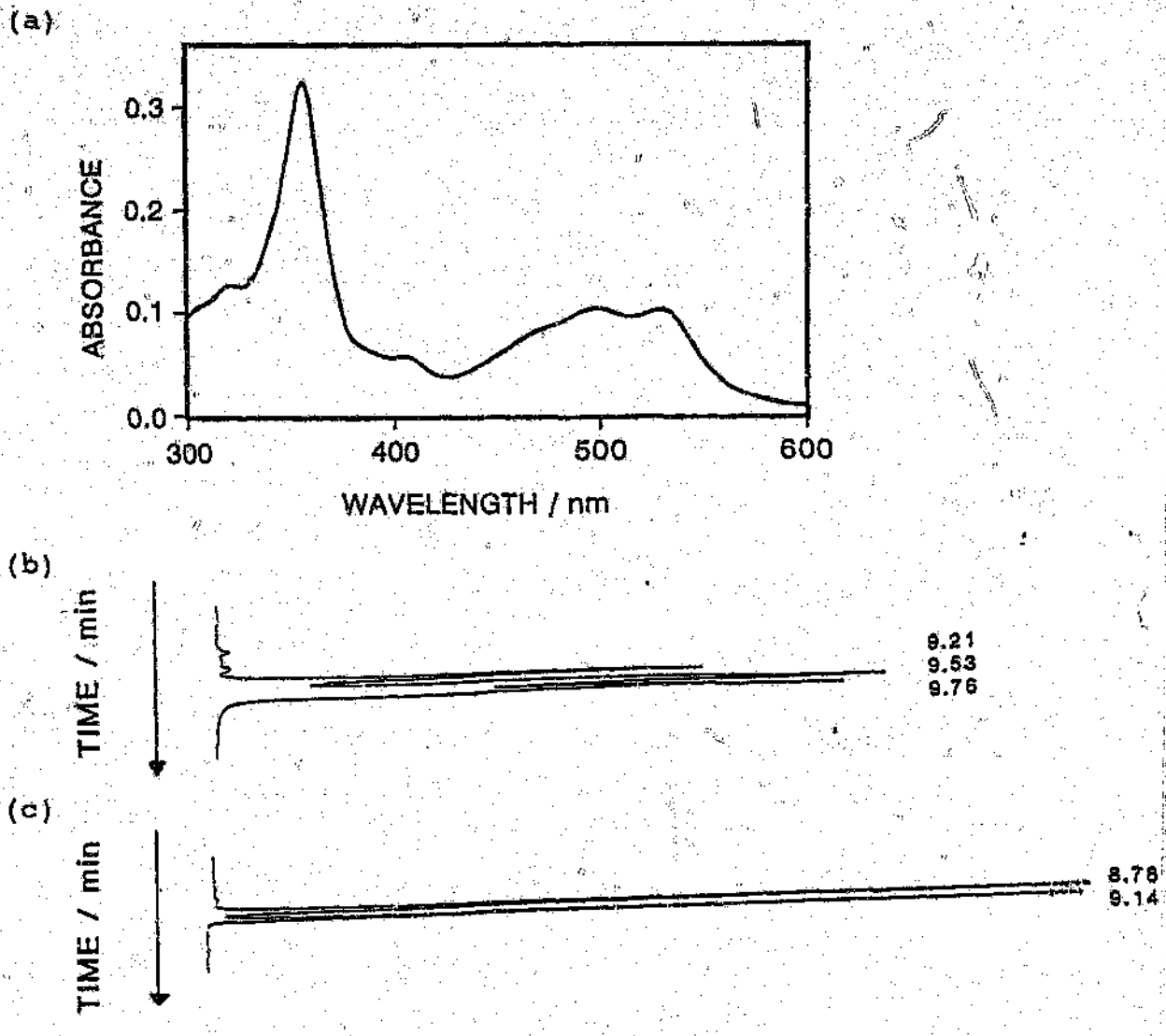


Table 2.1.1 HPLC elution program to analyse the fraction, believed to be Factor B (Fraction 3), on an analytical 100 mm X 4.6 mm C_{18} reverse phase column.

Time / min	% 50 mM Phosphate Buffer (pH 7.4 or 3.0)	% Acetonitrile	Flow Rate / ml min^{-1}
0	95	5	1.5
5	95	5	1.5
10	70	30	1.5
15	70	30	1.5
16	95	5	1.5
20	95	5	STOP

Fraction 3, containing Factor B, was concentrated and desalted using the same phenol/chloroform and ether serial extractions described above.

Table 2.1.2 Distribution of the various corrinoid reaction products (from 0,378 mmol vitamin B_{12}) after separation on a 2.5 cm X 35 cm SP-Sephadex C-25 cation (Na^+) exchange column.

Fraction	Amount / mol	% Composition of Reaction Mixture
1- Vitamin B_{12}	$1.90X10^{-5}$	5.0
2- Dicyanocobinamide	$2.36X10^{-6}$	6
3- Factor B	$2.78X10^{-4}$	
4- Factor B + SYC	$2.77X10^{-6}$	0.7
5- SYC		
6- SYC		
7- Factor B + SYC	$1.67X10^{-5}$	4.4
TOTAL	$3.19x10^{-4}$	84.4

2.2 SYNTHESIS OF DAC

Factor B (3.3×10^{-5} mol) was dissolved in 50 ml 5% (w/v) NH_4Br in methanol in a 3 necked round bottomed flask capped with serum stoppers with a glass frit gas feeder. Argon, passed through a prebubbler containing methanol to prevent evaporation, was used to deaerate the solution thoroughly for 1.5 hours. Zinc wool (0.5 g), freshened with 2 mol dm^{-3} HCl for a few minutes, was rinsed with methanol and added to the flask. The reduction proceeded for 1.5 hours under the circulating inert atmosphere. The orange solution turned brownish/yellow. Brown indicates that the solution should turn dark blue/grey at this point.[29] This colour change is probably indicative of the reduction of Co(III), preferentially a 6-coordinate species, to Co(I), preferentially a 4-coordinate species.[1] The axial ligands, H_2O and CN^-, would then be released into the methanol. A yellow solution is more indicative of a reduction to Co(II), preferentially a 5-coordinate species.[1] If the reduction proceeds via the scheme shown below, then an equilibrium condition exists between the two reduced ions, with the Co(II) in the majority in this instance.

$$e^- + Co(III) \rightleftharpoons Co(II)$$
$$2Co(II) \rightleftharpoons Co(III) + Co(I)$$

The solution was canula transferred into 100 ml 1 mol dm^{-3} HCl and left for a further 1.5 hours under argon. Free CN^- was protonated to form HCN, a gas which is insoluble in methanol, and was thus vented off with the circulating Ar. When the reaction solution was exposed to air, the Co(I) or Co(II) was reoxidised to Co(III). In the absence of CN^-, DAC is produced.

The solution was then desalted by extraction into 10 successive 10 ml portions of 1:1 phenol/chloroform. The organic layer was washed 3 times with 1 mol dm^{-3} HCl, diluted with 300 ml ether and back extracted into water (150 ml in 10 portions). The product was analysed using reverse phase analytical HPLC, using the elution program in table 2.2.1

Table 2.2.1 HPLC elution program to analyse DAC reaction mixture on an analytical 100 mm X 4.6 mm C_{18} reverse phase column.

Time / min	% 50 mM KH_2PO_4 Buffer (pH 3.0)	Acetonitrile	Flow Rate / ml min^{-1}
0	95	5	2
10	90	10	2
15	60	40	2
20	60	40	2
20.1	95	5	STOP

Table 2.2.2 HPLC elution program to analyse the DAC reaction mixture on a semi-preparatory 250 mm X 10 mm C_{18} Aquapore reverse phase column.

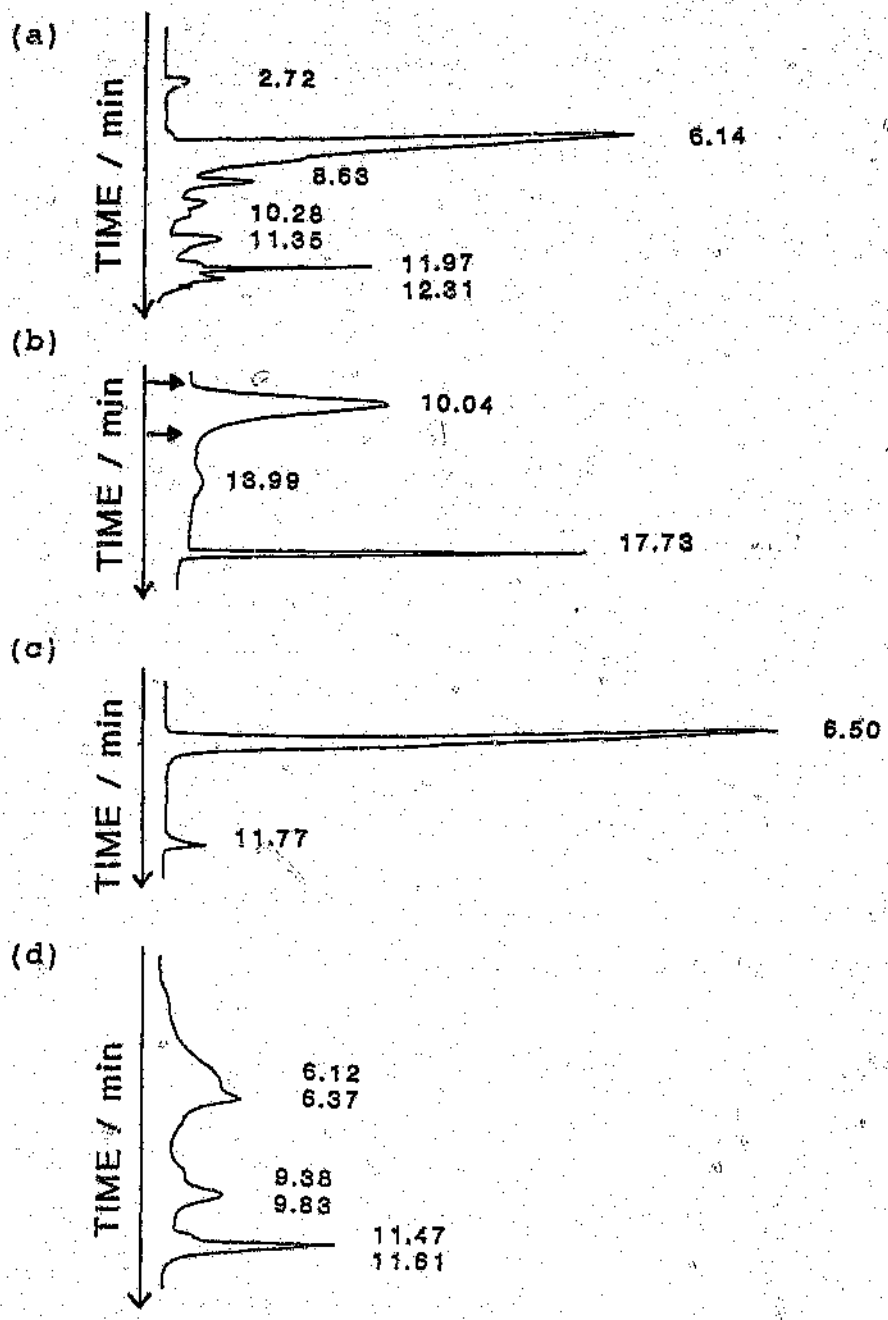
Time / min	% 50 mM KH_2PO_4 Buffer (pH 3.0)	% Acetonitrile	Flow Rate / ml min^{-1}
0	95	5	5
15	94.5	5.5	5
16	60	40	5
25	60	40	5
25.1	95	5	STOP

Table 2.2.3 HPLC elution program to analyse the separated fractions of the DAC reaction mixture on a semi-preparatory 250 mm X 10 mm C_{18} Aquapore reverse phase column.

Time / min	% 50 mM KH_2PO_4 Buffer (pH 3.0)	% Acetonitrile	Flow Rate / ml min^{-1}
0	95	5	5
8	90	10	5
12	60	40	5
20	60	40	5
20.1	95	5	STOP

Figure 2.2.1 (a) shows the chromatogram obtained. Using a peak area estimate (345 nm) DAC constituted 83% of the reaction mixture. The remaining peaks on the chromatogram are attributed to Factor B (verified by spiking with the starting material) and the inevitable degradation products. A semi-preparatory 250 mm X 10 mm C_{18} Aquapore reverse phase column with a 20 μm particle size (Brownlee Laboratories) was used to attempt a separation of the various reaction mixture constituents. Table 2.2.2 indicates the elution program used for the separation. Figure 2.2.1 (b) indicates how the elution program was designed to optimise the separation of DAC from the remaining unwanted reaction components. The arrows on the chromatogram indicate at what points the two fractions were collected.

Figure 2.2.1 HPLC chromatograms of (a) reaction mixture using elution program in Table 2.2.1, (b) reaction mixture using elution program in Table 2.2.2, (c) fraction expected to contain pure DAC using elution program in Table 2.2.3, (d) fraction containing starting material and stable yellow corrinoid species using elution program in Table 2.2.3.



The two fractions were reanalysed using a modified elution program given in Table 2.2.3. Figures 2.2.1 (c) and (d) indicate the chromatograms obtained. Improvement in the percentage purity of DAC was small, increasing at best to 96%. The inability to achieve a 100% pure DAC sample using this separation technique is likely to be a consequence of the instability of DAC in air.[3,5] Ford *et al.* reported that changes in the absorption spectrum of DAC were pronounced after only a few days, even when solutions were maintained frozen.[5] Exposure of DAC to air during the laborious separations probably negated the expected improvement in the percentage purity achieved by the separation. The DAC solution was nevertheless obtained free from starting material (Factor B) by this procedure.

The DAC was concentrated and desalted once more using phenol/chloroform and ether serial extractions. The pink solution was stored frozen under argon. In subsequent repetitions of this synthesis, the separated DAC was not desalted because desalting using phenol/chloroform or benzyl alcohol extractions has been implicated in the formation of stable yellow corrinoids.[3,29] Ultra-filtration[3] and high voltage paper electrophoresis[5] have been reported to remove electrolytes without effecting further degradation of the sample, but these methods was not attempted here. Comparable problems with exposure of DAC to air during these separations was not reported. DAC was then stored frozen under argon in a solution containing some phosphate buffer salts. HPLC analysis of the sample 6 months later indicated only very little (1% - 3%) degradation of the sample during storage.

2.3 OPTIMISATION OF THE CONDITIONS USED IN THE SYNTHESIS OF DAC FROM FACTOR B

Percentage yields for the conversion of Factor B to DAC using Brown's method[29] varied from 75% to 93%. Reaction mixtures at the end of the synthesis consisted of three components: unreacted starting material, DAC and stable yellow corrinoid species. Optimum reaction conditions were thus investigated in the hope that the yield of DAC could be improved and that the conditions contributing to this yield could be better understood.

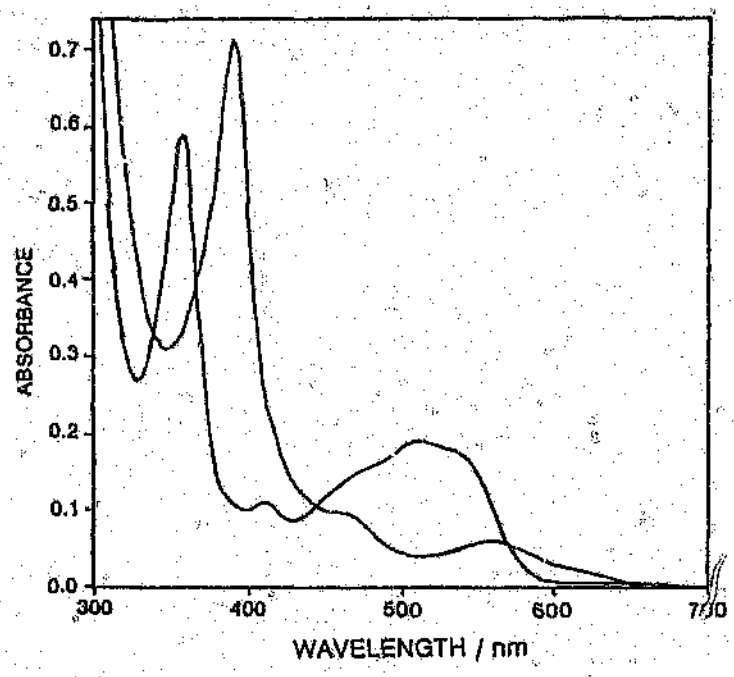
Investigation of an Alternative Reducing Agent

Incomplete conversion of Factor B to DAC and stable yellow corrinoid species is probably the result of incomplete reduction of Co(III) to Co(I) by the zinc wool. $NaBH_4$ was thus investigated as an alternative reducing agent. Preliminary spectroscopic studies of degassed Factor B in methanol before and after addition of degassed aqueous $NaBH_4$ suggested that the Co(III) had been successfully reduced to Co(I). Figure 2.3.1 shows the UV/VIS spectrum of the reaction mixture before and after the addition of $NaBH_4$. The solution changed from an orange/red (Co^{3+}) to a grey (Co^{+}) colour (maximum absorbance shifted from 358 nm to 391 nm).

The synthesis of DAC from Factor B was then attempted using $NaBH_4$ as the reducing agent. Factor B (3 mg, 3 μ mol) was dissolved in 100 ml methanol and deaerated using nitrogen for 1.5 hours. $NaBH_4$ (0.2 g) (Merck) in 10 ml water was similarly deaerated for 1.5 hours, then canula transferred to the Factor B solution. After 15 minutes the solution had turned amber, and not the expected grey. Leaving the reduction to continue for a further hour had no effect on this colour change (verified spectroscopically). A further 0.2 g $NaBH_4$ was added

to the solution. A virtually instantaneous colour change to grey was observed. Deaerated acetone was immediately added to scavenge excess borohydride. Deaerated 12 mol dm^{-3} HCl was added dropwise to the solution until the pH dropped from 12 to 3. The solution was then left under nitrogen for a further 1.5 hours. Using a canula, 100 ml deaerated 1 mol dm^{-3} HCl was added to the solution which was then left under nitrogen for a further 2 hours. HPLC analysis of the reaction mixture (elution program in table 2.2.1) indicated that complete conversion of Factor B had occurred, though only 58% had been converted to DAC. The remaining amount of Factor B was converted to stable yellow corrinoids. A substantially larger proportion of stable yellow corrinoids is thus produced when $NaBH_4$ rather than zinc wool is used as the reducing agent.

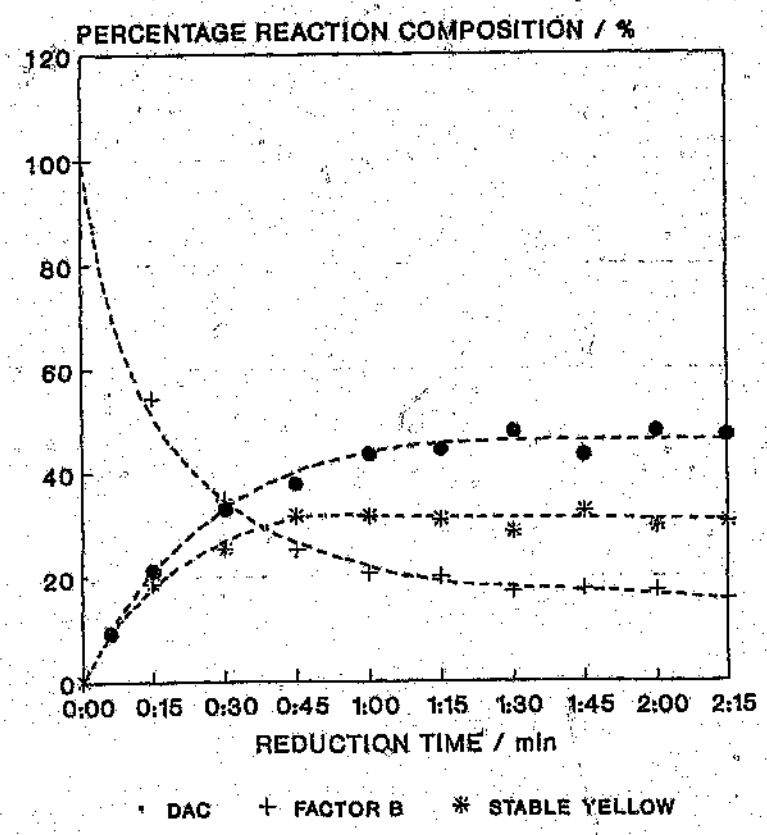
Figure 2.3.1 UV/VIS spectrum of DAC before and after the addition of $NaBH_4$.



Investigation of an Optimum Reduction Time

Conditions were then investigated to improve DAC yields using zinc wool as the reducing agent. The reduction time is one factor which was considered. Factor B was reduced as described in the previous section (2.2). Samples were withdrawn from the reaction mixture at regular intervals, added to the equivalent amount of 1.0 mol dm^{-3} HCl, and analysed using HPLC (elution program in table 2.2.1). Solutions were not left standing in acid under a circulating inert atmosphere and hence the overall DAC yields were low. Comparisons between the solutions are nevertheless useful and an optimum reduction time of ~1.5 hrs was confirmed. Figure 2.3.2 indicates how the composition of the reaction mixture changes with reduction time.

Figure 2.3.2 Changes in the reaction mixture composition in the conversion of Factor B to DAC with zinc wool as a function of reduction time.



Investigation of an Optimum Acid Concentration

The effect of the concentration of the acid on the conversion of Factor B to DAC was then investigated in the same manner as described above for the determination of an optimum reduction time. Samples were again analysed immediately and not left for some time under a circulating inert atmosphere to allow the elimination of CN^- as HCN, and thus the percent conversion of Factor B to DAC is again low. Nevertheless, table 2.3.1 does indicate that increasing the concentration of the acid resulted in a decrease in the percentage conversion of Factor B to DAC and a corresponding increase in the percentage decomposition products. Exposure to any acid is likely to lead to some degradation of the cobinamide, but is nevertheless necessary in order to facilitate removal of CN^- as gaseous HCN.

Table 2.3.1 Relationship between acid concentration and the percent conversion of Factor B to DAC.

[HCl] / mol dm^{-3}	% Conversion of Factor B to DAC
0.25	33.5
0.5	30.6
1.0	22.7
2.0	21.9
3.0	16.1

Investigation of an Optimum Time for Exposure to the Acid

Samples of the reaction mixture produced during the $NaBH_4$ reduction experiment were extracted regularly and analysed using HPLC (elution program in table 2.2.1) to determine the percent conversion of Factor B to DAC. Table 2.3.2 indicates the relationship between the time the reduced Factor B was left in acid and the percent conversion of Factor B to DAC. An optimum time of 1.5 hours was confirmed.

Table 2.3.2 Relationship between the time that the reduced Factor B is left in acid and the percent conversion of Factor B to DAC.

Time / min	% Conversion of Factor B to DAC
40	31
60	38
90	56
120	55
135	58

2.4 COMPARISON OF BROWN'S SYNTHETIC TECHNIQUE[29] WITH OTHER LITERATURE METHODS

It is difficult to compare the results obtained using Brown's synthesis[29] with those involving photolysis, of either Factor B directly[29], or of the methylcobinamide intermediate[3]. At best, using Brown's synthesis, a 93% pure DAC sample was achieved, though percentage purities as low as 75% were also obtained on occasion. Brown reported that his sample was 85% pure.[29] All these measurements were taken directly from the integration of the peaks in the HPLC chromatogram, and thus are susceptible to error due to incorrect integration of the peak area (a problem associated with tailing peaks as was found in the chromatograms of DAC), as well as the error introduced because of the different response factors at different wavelengths of different substances. Earlier, however, it was shown that HPLC peak integration is suitable for rough quantifications. Pratt reported no detectable levels of hydrolysis products when he used the technique of photolysis of Factor B to produce DAC[3], though other authors were not so fortunate.[5] Thin-layer chromatography was the technique cited for analysis of his DAC sample. HPLC is a far more sensitive technique and analysis of his reaction mixture using this technique might well have yielded a different result. Brown investigated the reaction products of the photolysis of methylcobinamide using HPLC. He reports achieving DAC percentage purities of around 70%.[29] Brown's method of synthesis is thus superior to the methylcobinamide method, but cannot be compared to Pratt's method until comparable HPLC analyses of these reaction mixtures are done.

Page 38 omitted in the pagination.

3 THE ACID DISSOCIATION CONSTANTS OF COORDINATED WATER IN DIAQUOCOBINAMIDE

Spectrophotometric titrations of DAC were used to determine the acid dissociation constants of its two axially coordinated water molecules (pK_1 and pK_2). The cobalt corrinoid molecules are well suited to spectroscopic investigation because their electronic structures are profoundly altered by the nature of the ligands attached to the metal atom.[1] As previously described, this characteristic was exploited in the synthesis of DAC, where colour changes were used to identify reaction intermediates and products. Spectrophotometric investigation of deprotonation equilibria reflect only those changes directly involving the chromophore (*i.e.* changes in the conjugated ring itself and in the nature of the ligands axially coordinated to the cobalt(III) atom) and not changes occuring at the periphery of the molecule (*e.g.* possible hydrolysis of the amide side chains).[28]

Table 3.1 gives available values of the acid dissociation constants of DAC's two axially coordinated water molecules. The effect of temperature on these quantities has not yet been investigated. Such information is important for the kinetic investigations described in subsequent chapters, and hence the relationship between temperature and these values was determined.

Table 3.1 Literature values of the acid dissociation constants of the two axially coordinated water molecules in DAC at 25°C and an ionic strength of 0.2 mol dm^{-3}, standard deviations in parenthesis.

Equilibrium	pK_a	Reference
DAC ⇌ AHC + H^+	5.40 (0.05) 5.9 (0.1)	5 3
AHC ⇌ DHC + H^+	10.30 (0.07) 10.3 (0.2)	5 3

3.1 EXPERIMENTAL PROCEDURES

The two deprotonation equilibrium constants of DAC were measured at four different temperatures. Figure 3.1.1 below indicates the arrangement of the apparatus used in the determinations. An aqueous solution of DAC (80% - 95% pure, 5 X 10^{-5} mol dm^{-3}) with an ionic strength of 1.0 mol dm^{-3}, achieved by using appropriate amounts of $NaClO_4$, was placed in the reaction vessel. The reaction vessel, surrounded by a water jacket insulated with cotton wool and aluminium foil, and the spectrophotometer cell holder were maintained at the required temperature by a circulating water bath (± 0.1°C). A peristaltic pump was used to transfer a fixed quantity of solution from the reaction vessel to the cuvette in the spectrophotometer cell holder. The cuvette hence remained stationary throughout the titration. Measurements were performed under reduced light conditions to minimise degradation of DAC. Solutions of HCl and NaOH (1.0, 0.1 and 0.01 mol dm^{-3}), were transferred by means of a capillary tube to the reaction vessel to alter the solution's pH during the titration in steps of 0.01 to 0.05. Volumes added were always

very small in order to minimise the volume change (and hence the concentration of DAC) during the course of the titration. The pH electrode, immersed in the solution, measured the solution's pH following addition of either acid or base. The pH of the equilibrated solution was measured, an aliquot was transferred to the cuvette and the absorbance of that solution at a specific wavelength was then recorded.

Figure 3.1.2 below shows the UV/VIS spectra of DAC, aquohydroxocobinamide (AHC), and dihydroxocobinamide (DHC). AHC can exist as two isomers and thus the spectrum of AHC is an average of the spectra of the two isomers. From these spectra, wavelengths were chosen where a maximim absorbance change accompanied a deprotonation. Wavelengths of 278 nm and 344 nm were thus identified. For the first equilibrium (DAC ⇌ AHC), isosbestic points were observed at 341 nm and 357 nm. For the second equilibrium (AHC ⇌ DHC), isosbestic points were observed at 341 nm and 377 nm.

Figure 3.1.1 Apparatus used in the determinations of the acid dissociation constants of the two axially coordinated water molecules in DAC.

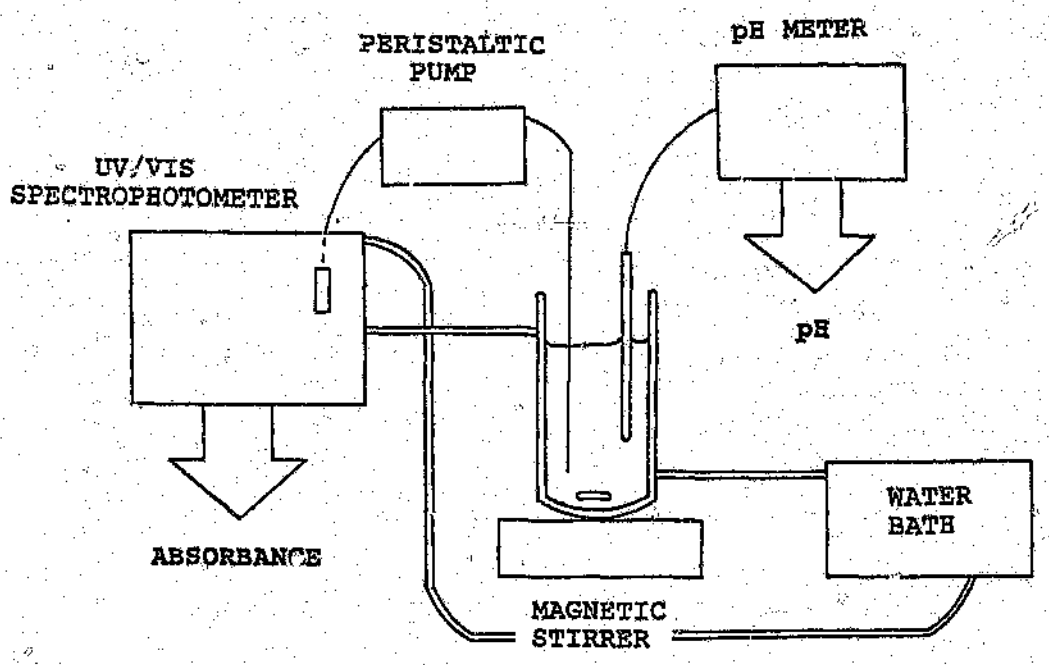
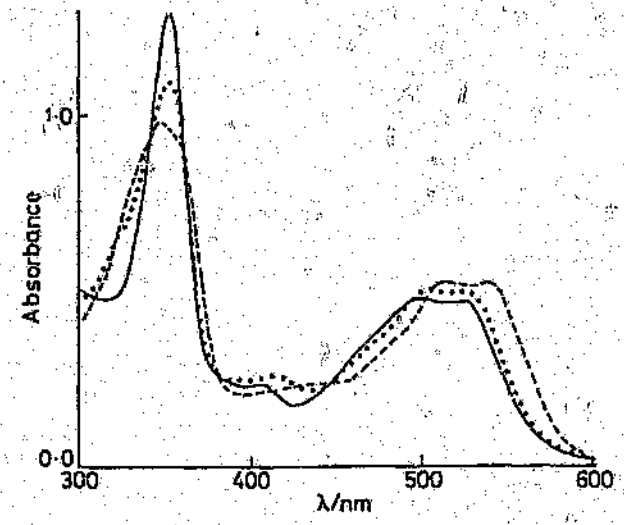


Figure 3.1.2 UV/VIS spectra of (a) DAC ——, (b) AHC ..., and (c) DHC ---, at 25°C.[3]



3.2 RESULTS

Tables 11.1.1 - 11.1.4 in the appendix give the absorbance data collected as a function of pH. For data collected at 35.0°C and 25.0°C, the absorbance change at 278 nm and 344 nm was collected over the whole pH range. The data collected for these titrations indicated that the first equilibrium was best followed at 344 nm, whilst the second equilibrium was best followed at 278 nm, though it can also be adequately followed at 344 nm. Suitability of the selected wavelength was based on using the wavelength at which the largest absorbance change accompanied deprotonation. Thus, for the other two temperatures investigated, absorbance change as a function of pH in the acid to neutral titration was only followed at 344 nm, whilst the neutral to basic titration was followed at 278 nm. Problems encountered with the spectrophotometer's monochromator necessitated duplication of some titrations. Data analysis (described later) was, whenever possible, performed on these duplicate data sets.

3.3 ANALYSIS AND INTERPRETATION OF DATA

The two reactions of interest are,

$$DAC \rightleftharpoons AHC + H^+ \qquad (K_{a1})$$
$$AHC \rightleftharpoons DHC + H^+ \qquad (K_{a2})$$

Then, $K_{a1} = \dfrac{[H^+]_{eq}[AHC]_{eq}}{[DAC]_{eq}}$ and, $K_{a2} = \dfrac{[H^+]_{eq}[DHC]_{eq}}{[AHC]_{eq}}$

These observed ionisations of DAC are macroscopic pK_as since AHC can exist as two stereoisomers.

Considering only the first equilibrium, then the absorbance measured when only DAC is present is A_o. If 100% conversion of DAC to AHC occurs, then the absorbance at the same wavelength, due only to the AHC is A_1. At any time during the equilibrium titration, the absorbance measured is A. Appendix 12.1 gives the derivation of equations 3.3.1 and 3.3.2.

$$\text{Then,} \quad K_{a1} = \frac{A_o - A}{A - A_1} \times [H^+]_{eq} \qquad \text{(equation 3.3.1)}$$

Similarly, considering only the second equilibrium: if 100% conversion of AHC to DHC occurs, then the absorbance at the same wavelength, due only to the DHC is A_2.

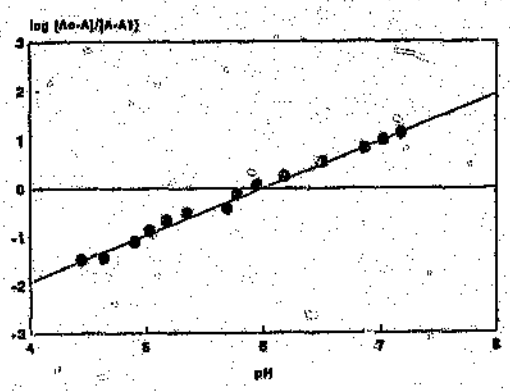
$$\text{Then,} \quad K_{a2} = \frac{A_1 - A}{A - A_2} \times [H^+]_{eq} \qquad \text{(equation 3.3.2)}$$

Plots of $\log[(A_o - A)/(A - A_1)]$ versus pH at 25°C for the first equilibrium, and $\log[(A_1 - A)/(A - A_2)]$ versus pH for the second equilibrium, determined at both wavelengths gave linear plots, shown in figure 3.3.1. This confirms the

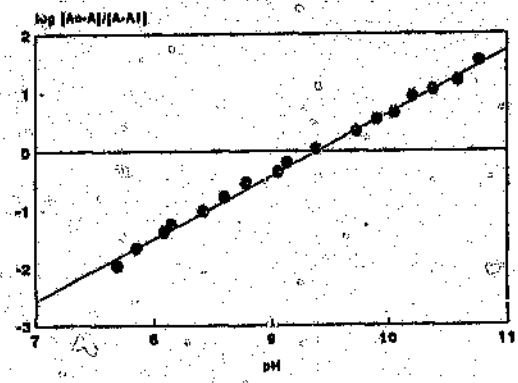
assumption made in the equations' derivation that each observed equilibrium corresponds to the transfer of one proton.

Figure 3.3.1 (a) $\log[(A_o - A)/(A - A_1)]$ versus pH at 25°C for data collected for pK_{a1} at 344 nm, (b) $\log[(A_1 - A)/(A - A_2)]$ versus pH at 25°C for data collected for pK_{a2} at 278 nm.

(a)



(b)



One problem with such a plot is that the values of A_o, A_1 and A_2 are not known and can only be extrapolated from the raw data. Values of pK_{a1} and pK_{a2}, derived by fitting a straight line to the data, will then be largely dependent on the accuracy of these estimated absorbance values. An equation was thus derived (appendix 12.1) which would describe the data without any assumptions regarding the values of A_o, A_1 and A_2 having to be made.

$$\text{Then } A_{total} = \frac{A_{DAC}[H^+]^2}{K_{a1}K_{a2} + K_{a1}[H^+] + [H^+]^2} \qquad \text{(equation 3.3.3)}$$

$$+ \frac{A_{AHC}K_{a1}}{K_{a1}K_{a2}/[H^+] + K_{a1} + [H^+]}$$

$$+ \frac{A_{DHC}K_{a1}K_{a2}}{K_{a1}K_{a2} + K_{a1}[H^+] + [H^+]^2}$$

When a titration to determine a single deprotonation equilibrium constant was performed, data was fitted by one of two simplified forms of equation 3.3.3,

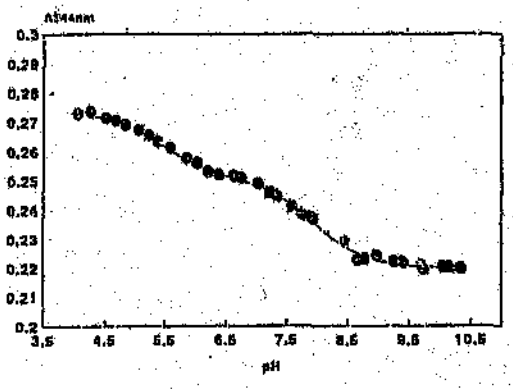
$$\text{then, } A_{total} = \frac{A_{AHC}}{1 + [H^+]/K_{a1}} + \frac{A_{DAC}}{1 + K_{a1}/[H^+]} \quad \text{(equation 3.3.4)}$$

$$\text{then, } A_{total} = \frac{A_{DHC}}{1 + [H^+]/K_{a2}} + \frac{A_{AHC}}{1 + K_{a2}/[H^+]} \quad \text{(equation 3.3.5)}$$

Figures 3.3.2 -3.3.5 show how equations 3.3.3 - 3.3.5 were fitted to the data tabulated in tables 11.1.1 - 11.1.4 (in appendix 11.1). Table 3.3.1 below gives the optimised values of pK_{a1} and pK_{a2}.

Figure 3.3.2 Spectrophotometric titration at 35°C, (a) data collected at 344 nm, curve fitted using equation 3.3.3, (b) data collected at 278 nm, curve fitted using equation 3.3.3.

(a) (b)



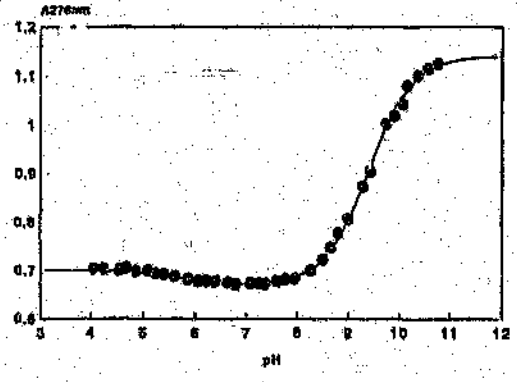


Figure 3.3.3 Spectrophotometric titration at 25°C, (a) data collected at 344 nm, curve fitted using equation 3.3.3, (b) data collected at 278 nm, curve fitted using equation 3.3.3.

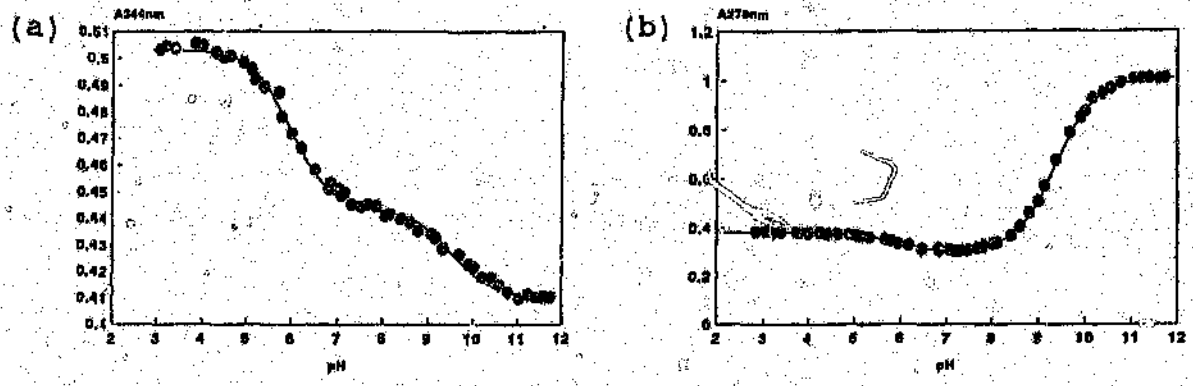


Figure 3.3.4 Spectrophotometric titration at 15°C, (a) data collected at 344 nm, curve fitted using equation 3.3.4, (b) data collected at 278 nm, curve fitted using equation 3.3.5.

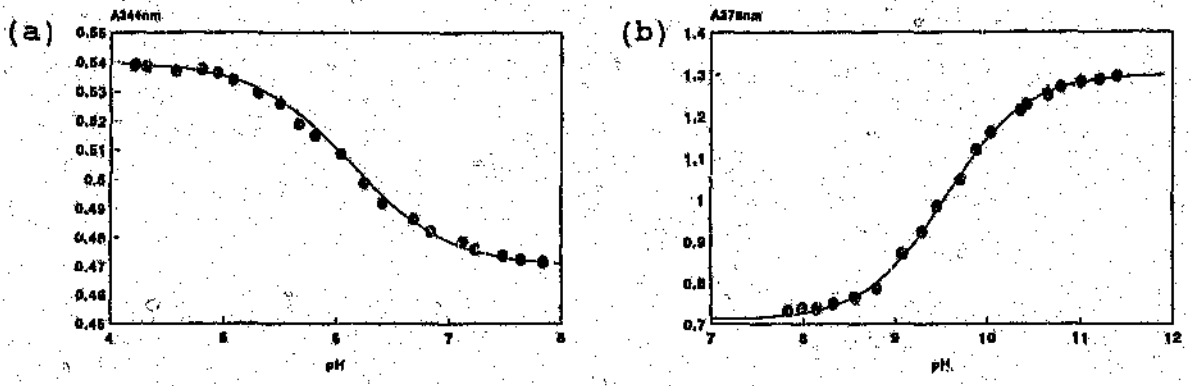
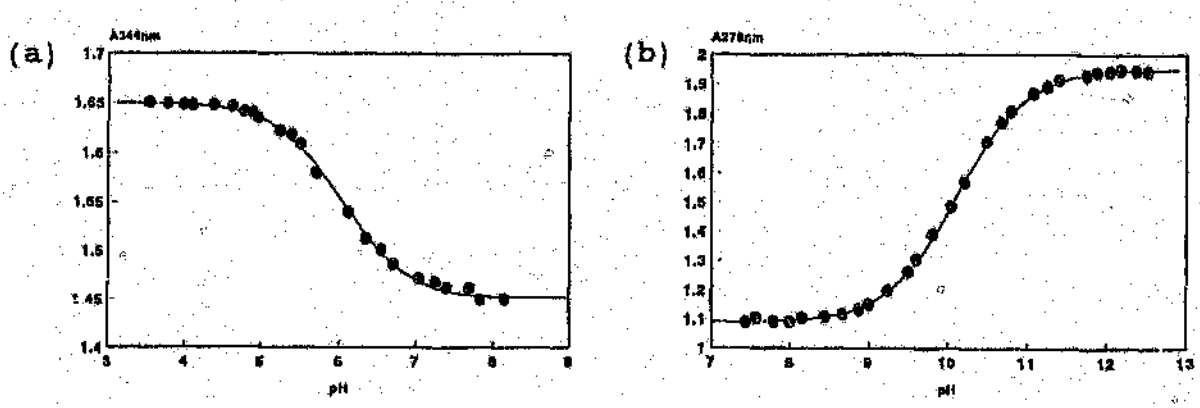


Figure 3.3.5 Spectrophotometric titration at 5°C, (a) data collected at 344 nm, curve fitted using equation 3.3.4, (b) data collected at 278 nm, curve fitted using equation 3.3.5.



Thermodynamic parameters for the averaged deprotonation equilibria were determined using equation 3.3.6,

$$\ln K_{eq} = -\frac{\Delta H^\circ}{RT} + \frac{\Delta S^\circ}{R} \qquad (3.3.6)$$

Table 3.3.2 shows the data used to produce figure 3.3.6. The thermodynamic parameters thus derived are given in table 3.3.3.

Table 3.3.1 Acid dissociation constants of the two coordinated water molecules in DAC, standard deviations in parenthesis.

	Temperature / °C			
	35.0 ± 0.1	25.0 ± 0.1	15.0 ± 0.1	5.0 ±0.1
pK_{a1}	5.56(0.16)[a] 5.54(0.04)[b]	5.95(0.03)[a] 5.87(0.06)[b]	6.14(0.03)[b]	6.04(0.03)[b] 6.76(0.80)[b]
Av.	5.55	5.91	6.14	6.40
pK_{a2}	9.40(0.02)[a] {7.90(0.05)[b]}	9.55(0.06)[a] 9.38(0.01)[b]	9.46(0.01)[a] 9.54(0.01)[a]	10.11(0.01)[a]
Av.	9.40	9.47	9.50	10.11

[a] measured at 278 nm

[b] measured at 344 nm

Table 3.3.2 Data used to calculate the thermodynamic parameters for the acid dissociation constants of the two axially coordinated water molecules in DAC.

T / °C	T^{-1} (K)	$ln\ K_{a1}$	$ln\ K_{a2}$
35.0	3.25×10^{-3}	-12.78	-21.64
25.0	3.36×10^{-3}	-13.61	-21.81
15.0	3.47×10^{-3}	-14.14	-21.88
5.0	3.60×10^{-3}	-14.74	{-23.28}

Figure 3.3.6 Linear plots of data in table 3.3.2.

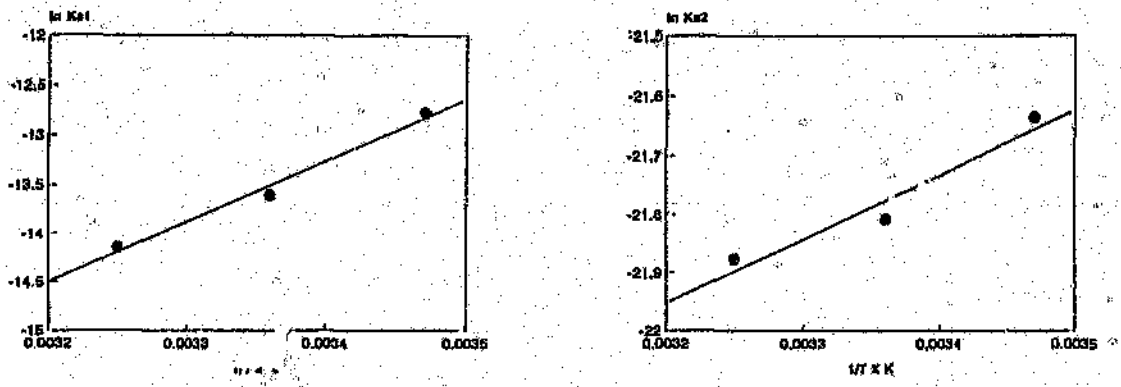


Table 3.3.3 Thermodynamic parameters for the acid dissociation constants of the two axially coordinated water molecules in DAC, standard deviations in parenthesis.

Deprotonation Equilibrium	ΔH° / kJ mol^{-1}	ΔS° /J K^{-1} mol^{-1}
DAC ⇌ AHC + H^{+}	44 (4)	-35 (15)
AHC ⇌ DHC + H^{+}	37 (15)	-59 (50)

3.4 DISCUSSION

The measured value of pK_{a1} at 25°C compares well with the published values in table 3.1. The same, however, cannot be said for the value of pK_{a2}. Both Baldwin[3] and Ford[5] collected data for both equilibria at 348 nm, whereas the data collected for pK_{a1} here was at 344 nm, and the data for pK_{a2} at 278 nm. This suggests that the discrepent pK_{a2} results could be a wavelength-dependent phenomenon. However, at 25°C and 35°C, data for both pK_as were collected at both wavelengths. At 25°C, the two values for pK_{a1} and pK_{a2}, are, within error, the same, and hence a wavelength-dependent phenomenon is not supported. At 35°C, the two values for pK_{a1} are very close whilst the two values for pK_{a2} are very different. It is however the measurement at 344 nm which appears discrepent, rather than that at 278 nm. A wavelength-dependent discrepency is thus not supported. Alternative reasons must then be sought to explain the discrepent set of pK_{a2} values, and the exceedingly low pK_{a2} value measured at 344 nm.

Marques has determined the temperature dependence of the pK_{a2} of DAC.[31] The value obtained at 25°C compares well with the other published results and hence these results (ΔH° = 27 kJ mol^{-1}, ΔS° = -109 J K^{-1} mol^{-1}) were used in subsequent calculations (later chapters). Table 3.4.1 compares these values to those calculated here.

Table 3.4.1. Dependence of the acid dissociation constant of the axially coordinated water molecule in aquohydroxocobinamide, pK_{a2}, on temperature.

Temperature / °C	pK_{a2} - Marques[31]	pK_{a2} - this work
5.0	10.77	10.11
15.0	10.59	9.50
25.0	10.43	9.47
35.0	10.27	9.40

Both series exhibit the same trend, with the magnitude of pK_{a2} decreasing with increasing temperature. A moderate dependence on temperature is evident in both cases. A fairly consistent difference exists between the two series, indicating that the "slope" of the two series are similar. Experimental error associated with the pH measurement could explain the discrepent pK_{a2} series measured here. An incorrectly calibrated pH meter, as a result of a defective electrode or defective standard solutions, could produce this result.

4 BINDING CONSTANTS OF AQUOHYDROXOCOBINAMIDE (AHC) WITH FIVE SELECTED LIGANDS

The primary aim of this work was to measure the binding constants of chosen ligands to AHC, and hence to determine the suitability of these ligands for subsequent kinetic investigation. Very small binding constants, for example, complicate kinetic determinations because detection of the substituted product is more difficult.

DAC can exist as a mixture of four possible species, DAC, AHC (the α - and β -isomers), and DHC, depending on the pH of the solution. Baldwin *et al.* reported that DAC and AHC are kinetically labile, whereas DHC is kinetically inert.[29] It was assumed that the ligand substitution kinetics of DAC would be more complicated than those for AHC since DAC has two possible coordinated water molecules for substitution and hence multiphase kinetics can be expected. In contrast, AHC, with only one water for possible substitution, was expected to exhibit much simpler kinetics. The hydroxide ligand was reported to be inert to substitution.[1] Since the AHC sample comprises a mixture of the α - and β -aquo complexes, biphasic kinetics were not ruled out. Kinetic studies, and thus preliminary binding studies too, were then planned at a high pH (12.0), to limit the number of observable reactions by ensuring that only one labile corrin species, AHC (with two isomers), would be present.

Three classes of ligands were identified for thermodynamic and kinetic investigation, anions, aromatic amines and primary amines. Six ligands were chosen to investigate their binding constants with AHC: sulphite, cyanide, azide, pyridine, N-methylimidazole and 3-amino-1-propanol. With the exception of SO_3^{2-} and CN^-, all ligands were N-donor ligands. An IR spectrum of the solid product of the reaction of aquocobalamin with SO_3^{2-}

indicates that SO_3^{2-} bonds through sulphur.[32] The CN^- ligand can potentially bind through both its C and N ends, but only binding through the C with cobalamins and cobinamides has been reported.[1]

Two structural isomers of AHC are expected to exist, and hence two isomers will be produced in their ligand substitution reactions. Pratt *et al.*[33] were unable to detect the two expected isomers when DAC was reacted with imidazole and ammonia, probably because the differences in the spectra of the two isomers are slight. Since isomers are present at equilibrium in aqueous solution in approximately equal amounts in all cyanoaquocorrinoids so far studied,[1] and in an approximately 2:1 ratio in the two cobinamide isomers,[50] the formation constants for the substitution of coordinated water by CN^- in the two different coordination sites must be almost identical. Pratt assumed that the same was true for the substitution of ammonia and imidazole and hence the possible existence of isomers was neglected.[33] The same approach was used in this work. Equilibrium constants reported here are thus macroscopic equilibrium constants.

4.1 EXPERIMENTAL PROCEDURES

Equilibrium constants for the substitution of coordinated H_2O in AHC in aqueous solution (adjusted to pH 12.0 using NaOH and an ionic strength of 1.0 mol dm^{-3} using $NaClO_4$) were determined spectrophotometrically at 25.0°C (temperature maintained ±0.1°C with a circulating water bath). Preliminary spectroscopic studies indicated the optimum wavelength (refer to table 4.2.1) for observing the absorbance changes which accompany binding of the ligand. An in-cell titration of a solution of cobinamide ([DHC + AHC] = $2X10^{-5}$ mol dm^{-3}) was then performed by observing the absorbance change at the chosen wavelength as a function of the amount of ligand added.

The chosen ligands or where the ligands were charged, their salts, were; NaCN (Merck), NaN_3 (Merck), 3-amino-1-propanol (Aldrich), N-methylimidazole (Aldrich), pyridine (Merck) and Na_2SO_3 (Merck).

4.2 RESULTS

Preliminary spectroscopic investigations of the reaction of AHC with SO_3^{2-} indicated that SO_3^{2-} reacted with AHC to produce stable yellow corrinoids, and hence this determination was not continued. Firth *et al.*[32] observed a similar reaction when investigating the reaction of AHC with SO_3^{2-} at pH 14-15. They observed that the treatment of AHC with a slight excess of sodium sulphite showed a rapid and reversible equilibrium with a reddish complex and also a slower, irreversible decomposition which prevented a quantitative study of the first equilibrium.

Figures 4.2.1 - 4.2.3 below show the UV/VIS spectra produced during the titrations of AHC with cyanide, azide, pyridine, N-methylimidazole and 3-amino-1-propanol. Table 4.2.1 shows the wavelengths selected at which the greatest absorbance change accompanied the substitution. Isosbestic points in each titration are also given in table 4.2.1. Tables 11.2.1 - 11.2.5 in the appendix give the absorbance versus the amount of ligand added data for these titrations. Absorbance data are corrected for dilution effects which accompanied the titration.

Figure 4.2.1 UV/VIS spectra of the titations of AHC (pH 12.0) with (a) sodium cyanide and (b) sodium azide at 25.0°C.

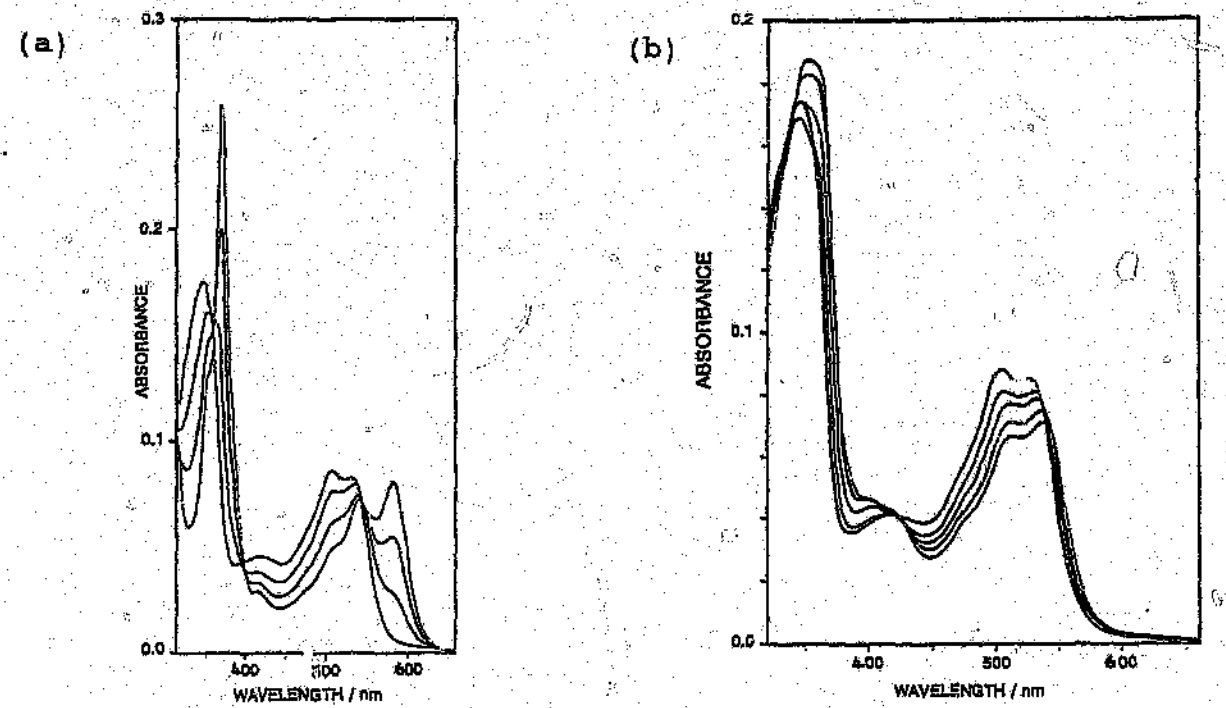


Figure 4.2.2 UV/VIS spectra of the titations of AHC (pH 12.0) with (a) pyridine and (b) N-methylimidazole at 25.0°C.

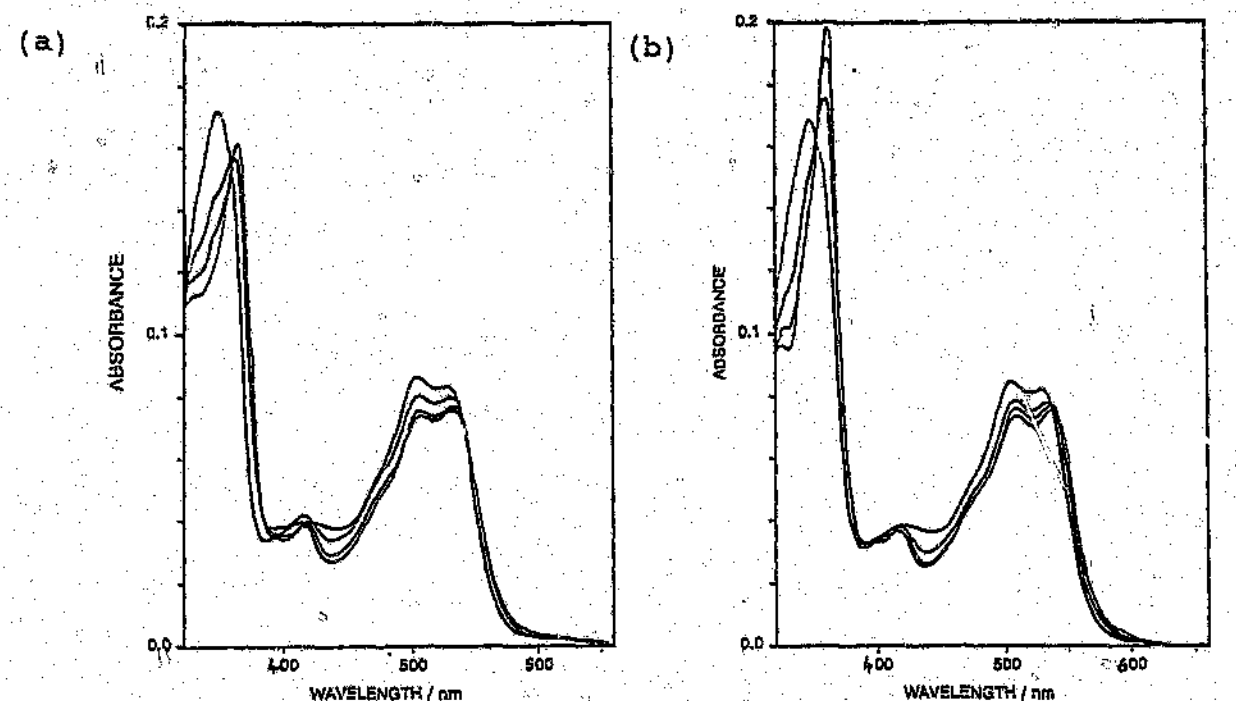


Figure 4.2.3 UV/VIS spectra of the titation of AHC (pH 12.0) with 3-amino-1-propanol at 25.0°C.

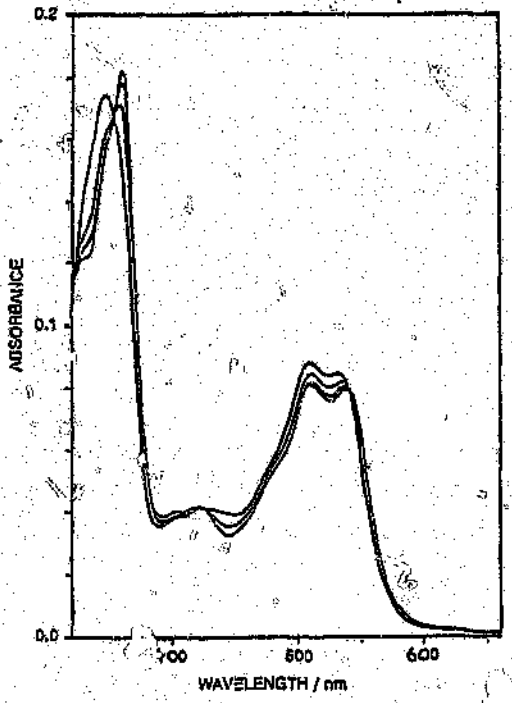


Table 4.2.1 Spectroscopic data associated with the titration of AHC with the five chosen ligands.

Ligand	Titration wavelength / nm	Isosbestic points / nm
cyanide	348	402, 544
azide	370	543
pyridine	368	542
N-methylimidazole	365	391
3-amino-1-propanol	364	376

4.3 ANALYSIS AND INTERPRETATION OF DATA

Absorbance versus ligand concentration data can be analysed to determine ligand binding stoichiometry using a Hill plot, as was described in chapter 3 to determine deprotonation equilibrium constants. For the reaction represented by,

$$AHC + nL \rightleftharpoons AHC\text{-}L_n + nH_2O \quad (K_{eq})$$

It follows that $\dfrac{(A - A_o)}{(A_1 - A)} = K_{eq} \times [ligand]^n$

and $\log[(A - A_o)/(A_1 - A)] = \log K_{eq} + n\log[ligand]$

where A is the measured absorbance
A_o is the absorbance of AHC
A_1 is the absorbance of the substitution product (100% conversion)
[ligand] is the concentration of free ligand
n is the ligand binding stoichiometry

If $[AHC] \ll [ligand]_{total}$, then $[ligand]_{total} \sim [ligand]_{free}$

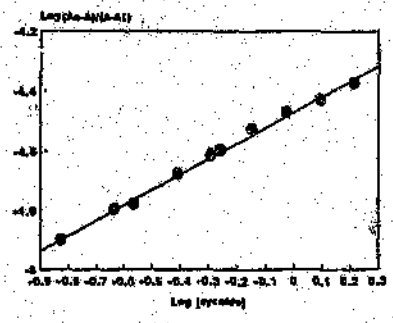
This assumption is valid for all ligands investigated, except CN^-, because log K values for the binding of these ligands to AHC are modest. Observed binding constants are macroscopic pK_{eq}s since a sample of AHC contains two stereoisomers.

As discussed before, the inherent problem with such a plot is that it requires accurate values for A_o and A_1 if accurate values for n and K_{eq} are expected. Nevertheless the plot is useful for determining ligand binding stoichiometry. Data collected when $A \sim A_1$ were not used in these plots because small errors in A are magnified in the course of the analysis, resulting in significant skewing of the fitted straight line.

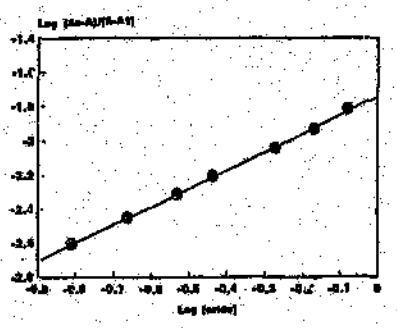
Table 4.3.1 below has the values of n and K_{eq} produced using the Hill plot. Figure 4.3.1 indicates the straight lines fits which were obtained.

Figure 4.3.1 Hill plots for the substitution reactions of AHC (pH=12) with (a) cyanide, (b) azide, (c) pyridine, (d) N-methylimidazole, and (e) 3-amino-1-propanol.

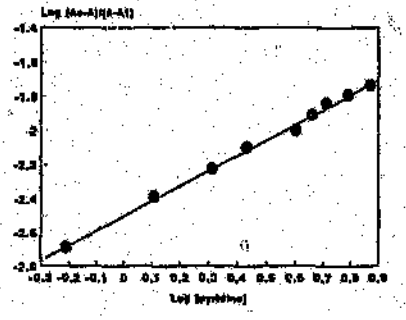
(a)



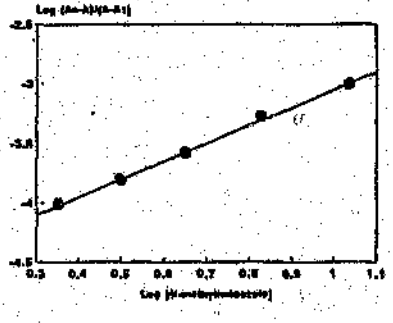
(b)



(c)



(d)



(e)

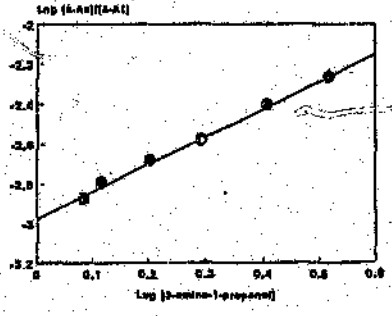


Table 4.3.1 Values for n and K_{eq} for the substitution reactions of AHC (pH=12) with the five selected ligands, obtained using a Hill plot.

Ligand	A_o	A_1	n	$\log K_{eq}$
Cyanide	0.7558	0.5824	2.00(0.16)	9.09(0.72)*
Azide	0.1662	0.3100	0.91(0.03)	1.54(0.07)
Pyridine	0.2466	0.4094	1.09(0.03)	2.75(0.06)
N-methylimidazole	0.5111	0.7520	0.94(0.05)	4.09(0.21)
3-amino-1-propanol	0.5867	0.8046	0.97(0.05)	2.79(0.15)

*$\log K_1K_2$

standard deviations in parenthesis

These results suggest that, in all cases except for cyanide, only one ligand coordinated to the AHC (producing the ligand-hydroxocobinamide complex, HC-L). For cyanide, two ligands appear to bind to AHC (producing the cobinamide complex, NC-Co-CN). Cyanide is well known to exert a strong *trans*-effect on other axial ligands.[1] This strong *trans*-labilising effect can be interpreted in one of two ways, the net results of which (sufficient labilisation of the remaining axial position to allow a second CN^- substitution) are indistinguishable. Firstly, the strong *trans*-labilisation of CN^- could increase the pK_a of the remaining water in the cyanohydroxocobinamide to a value greater than 12, so that the equilibrium between the OH^- and H_2O *trans* to the CN^- would shift in favour of the water. Water is not substitutionally inert, and hence a second substitution could occur. The pK_a of coordinated water in cyanoaquocobinamide (Factor B) is reported to be 10.95[1], and hence only a very small proportion of hydroxcyanocobinamide will be present as aquocyanocobinamide at pH 12.00. A second possible explanation for the observed bisubstitution is that, OH^-, generally inert

to substitution, could be labilised sufficiently by the *trans*-CN^- to allow substitution of a second CN^-. Marques however has shown that hydroxocyanocobinamide is inert to substitution[31] and hence the first mechanism is more likely to be operable. The other ligands investigated here exert weaker *trans*-effects, and thus the OH^- remains firmly held by the substituted AHC.

As explained in chapter 3, an equation can be derived to fit the absorbance data without pre-knowledge of the values of A_o and A_1. Equation 4.3.1, derived in appendix 12.2, was used to fit data from the azide, pyridine, N-methylimidazole, and 3-amino-1-propanol titrations. The optimised K_{eq} values are in table 4.3.3.

For the reaction represented by,

$$AHC + L \rightleftharpoons HC\text{-}L + H_2O$$

$$\text{then, } K_{eq} = \frac{[HC\text{-}L]}{[AHC][L]}$$

$$\text{and, } A = \frac{A_{AHC} + A_{HC\text{-}L}K_{eq}[L]}{1 + K_{eq}[L]} \qquad (4.3.1)$$

In the case of cyanide, two ligands bind to AHC. Two models can be used to describe this process, a sequential substitution model where the reaction proceeds through the formation of a mono-ligated intermediate which, at higher ligand concentrations, binds a second ligand to form the final bis-ligated species, or a simultaneous substitution model where the binding constant for the second ligand is similar in

magnitude to, or larger than, the binding of the first ligand so that the the two substitution reactions cannot be distinguished.

Derivation of the equation describing the simultaneous substitution model is in appendix 12.2. For the simultaneous substitution model, the reaction under consideration is represented by,

$$AHC + 2L \rightleftharpoons L\text{-}Co\text{-}L + 2H_2O$$

Only an overall equilibrium constant, β_2, can be determined,

$$\beta_2 = \frac{[L\text{-}Co\text{-}L]}{[AHC][L]^2}$$

and,
$$A = \frac{A_{AHC}}{1 + K_{eq}[L]^2} + \frac{A_{L\text{-}Co\text{-}L}}{1 + 1/K_{eq}[L]^2} \qquad (4.3.2)$$

However, the assumption that $[L] \sim [L]_{total}$ is no longer necessarily valid since a high binding equilibrium constant means that saturation is reached with very low concentrations of ligand. A polynomial equation was derived (appendix 12.2) to express the free ligand concentration, [L], in terms of the total and bound ligand concentrations respectively, and the solutions to this equation, obtained by an iterative procedure using Newton's method, were then substituted into equation 4.3.2.

For the sequential substitution model, the reactions under consideration are represented by,

$$AHC + L \rightleftharpoons HC\text{-}L + H_2O$$
$$HC\text{-}L + L \rightleftharpoons L\text{-}Co\text{-}L + H_2O$$

then,

$$K_1 = \frac{[HC\text{-}L]}{[AHC][L]}$$

$$K_2 = \frac{[L\text{-}Co\text{-}L]}{[HC\text{-}L][L]}$$

This situation is analogous to the deprotonation of DAC, dealt with in chapter 3 (equation 3.3.1),

thus,

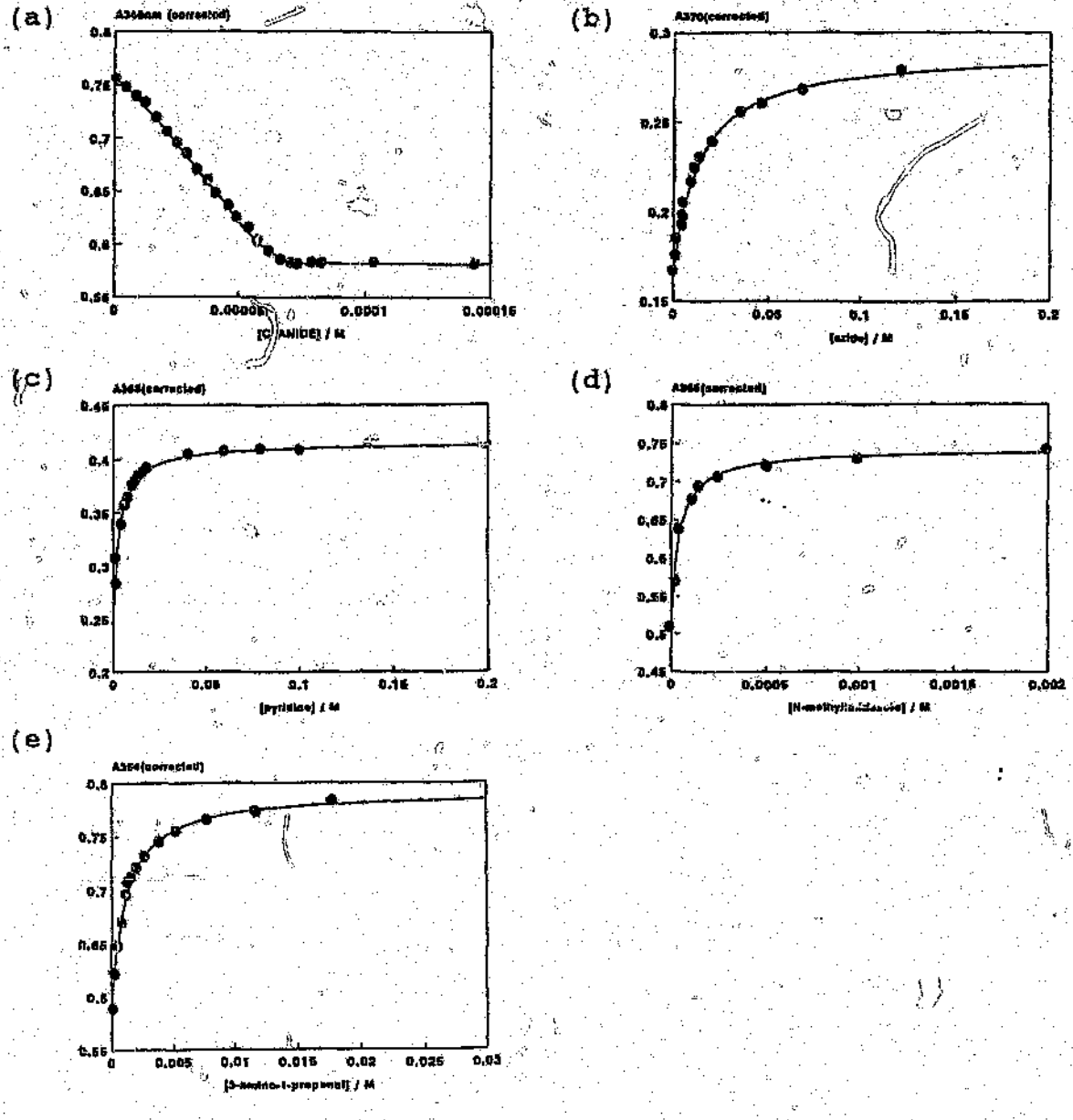
$$A = \frac{A_{AHC}}{1 + K_1[L] + K_1K_2[L]^2} + \frac{A_{HC\text{-}L}}{1 + K_2[L] + 1/K_1[L]}$$

$$+ \frac{A_{L\text{-}Co\text{-}L}}{1 + 1/K_2[L] + 1/K_1K_2[L]^2} \qquad (4.3.3)$$

Again, the assumption that $[L] \sim [L]_{total}$ is no longer necessarily valid. An equation was once more derived (appendix 12.2) to describe [L], and the solutions to this equation were then substituted into equation 4.3.3.

Both the sequential and the simultaneous substitution models were fitted to the cyanide data. Meaningful results were only obtained using the latter model. For the sequential substitution model a strong correlation between the values of K_1 and K_2 and unstable iterations during the optimisation process prevented the determination of meaningful values of K_1 and K_2. Only the overall stability constant for the binding of two ligands to AHC was thus obtained. Table 4.3.3 gives the values for $\log K_{eq}$ and $\log \beta_2$ for the substitution reactions of AHC, produced by fitting equations 4.3.1 and 4.3.2 to the data. Figure 4.3.2 indicates the fits obtained.

Figure 4.3.2. Plots of $A_{corrected}$ versus [L] for the substitution reactions of AHC with (a) cyanide, (b) azide, (c) pyridine, (d) N-methylimidazole, and (e) 3-amino-1-propanol. Data fitted using equation 4.3.2 (a) or equation 4.3.1 (b)-(e).



The values of A_o and A_1 can be compared with the experimentally determined approximate values in table 4.3.1. The experimentally determined and calculated values are in all cases consistent. With the exception of CN^- the $\log K_{eq}$ values calculated here are consistent with those determined using a Hill plot. Data used in the Hill plots were analysed using the assumption that $[L]_{total} - [L]_{free}$, which as explained before, is inappropriate for the CN^- data. It would thus seem probable that the calculated $\log\beta_2$ value for CN^-, the determination of which involves the calculation of $[L]_{free}$, would be the more correct value.

Table 4.3.3 Optimised values of A_o, A_1 and $\log K_{eq}$ obtained by fitting equations 4.3.1 and 4.3.2 to the absorbance data.

Ligands	A_o	A_1	$\log K_{eq}$
Cyanide	0.756(0.004)	0.574(0.002)	17.1(1.3)*
Azide	0.169(0.003)	0.302(0.003)	1.74(0.04)
Pyridine	0.246(0.002)	0.415(0.001)	2.48(0.01)
N-methylimidazole	0.512(0.006)	0.748(0.003)	4.35(0.04)
3-amino-1-propanol	0.585(0.005)	0.796(0.004)	2.95(0.04)

*$\log K_1K_2$ or $\log\beta_2$
standard deviations in parenthesis

Given a *trans*-labilising order of H_2O < bzm < OH^- < CN^-[14], it follows that the binding constants for the reactions of AHC with various ligands should be less than for the analogous reactions with vitamin B_{12a}, which again should be less than for the analogous reactions of DAC. The $\log\beta_2$ value for the reaction of AHC with CN^- cannot be directly compared with any reported $\log K_{eq}$ values. Assuming a reaction scheme of,

$$HO\text{-}Co\text{-}OH_2 \xrightarrow[H^+]{CN^-} H_2O\text{-}Co\text{-}CN \xrightarrow{CN^-} NC\text{-}Co\text{-}CN$$

then a $\log K_{eq}$ value for a single substitution of AHC by CN^- can be calculated by subtracting the $\log K_{eq}$ value for the substitution of water by CN^- in Factor B (8.4)[1] from the $\log \beta_2$ value for the reaction of AHC (18.8). The calculated $\log K_{eq}$ value is then 10.4, which is consistent with the reported data on Factor B and vitamin B12a (table 4.4.1 below). Baldwin *et.al* reported an approximate $\log K_{eq}$ value for the substitution reaction of AHC with CN^- of > 9.[14] Assumptions made in the above reaction scheme are that DHC and hydroxocyanocobinamide are inert and that the equilibrium constants involving HCN are very much smaller than those involving CN^- and thus can be ignored.

The optimised values of K_{eq} are conditional binding constants because of the dependence of K_{eq} on pH. The pH is an important factor in these measurements. Heterocyclic bases, for example, can coordinate to corrinoids in several forms *e.g.* the imidazole molecule and the imidazolate anion. Formation constants are several orders of magnitude greater for the coordination of the anion than for the corresponding neutral molecule.[33] Here, at pH 12 all ligands are in their protonated forms. However, at pH 12 the proportion of labile corrin, AHC, is very small and hence the pH dependence of these equilibrium constants on the measured values will be large (DHC is inert[29]). An equation was thus derived (appendix 12.2) to determine the unconditional binding constants of L to AHC.

At any pH, the experimental binding constant for the reaction represented by,

$$\text{corrin} + L \rightleftharpoons Co\text{-}L + H_2O$$

$$\text{is, } K_{exp} = \frac{[Co\text{-}L]}{[L]_{total}[corrin]_{total}}$$

The reaction of interest however is represented by,

$$AHC + L \rightleftharpoons Co\text{-}L + H_2O$$

$$\text{for which, } K \approx \frac{[Co\text{-}L]}{[L][AHC]} \text{ at high pH}$$

The unconditional binding constant, K, can then be related to the conditional binding constant, K_{exp},

$$K = \frac{K_{exp}([H^+] + K_{a2})}{[H^+]} \qquad (4.3.4)$$

Table 4.3.4 below shows the unconditional binding constants calculated using the above equation.

Table 4.3.4 Unconditional binding constants, given as log K, for the reaction of AHC with the five ligands at 25°C.

Ligand	log K
Cyanide	18.8*
Azide	3.45
Pyridine	4.19
N-methylimidazole	6.06
3-amino-1-propanol	4.66

* $\log\beta_2$, using K_{exp} = 17.1

4.4 DISCUSSION

A large number of binding constants for the substitution reactions of the cobalt corrinoids have been determined. Experimental conditions (temperature, ionic strength, etc.) used in the determination of the formation constants vary considerably, but Pratt *et al.*[12] claim that the differences which are significant for the study of *cis*- and *trans*-effects are, in most cases, greater than the differences which would be caused by a change in the experimental conditions. Table 4.4.1 below shows the binding constants for the substitution of coordinated H_2O in cobalt(III) corrinoids by various ligands Z, with several different ligands X in the *trans*-position.[1] A single order of equilibrium constants for different ligands X is predicted for all Z (here equilibrium constants should decrease across the table). In general, as X becomes a better σ-donor (across the table), so the equilibrium constants fall, a manifestation of the thermodynamic *trans*-effect; H_2O < bzm < OH^- < CN^-.[14]

Table 4.4.1 Log K_{exp} values for the ligand substitution reactions of various corrins,
X-Co(III)-H_2O + Z ⇌ X-Co(III)-Z + H_2O.[1,14]

Ligand, Z	X = H_2O	X = bzm	X = CN^-
azide		4.9	2.7
hydroxide	8.0	6.3	3
imidazole	7.5	4.6	4.1
ammonia	> 9	7	3.35
cyanide	14	14.1	8.4

Earlier it was shown that conditional binding constants can vary quite considerably from their unconditional counterparts (by almost two orders of magnitude here), and hence the

trans-labilising order given above is not necessarily correct. Unless the pH of the reaction solution is known, the validity of these comparisons and apparent orders cannot be tested. It has proved impossible to reconstruct the above table using unconditional binding constants because, in most cases, the primary literature gives no indication of the pH at which the measurements were made. The results discussed here, retabulated in table 4.4.2 for convenience, do nevertheless fit the predicted sequence and hence the proposed *trans*-labilising order; bzm < OH^- < CN^-[14], is supported.

Table 4.4.2 Comparison of the log K_{exp} (log K when X = OH^-) values for the ligand substitution reactions of various corrins, X-Co(III)-H_2O + Z ⇌ X-Co(III)-Z + H_2O.[1,14,31]

Ligand, Z	X = bzm	X = OH^-	X = CN^-
azide	4.9	3.45	2.7
pyridine		4.19	2.6
3-amino-1-propanol	> 6	4.66	
N-methylimidazole		6.06	
cyanide	14.1	12.0	8.4

Pratt noted that although the binding constants for the substitution of water by nitrogenous bases decrease as X becomes a better σ-donor, the sensitivity of K to the nature of X still varies with the nature of Z.[1] Such a difference in sensitivity could then lead to a change in the relative order of stabilities as X is varied. Table 4.4.2 shows how the ligands investigated here can be arranged in an ascending order of binding constants for the substitution of water (down a column); azide < pyridine < 3-amino-1-propanol < N-methylimidazole < cyanide. Insufficient comparative data are available for comment on the possible different orders of sensitivity exhibited by analogous corrins with different

trans-ligands, though no anomalies are observed here. The factors which contribute to these orders are not yet fully understood. Both electronic and steric effects were considered in an attempt to rationalise the order recorded for the substitution reactions of AHC.

Table 4.4.3 Comparison between the acid dissociation constants of the ligands, shown here as pK_a, and the ligand binding constants of AHC, log K.

Ligand (Z)	pK_a	log K
azide	4.1	3.45
pyridine	5.25	4.19
N-methylimidazole	7.21	6.06
cyanide	9.31	12.0
3-amino-1-propanol	10.44	4.66

In table 4.4.3 above, comparison between the pK_a of the ligands and the binding constants of these ligands with AHC, log K, shows a good correlation except for the case of the ligand, 3-amino-1-propanol. In general, the greater the basicity of the ligand, the greater the binding constant of the ligand to AHC. Whilst this correlation suggests that electronic effects are important in determining the magnitude of the ligand binding constant, they must certainly not be the only factor to be considered. Alternative factors must be responsible for the anomalous behaviour of 3-amino-1-propanol.

The importance of steric effects on the ligand binding constant sequence was considered by calculating the molecular surface areas and volumes of these ligands using the program QCPE 509.[35] ALCHEMY II[36] was used to construct molecular fragments of the ligands of interest and the force field parameters built into the program were used to find an

energy-minimised structure of each ligand. These molecular fragments were then submitted to QCPE 509 for analysis. Molecular surface area, given in table 4.4.4, increases in the order; cyanide < azide < pyridine < N-methylimidazole < 3-amino-1-propanol; whilst molecular volume increases in the order; cyanide < azide < 3-amino-1-propanol, N-methylimidazole < pyridine. A comparison between the molecular volumes and ligand binding constants reveals a trend, with azide being the only ligand not conforming to the trend. High ligand binding constants are correlated with small molecular volumes.

Table 4.4.4 Molecular surface areas and volumes of the five ligands, calculated using QCPE 509.[35]

Ligand	Molecular area / Å^2	Molecular volume / Å^3
cyanide	46.3	29.0
azide	59.4	35.4
pyridine	110.1	87.5
N-methylimidazole	112.2	83.4
3-amino-1-propanol	122.6	83.3

An explanation for the observed ligand binding order is likely to be found in a combination of steric and electronic factors. In general, the expected trend of the smallest, strongest nucleophile having the largest binding constant seems consistent with the data.

4.5 CONCLUSIONS

The primary aim of the work discussed in this chapter; to determine the suitability of these ligands for kinetic investigation, was successful. All five N-donor ligands were found suitable for further investigation. The data collected appears consistent with the established *trans*-labilising order, despite the limited availability of unconditional binding constants. Both steric and electronic factors are important in arriving at an explanation as to the order of stability of the substituted complexes.

5 pH PROFILE OF THE KINETICS OF THE REACTION OF DAC WITH AZIDE

The mechanism of ligand substitution in vitamin B_{12a}, the parent molecule of DAC, is generally accepted to be dissociative. The rate of substitution of the axially coordinated water molecule in the B_{12a} molecule by a variety of ligands varies only by about two orders of magnitude, whereas the corresponding stability constants vary by about eleven orders of magnitude.[9] *Firth et al.* observed five coordinate corrin complexes when investigating the removal of co-ordinated water from organocobinamides.[37] These five co-ordinate complexes are analogous to the intermediates in S_N1 ligand substitution reactions.

We assumed that the substitution reactions of DAC would similarly be dissociative. Whether the mechanism is interchange dissociative, I_D, or purely dissociative, D, will be addressed in the following chapters. Observed rate constants of B_{12a} reactions are known to be pH dependent, since hydroxocobalamin is substitutionally inert.[1] A similar pH dependence is expected for DAC, since DHC is also substitutionally inert.[3]

5.1 EXPERIMENTAL PROCEDURES

The kinetics of the substitution of coordinated H_2O in DAC/AHC were followed by observing the change in absorbance with time at 370 nm using stopped flow spectrophotometry (see appendix 13 for more details). Both azide and DAC/AHC solutions were prepared with an ionic strength of 1.0 mol dm^{-3}. The pH of solutions, buffered with phosphate buffers, was adjusted using either NaOH or HCl as appropriate. The concentration of DAC, quantified by conversion to dicyanocobinamide, was $2X10^{-5}$ mol dm^{-3}. The temperature was maintained at 25°C using a circulating water bath (±0.1°C). The pseudo-first-order rate constants, k'_{obs}, were determined by fitting the

absorbance-time traces to an exponential function, $A_{meas} = A_1 exp(-k'_{obs}t) + A_2$, using a non-linear least squares routine employing a Newton-Raphson procedure.

5.2 RESULTS

Table 11.3.1 in the appendix gives the observed pseudo-first-order rate constants, k'_{obs}, as a function of ligand concentration and pH at 25°C. Figure 5.2.1 shows that a linear relationship exists between the pseudo first order rate constants and the concentration of azide. The slopes of these linear least squares fits produce second order rate constants, k_{II}^{obs}, where k_{II}^{obs} refers to the equation,

$$Co_T + L_T \rightleftharpoons L\text{-}Co\text{-}OH/OH_2$$

where $[Co_T] = [H_2O\text{-}Co\text{-}OH_2] + [H_2O\text{-}Co\text{-}OH] + [HO\text{-}Co\text{-}OH]$

$[L_T] = [HN_3] + [N_3^-]$

$$\frac{d[L\text{-}Co\text{-}OH/OH_2]}{dt} = k_{II}^{obs} \times [Co_T] \times [L_T]$$

Table 5.2.1 gives the values of k_{II}^{obs} as a function of pH.

Figure 5.2.1 Plot of k'_{obs} versus $[N_3^-]$ at pH 10.0.

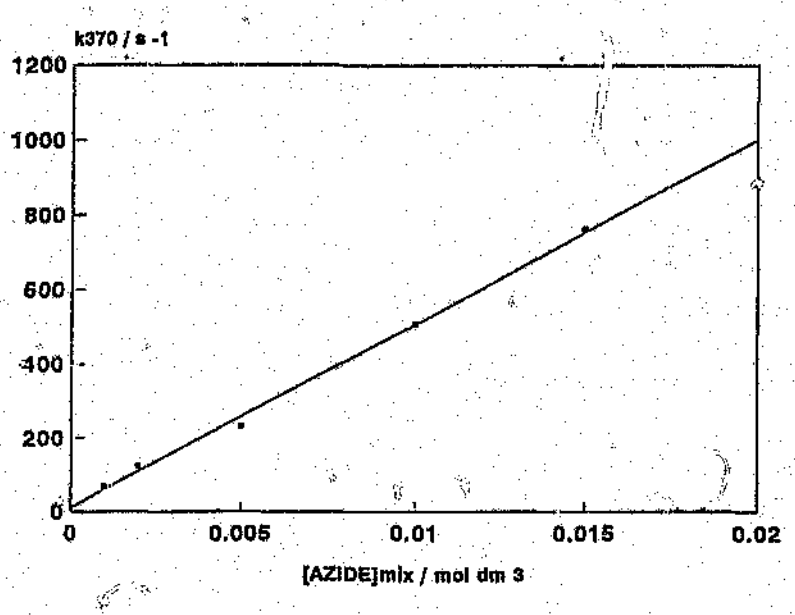


Table 5.2.1 The dependence of k_{II}^{obs} on pH for the substitution of a H_2O in DAC (or AHC) by N_3^- (or HN_3) at 25°C.

pH	k_{II}^{obs} / $dm^3\ mol^{-1}\ s^{-1}$
12.0*	$1.4X10^3$ ($3X10^2$)
11.5	$8.8X10^3$ ($9X10^2$)
11.0	$1.02X10^4$ ($6X10^2$)
10.5	$2.8X10^4$ ($1X10^3$)
10.0	$4.3X10^4$ ($4X10^3$)
9.5	$6.45X10^4$ ($2X10^1$)
9.0	$6.7X10^4$ ($4X10^3$)
8.5	$7.6X10^4$ ($5X10^3$)
8.0	$8.2X10^4$ ($6X10^3$)
7.5	$1.12X10^5$ ($5X10^3$)
7.0	{$1.06X10^5$ ($5X10^3$)}
6.5	$1.59X10^5$ ($6X10^3$)
6.0	$1.46X10^5$ ($9X10^3$)
5.5	$1.02X10^5$ ($5X10^3$)
5.0	$6.5X10^4$ ($7X10^3$)
4.5	{$5.4X10^4$ ($4X10^3$)}
4.0	$4.4X10^4$ ($7X10^3$)
3.5	$5.28X10^4$ ($9X10^2$)
3.0	$4.6X10^4$ ($2X10^3$)

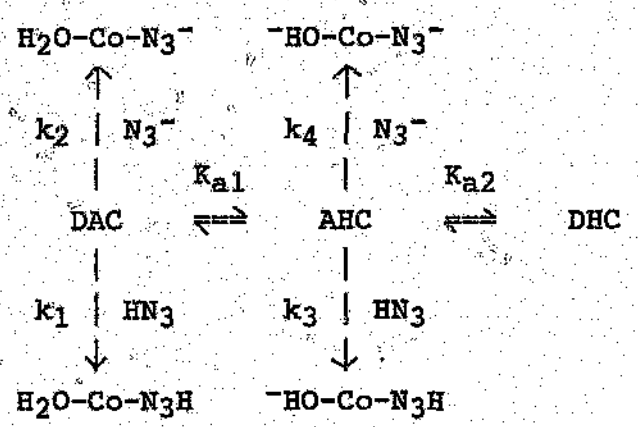
* from work described in chapter 7

5.3 DISCUSSION

The absorbance/time traces for the substitution of water in DAC/AHC by azide over the whole pH range investigated were monophasic. This does not necessarily imply that only one of the axially coordinated water molecules in DAC is available

for substitution, but rather that the first substitution is kinetically indistinguishable from the second because the rate of substitution of the first water molecule is much slower than that of the second. Monophasic kinetics similarly indicate that the technique was unable to differentiate between the reactions of the two structural isomers of AHC so that k_{II}^{obs} is a macroscopic rather than a microscopic rate constant. This result can be interpreted in one of three ways; (1) only one isomer is present (>90% total), (2) both isomers are present and react at very similar rates, and (3) the interconversion of the two stereoisomers is rapid compared to the rate of reaction of either with the incoming ligand. This third option is most likely since the interconversion between the two isomers requires only a proton transfer (generally at or near the diffusion controlled limit in water) and not ligand substitution. Baldwin *et al.*[3] reported that AHC exists as a mixture of two or more isomers and Brown *et al.*[50] indicate that the diastereoisomers in aquocyanocorrinoids are present in approximately the ratio of $\alpha : \beta = 2:1$. This suggests that the monophasic kinetics must be interpreted in terms of the two isomers reacting at very similar rates.

An equation was derived (appendix 12.3) to describe the relationship between k_{II}^{obs} and pH. The reaction scheme below indicates all the possible forward reactions that can contribute to the value of k'_{obs}, and hence k_{II}^{obs}. Reverse reactions have been ignored for simplicity. Both DAC and AHC react with azide, though in the case of DAC a second substitution reaction is possible. However, since the first substitution reaction is rate determining, a second substitution will not contribute to the magnitude of k'_{obs}, and hence this possibility is ignored in the reaction scheme. Both N_3^- and HN_3 can coordinate to DAC/AHC.[11]



$$k'_{obs} = \frac{k_1[H^+]^3 + k_2[H^+]^2K_L + k_3K_{a1}[H^+]^2 + k_4K_{a1}[H^+]K_L}{(K_{a1}K_{a2} + K_{a1}[H^+] + [H^+]^2)(K_L + [H^+])} \qquad (5.3.1)$$

A non-linear least squares technique employing a Newton-Raphson procedure and Marquardt's algorithm was used to fit the data in table 5.2.2 with equation 5.3.1. Figure 5.3.1 below indicates the fit obtained. Table 5.3.1 has the optimised values of the component rate constants and equilibrium constants thus obtained, and table 5.3.3 the correlation matrix.

Figure 5.3.1 Plot of k_{II}^{obs} versus pH for the substitution reaction of DAC/AHC with HN_3/N_3^- at 25°C; data fitted using equation 5.3.1.

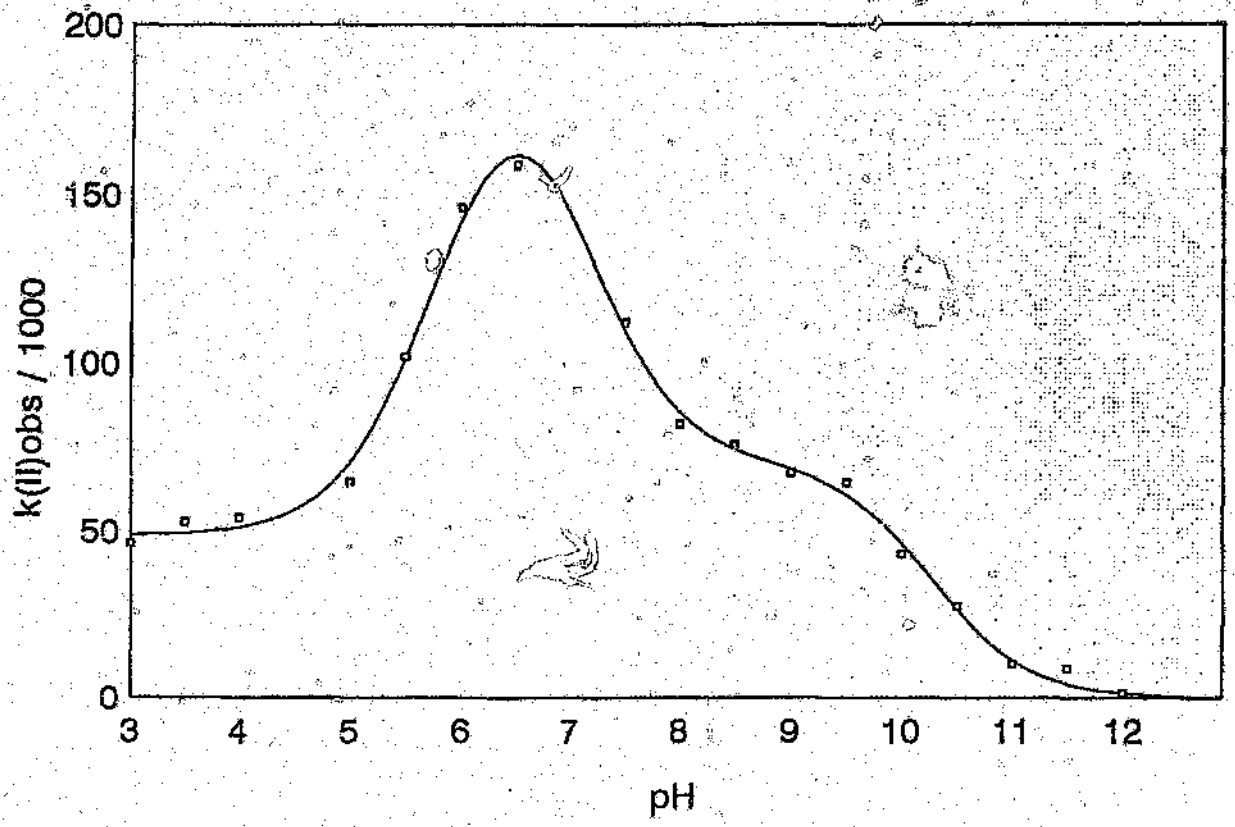


Table 5.3.1 Optimised values of the parameters in equation 5.3.1 after fitting with data in table 5.2.2.

Parameter	Optimised Value
k_1	$4.9X10^4$ $(2X10^3)$
k_2	$1.7X10^5$ $(2X10^{10})$
k_3	$9.2X10^5$ $(3X10^{11})$
k_4	$7.0X10^4$ $(3X10^3)$
pK_1	7.09 (0.08)
pK_2	10.28 (0.08)
pK_L	5.82 (0.08)

Table 5.3.3 Correlation matrix of the parameters in equation 5.3.1 after fitting with data in table 5.2.2.

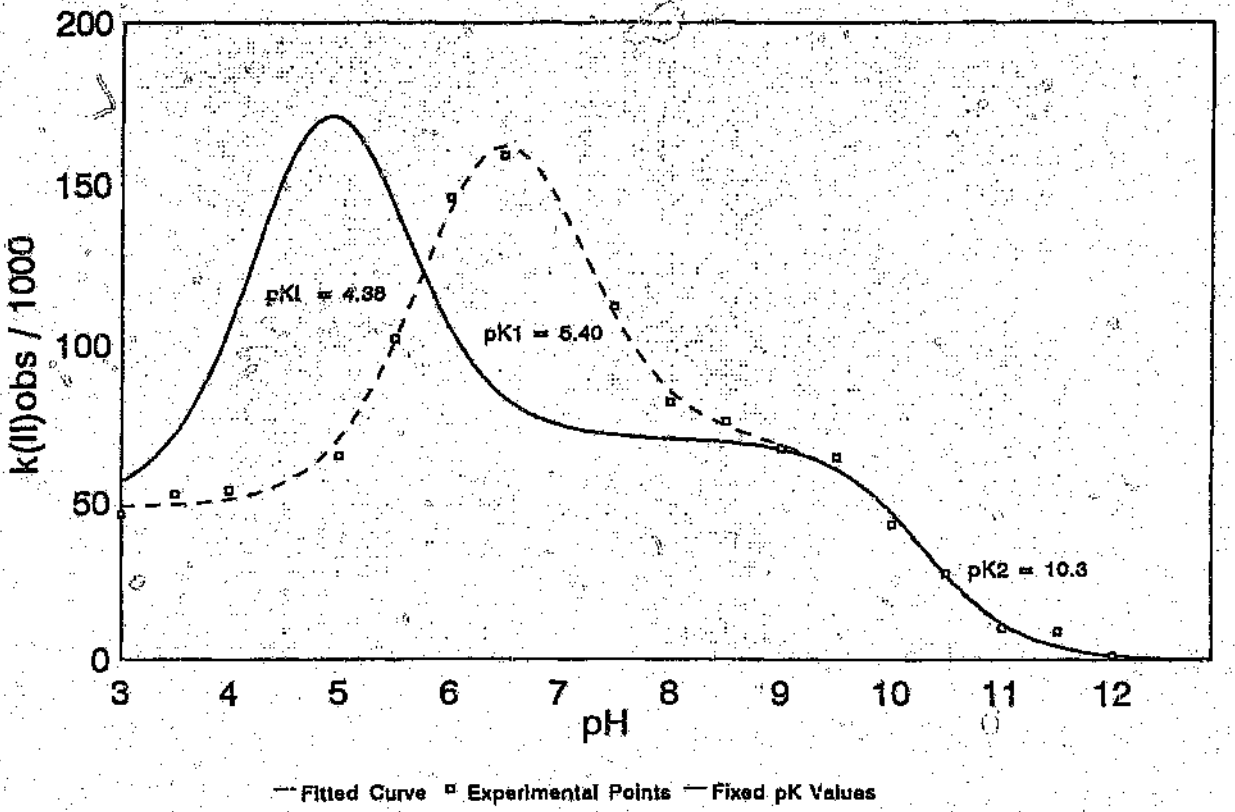
	k_1	k_2	k_3	k_4	pK_{a1}	pK_{a2}	pK_L
k_1	1.00						
k_2	0.38	1.00					
k_3	0.26	-0.88	1.00				
k_4	-0.15	-0.47	-0.42	1.00			
pK_{a1}	0.79	0.46	0.47	-0.98	1.00		
pK_{a2}	0.00	0.00	0.57	-0.11	0.13	1.00	
pK_L	-0.80	-0.50	-0.42	0.99	-0.99	-0.20	1.00

Although component rate constants can theoretically be determined by fitting equation 5.3.1 to the data, the large errors associated with these values indicate that few conclusions can be drawn from them. The extremely large error associated with the parameters k_2 and k_3 could be the result of a strong correlation between the two, shown in the correlation matrix in table 5.3.3.

The value of pK_{a2} is in good agreement with the literature value[5] (10.30), whereas the values for pK_{a1}[5] and pK_L[38] (5.40 and 4.38 respectively) are not. A strong correlation between these two factors could play some part in this. However, if the values of pK_L, pK_{a1} and pK_{a2} are kept constant (using the literature values) then the fit obtained when equation 5.3.1 is applied to the data is not good. Figure 5.3.2 shows how the data at low pH are inconsistent with the relevant pK_{a2} and pK_L values. The optimised values of these parameters given in table 5.3.1 are thus not artefacts, produced as a consequence of a close correlation between the two parameters. No reason

could be found for the real elevation of the magnitude of these parameters, and no precedent for such an elevation is available in the literature.

Figure 5.3.2 Plot of k_{II}^{obs} versus pH for the substitution reaction of DAC/AHC with HN_3/N_3^- at 25°C; data fitted using equation 5.3.1, fixing the values of pK_L, pK_{a1} and pK_{a2} at 4.38[38], 5.40[5] and 10.30[5] respectively.



If an incorrect reaction scheme had been proposed then an incorrect equation would have been derived to describe the data. Binding studies of AHC with azide at pH 12 had indicated that the AHC was singly substituted by the azide. However, analogous measurements were not done at lower pHs, and thus it is quite conceivable that DAC would react with two azide ligands to produce a doubly substituted product. N_3^- and OH^- exert similar *trans*-labilising effects, both being greater

than H_2O[1], and thus since HO^--Co-OH_2 (AHC) undergoes substitution of the H_2O, it is likely that the H_2O in N_3^--Co-OH_2 will similarly undergo substitution. The effect of a second substitution of the mono-substituted DAC species was thus considered. If this second substitution was faster than the first, then such an occurence would not effect the kinetic data since the rate determining step would remain the substitution of the first azide ligand. If the second substitution was slower, however, then the kinetic data would have shown biphasic behaviour. Monophasic kinetics were observed at all pHs investigated, and hence such a possibility is unlikely.

Assuming then that the proposed mechanism is correct, the elevated pK_{a2} and pK_L values must then be the result of some other experimental error. At low pH, azide, in the protonated form, is volatile. Skewing of the results at low pH could then be the result of real ligand concentrations being considerably less than expected. In an analogous study using vitamin B_{12a}, Marques *et al.* did not encounter any such problems.[45] In that study kinetic measurements were obtained over the pH range from 10 to 2, with no inexplicable deviations occuring at lower pHs.

5.4 CONCLUSIONS

The fit of equation 5.3.1 to the pH profile data indicates that, at least at high pH, the postulated mechanism is supported. The assumption that DHC is inert to substitution has been verified. Subsequent measurements of AHC substitution rate constants (pH 12) can thus be corrected in order to produce a pH independent rate constant. The low pH data clearly requires further investigation.

6 THE USE OF SATURATION KINETICS TO DISTINGUISH BETWEEN AN I_D AND A D MECHANISM OF LIGAND SUBSTITUTION: TEST CASE USING AQUOCOBALAMIN.

Two extreme possibilities for the mechanism of ligand substitution reactions at octahedrally-coordinated metal atoms have been identified.[34] For the dissociative mechanism, D, the bond to the leaving ligand, L, is entirely severed to generate a five-coordinate intermediate which then reacts with an incoming ligand, L′, to reform a six-coordinate substitution product. At the other extreme is the associative mechanism, A, in which the new ligand becomes fully bound, thus generating a seven-coordinate intermediate before one of the original ligands is lost. These extreme mechanisms are often too inflexible to deal with the subtle variations in real mechanisms and hence variations on these two basic mechanisms have been proposed. The dissociative interchange mechanism, I_D, is characterised by a transition state involving considerable extension of the M-L bond, but not its complete rupture, together with some incipient interaction with the incoming ligand. This incipient interaction positions the new ligand to enter the first coordination sphere on the departure of L. The associative interchange mechanism, I_A, is characterised by a similar transition state, but here the interaction between M and L′ is more advanced and the M-L′ bonding is important in defining the activated complex.

In the real world there are processes whose mechanisms define a continuous gradation from D through increasingly associated interchanges to A. In any given case it is difficult to give an exact description since the experimental criteria are seldom definitive.[34] Interest in the mechanism of substitution of vitamin B_{12a} has nevertheless been great.[1]

Hague and Halpern showed that for a series of seven singly charged anions, rate constants for the substitution of H_2O in an aquocobalamin molecule varied by about one order of magnitude although the stability constants for the formation of the complexes varied by about 12 orders of magnitude.[44] In addition, Thusius showed that the formation rate constants for the substitution of H_2O in an aquocobalamin molecule with various anionic ligands varied from 170 to 2300 $dm^3\ mol^{-1}\ s^{-1}$, whereas the dissociation rate constants varied between 590 and $< 10^{-5}$ s^{-1}.[22] This behaviour is typical of mechanisms in which direct bonding of the entering group does not commence until after the rate determining transition state has been passed.

There is thus general agreement that the mechanism of the ligand substitution reactions of aquocobalamin are dissociative; nevertheless there remains some disagreement concerning whether the intimate mechanism is purely dissociative, D,[14,22,23,24,25] or interchange dissociative, I_D.[23,26] Here the limiting dissociative mechanism is characterised by a rate determining step involving the unimolecular dissociation of H_2O from the Co(III) coordination sphere to produce a five coordinate transition state. The I_D mechanism, in contrast, requires some degree of participation of the incoming ligand in the transition state (which is thus never fully 5 coordinate).

A modest dependence of the substitution rate constants on the identity of the incoming ligand has been cited as evidence for a D mechanism. However, compensating changes in ΔH^* and ΔS^* for the reaction with a series of primary amines has been reported.[39,40] The slope of the plot of ΔH^* against ΔS^* happens to be such that, near room temperature, these ligands react at a similar rate, and thus the independence of the substitution rate on the nature of the incoming ligand, in this case, is not necessarily indicative of a D mechanism. Researchers

have attempted to use measurements of the volumes of activation of the reactions to solve the question of interpretation of these results[24,25], but interpretation of the data was complicated and proved unsuitable for solving the question.[41]

Activation enthalpies and entropies for the substitution of H_2O by small anionic ligands such as SCN^-, $S_2O_3^{2-}$, NO_2^- and HSO_3^- are all very similar. This is evidence for a D mechanism.[41] The transition state for the substitution of H_2O by CN^-, however, is enthalpically stabilised by more than 20 kJ mol^{-1} relative to the substitution by HCN, and the ΔS^* for the two reactions is -25 and +50 J K^{-1} mol^{-1}, respectively.[41,42] This evidence supports an I_D mechanism. Furthermore, the rate of substitution of bound H_2O by a series of imidazoles was found to vary linearly with the basicity of the incoming ligand.[43] This research team was thus of the opinion that the ligand substitution reactions of aquocobalamin involve the nucleophilic participation of the incoming ligand in the transition state, which is characteristic of an I_D mechanism.[27]

Stochel and van Eldik found that for the substitution of H_2O in aquocobalamin (shown below as dmbzim-Co-H_2O, dmbzim = 5,6-dimethylbenzimidazole, where only the axial ligands are shown and the overall charge is neglected for convenience) with pyridine, a plot of observed rate constant against ligand concentration showed saturating behaviour at high (*i.e.* > 0.5 mol dm^{-3}) ligand concentrations.[25] No other observations of saturating behaviour could be found in the literature. They indicated that this saturating behaviour can be explained using both a D and an I_D mechanism. For a D mechanism, equations 6.1 and 6.2 apply. If k_{-2} is significant, then the observed rate constant, k_{obs}, is related to the microscopic rate constants by equation 6.3 (derivation in appendix 12.4); if not, then equation 6.3 simplifies to equation 6.4.

$$\text{dmbzim-Co-}H_2O \underset{k_{-1}}{\overset{k_1}{\rightleftharpoons}} \text{dmbzim-Co} + H_2O \qquad (6.1)$$

$$\text{dmbzim-Co} + L \underset{k_{-2}}{\overset{k_2}{\rightleftharpoons}} \text{dmbzim-Co-L} \qquad (6.2)$$

$$k_{obs} = \frac{k_1k_2[L] + k_{-1}k_{-2}}{k_{-1} + k_2[L]} \qquad (6.3)$$

$$k_{obs} = \frac{k_1k_2[L]}{k_{-1} + k_2[L]} \qquad (6.4)$$

In the case of an I_D mechanism (equations 6.5 - 6.6), the observed rate constant is given by equation 6.7 if k_{-4} is significant (derivation in appendix 12.4), and equation 6.8 if not.

$$\text{dmbzim-Co-}H_2O + L \overset{K}{\rightleftharpoons} \{\ H_2O\ldots\text{dmbzim-Co}\ldots L\ \} \qquad (6.5)$$

$$\{\ H_2O\ldots\text{dmbzim-Co}\ldots L\ \} \underset{k_{-4}}{\overset{k_4}{\rightleftharpoons}} \text{dmbzim-Co-L} + H_2O \qquad (6.6)$$

$$k_{obs} = \frac{k_4K[L]}{1 + K[L]} + k_{-4} \qquad (6.7)$$

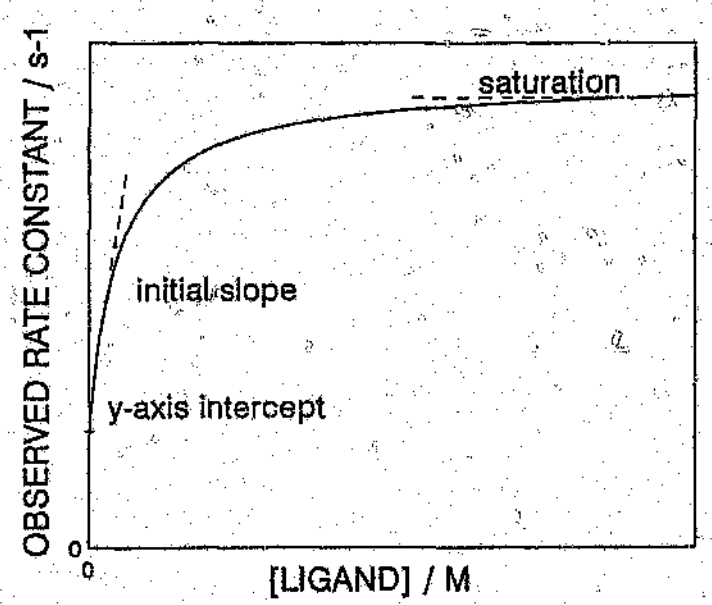
$$k_{obs} = \frac{k_4K[L]}{1 + K[L]} \qquad (6.8)$$

Equations 6.3 and 6.7 (and 6.4 and 6.8) have the same hyperbolic form. The microscopic rate constants, or combinations thereof, which describe the three sections of the hyperbola shown in figure 6.1 below, *viz.*, the y-axis intercept, the initial slope, and the saturating rate constant, k_{sat}, are given in table 6.1 below.

Table 6.1 The microscopic rate constants, or combinations thereof, which describe the three areas of the observed hyperbola of the graph of k_{obs} versus [L] for the substitution of H_2O in aquocobalamin with pyridine.

Mechanism	y-axis intercept	initial slope	k_{sat}
D , k_{-2} significant	k_{-2}	k_1k_2/k_{-1}	k_1
, k_{-2} insignificant	origin	k_1k_2/k_{-1}	k_1
I_D , k_{-4} significant	k_{-4}	$(k_4 + k_{-4})K$	$k_4 + k_{-4}$
, k_{-4} insignificant	origin	k_4K	k_4

Figure 6.1 The three sections of a hyperbolic function.



A distinction between the two mechanisms is not possible unless a series of ligands showing saturating behaviour are compared. For a D mechanism, k_{sat} corresponds to the rate constant for the unimolecular release of water from the Co(III) coordination sphere. The value of k_{sat}, and its activation parameters, should then be independent of the nature of L. In the case of an I_D mechanism, k_4, obtained from the difference between k_{sat} and the intercept, and its activation parameters, should depend on L.[27]

Saturation kinetics of aquocobalamin with 6 N-donor ligands, viz. hydroxylamine, methyl glycinate, imidazole, pyridine, 4-methylpyridine and histamine; are discussed in this thesis. The author was only directly involved with the substitution reactions with pyridine and experimental data is thus discussed for this ligand. Although saturation kinetics have been reported for the substitution reaction of aquocobalamin with pyridine[25], these measurements were repeated in order to verify the results, and to collect more data in the high pyridine concentration region.

6.1 EXPERIMENTAL PROCEDURES

The substitution of H_2O in aquocobalamin by pyridine was studied under pseudo first-order conditions at a single pH (6.50), halfway between the pK_a of the N-donor of the ligand (5.25 at 25.0°C)[47] and the pK_a of coordinated H_2O in B_{12a} (8.10 at 25.0°C)[1] and at four different temperatures (5.0°C, 15.0°C, 25.0°C, and 35.0°C). An 80 μ mol dm^{-3} solution of B_{12a}, with a total ionic strength adjusted to 1.00 mol dm^{-3} with KCl, was buffered with phosphate (0.1 mol dm^{-3}) and adjusted to pH 6.5 using additions of NaOH and HCl, as appropriate. Fifteen ligand solutions, varying in concentration between 0.01 mol dm^{-3} and 1.0 mol dm^{-3}, were similarly prepared. Preliminary spectrophotometric

observations indicated two possible wavelengths at which the reaction could be monitored (the requirement being a large absorbance change accompanying the reaction) *viz.* 362.5 nm (the γ-band of the complex), and 351.0 nm (the γ-band of the aquocobalamin). The reaction was monitored at both wavelengths by mixing equal volumes (100 μ dm^3) of the two solutions using a Hi-Tech Scientific SF-51 stopped flow spectrometer (cell pathlength 1.00 cm) interfaced through a DAS-50 A/D board with an IBM-type PC. The experimentally determined rate constants, k'_{obs}, were found by fitting the absorbance/time trace to an equation of the form $A_1\exp(-k'_{obs}t) + A_2$, or, where appropriate (see Results), to $A_1\exp(-k'_{1,obs}t) + A_2\exp(-k'_{2,obs}t) + A_3$ using a non-linear least squares technique employing a Newton-Raphson procedure. The temperature of the system was maintained (±0.1°C) with a circulating water bath. Data analysis, elaborated on below, was by means of either a non-linear least squares technique employing a Newton-Raphson procedure and Marquardt's algorithm, or by standard linear least squares methods.

6.2 RESULTS

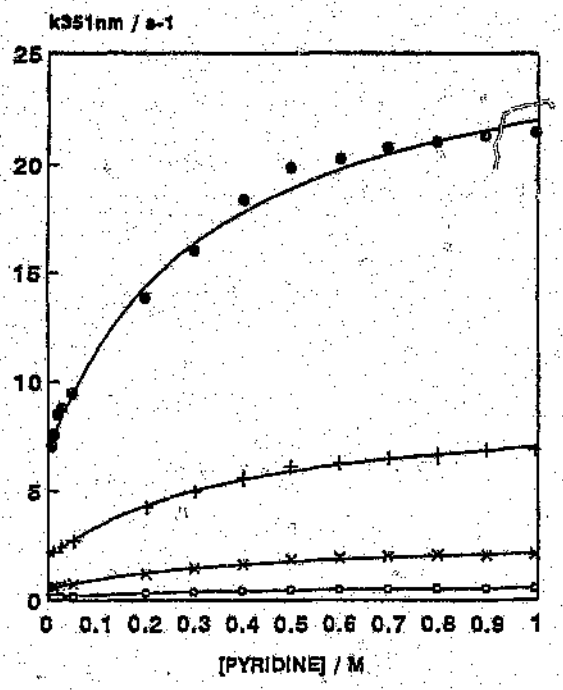
The absorbance time traces used to follow the kinetics of the substitution of H_2O in aquocobalamin with pyridine were followed at two wavelengths. Those traces followed at 362.5 nm were best fitted by a two-exponential expression, in contrast to those measured at 351 nm which were best fitted with a single exponential trace. No analogous effects were reported for the other five ligands investigated, though the kinetics of these reactions were only followed at one wavelength, the γ-band of the cobalamin.

The dependence on pH of the experimentally determined pseudo first-order rate constants, k'_{obs}, for the ligand substitution reactions of B_{12a} is well established.[40,41,42,45,46] Hydroxocobalamin is inert to substitution, and protonated amines will not coordinate. The reaction was thus studied at a single pH (6.50), where the observed reaction rate is at a maximum (halfway between the pK_a of the N-donor of the ligand (5.25) and the pK_a of coordinated H_2O in B_{12a} (8.10)). The pH-dependent rate constant, k'_{obs}, was converted to a pH independent rate constant, k_{obs}, using equation 6.2.1. The values of k_{obs} and k'_{obs}, are given in appendix 11.4. The graphs of k_{obs} versus [pyridine] at the four temperatures investigated are given in figure 6.2.1 below.

$$k_{obs} = k'_{obs}(1 + [H^+]/K_L)(1 + K_{Co}/[H^+]) \qquad (6.2.1)$$

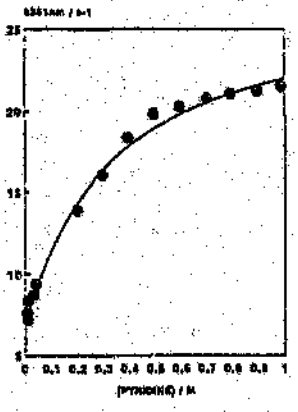
For pyridine (in agreement with the observations of Stochel and van Eldik[25]) and 4-methylpyridine, the rate constant for the dissociation of the ligand from Co(III) is significant. For hydroxylamine, methyl glycinate, histamine, and imidazole, the y-axis intercepts were within two standard deviations of the origin, which means that the reverse rate constants (k_{-2} in equation 6.3 or k_{-4} in equation 6.6) are very small. Figure 6.2.2 shows the plots of k_{obs} versus [ligand] for the six ligands investigated. It is evident from this figure that the saturating rate constants vary significantly for the different ligands investigated. This suggests that an I_D mechanism (equations 6.5 and 6.6) is appropriate and the data was thus fitted with equations 6.7 and 6.8.

Figure 6.2.1 Dependence of k_{obs} on [pyridine] and temperature for the reaction of pyridine with aquocobalamin.

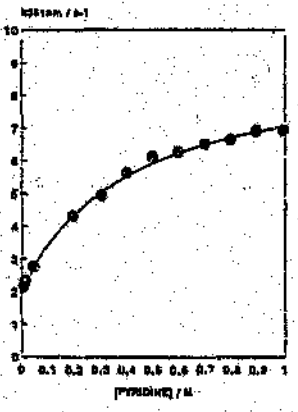


• T = 35°C + T = 25°C * T = 15°C ° T = 5°C

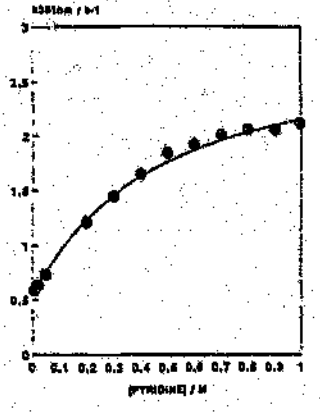
(a) T = 35°C



(b) T = 25°C



(c) T = 15°C



(d) T = 5°C

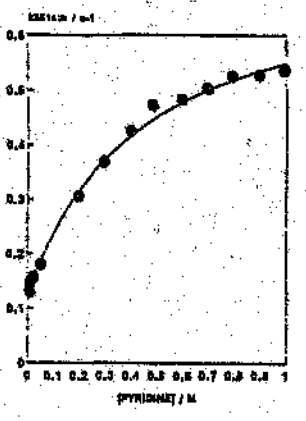
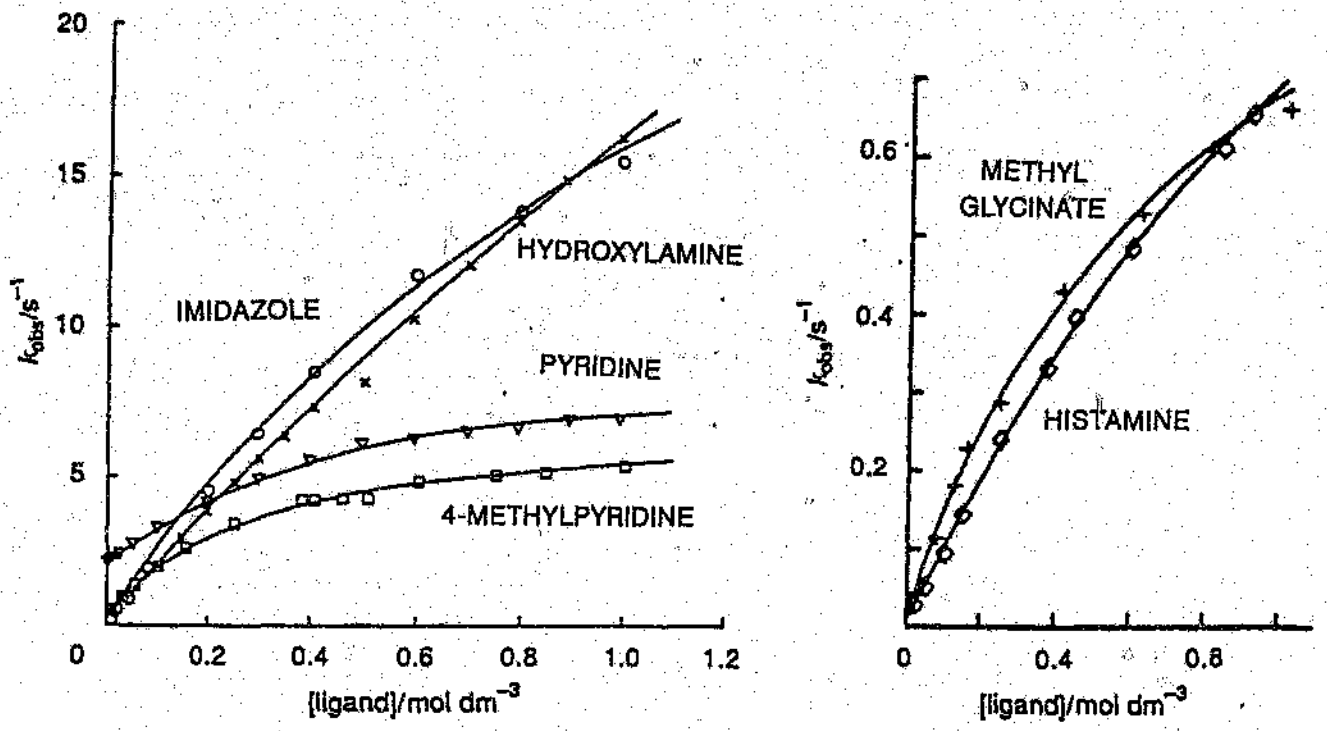


Figure 6.2.2 Dependence of k_{obs} on ligand concentration. All data at 25.0°C except for histamine (24.2°C) and methyl glycinate (25.2°C).



Although significant curvature is seen in all plots it is clear that complete saturation is not attainable in the ligand concentration range studied so that reliable values for the saturating rate constant are difficult to obtain. Higher ligand concentrations could not generally be used. In the case of pyridine, 4-methylpyridine and histamine, a large initial signal change occurs on first mixing, before the onset of the exponential absorbance change which can be attributed to the reaction. The size of this initial signal increased with ligand concentration and we suspect that it is due to the mixing of solutions of very different refractive indices. (No such effects were noted with comparable concentrations of solutions of ionic salts, such as ferric nitrate and potassium

thiocyanate, for example). The inevitable consequence of this mixing effect was that significant fractions of the absorbance change due to the reaction were lost at the higher ligand concentrations (the mixing signal increased in intensity as the ligand concentration increased, and the rate constant increased too; thus the overlap between the mixing and the rate signals increased).

Table 6.2.1 gives the values of k_{sat} (k_4) obtained by fitting equations 6.7 and 6.8 to the data. Alternative ways of obtaining estimates of k_{sat} were also explored. Equations 6.7 and 6.8 were manipulated to yield equations 6.2.2 - 6.2.5 (derivation in appendix 12.4). One of the problems associated with reciprocal plots such as used in equations 6.2.2 and 6.2.3 is the excessive weighting which the data points corresponding to low ligand concentrations will carry. Even small errors in these values lead to a significant skewing of the fit parameters, and especially the intercept. For this reason, only the last 6 or 7 points of each data set (corresponding to the higher ligand concentrations) were used for obtaining values of k_4; however the complete data set was used for obtaining the values of K. Figures 6.2.3 and 6.2.4 show the fits obtained when equations 6.2.2 and equations 6.2.4 were fitted to the pyridine data. Values for k_4, k_{-4} and K, and their averages, thus obtained, are given in table 6.2.1. Table 6.2.2 shows the average values of k_4, k_{-4} and K for the other five ligands investigated.

$$\frac{1}{k_{obs} - k_{-4}} = \frac{1}{k_4 K[L]} + \frac{1}{k_4} \qquad (6.2.2)$$

$$\frac{1}{k_{obs}} = \frac{1}{k_4 K[L]} + \frac{1}{k_4} \qquad (6.2.3)$$

$$\frac{k_{obs} - k_{-4}}{[L]} = -k_{obs}K + (k_4 + k_{-4})K \qquad (6.2.4)$$

$$\frac{k_{obs}}{[L]} = -k_{obs}K + k_4K \qquad (6.2.5)$$

Figure 6.2.3 Plots of k_{obs}^{-1} against [pyridine]$^{-1}$ for the reaction of pyridine with aquocobalamin; data fitted using equation 6.2.2.

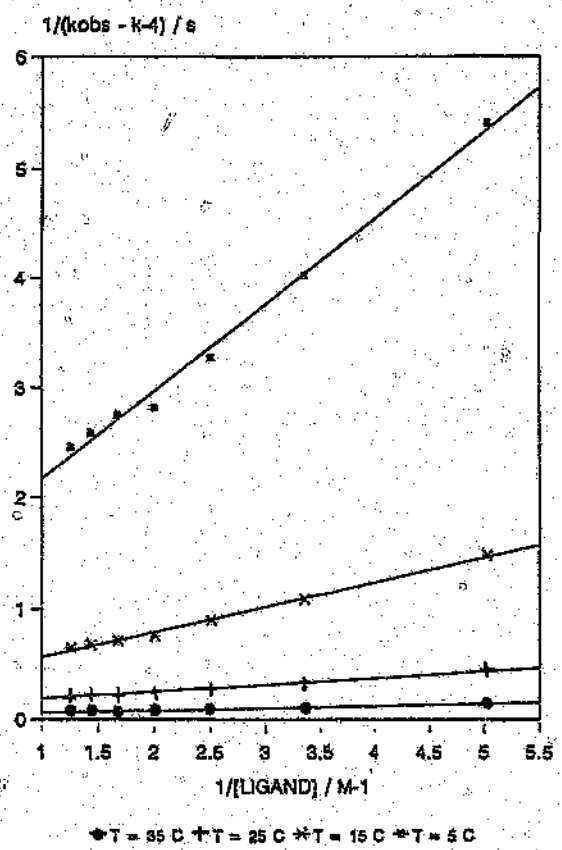
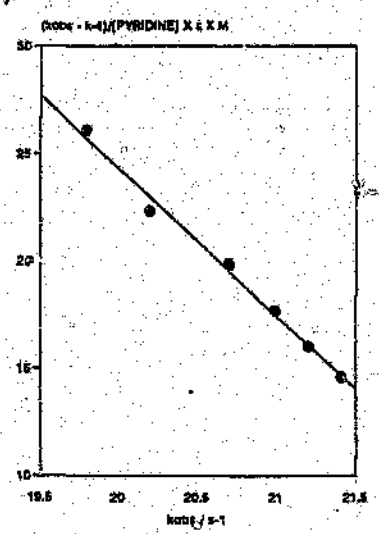
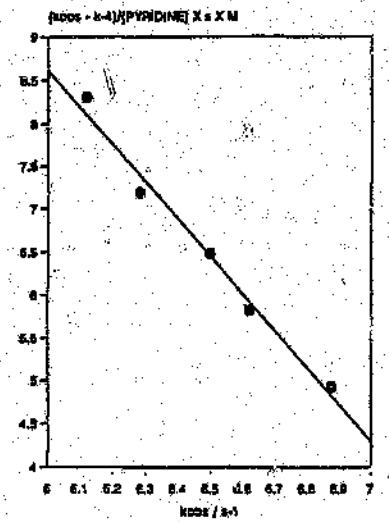


Figure 6.2.4 Plots of k_{obs}/[pyridine] against k_{obs} for the reaction of pyridine with aquocobalamin; data fitted using equation 6.2.4.

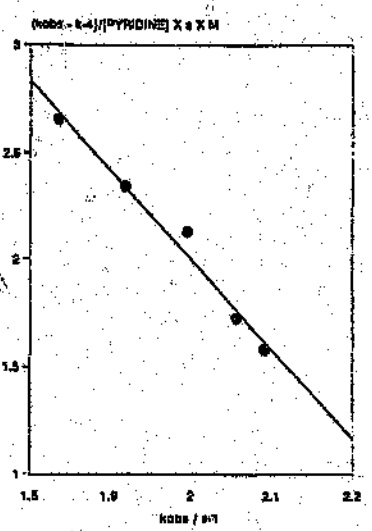
(a) T = 35°C



(b) T = 25°C



(c) T = 15°C



(d) T = 5°C

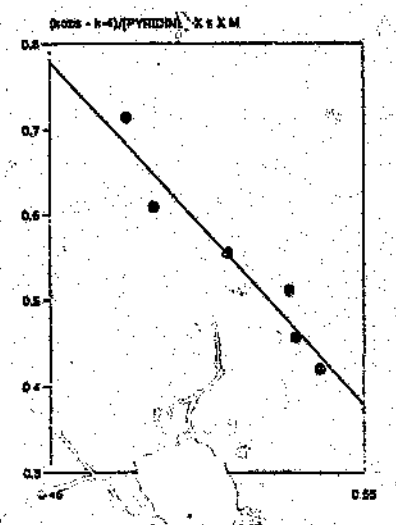


Table 6.2.1 Rate and equilibrium constants for the coordination of pyridine by aquocobalamin.

Parameter	Temp. / °C	Using equation	351 nm Value	351 nm Average	362.5 nm Value
K / $dm^3\ mol^{-1}$	5.0	6.7	2.5±0.3	2.5±0.1	4.3±0.6
		6.2.2	(3.3±0.5)		
		6.2.4	2.4±0.2		
	15.0	6.7	2.2±0.3	2.3±0.3	3.0±0.3
		6.2.2	2.5±0.3		
		6.2.4	2.0±0.1		
	25.0	6.7	2.5±0.2	2.4±0.1	2.4±0.4
		6.2.2	2.4±0.2		
		6.2.4	2.4±0.1		
	35.0	6.7	2.9±0.4	3.5±0.7	2.1±0.5
		6.2.2	(7.2±2.1)		
		6.2.4	4.0±0.7		
k_{-4} / s^{-1}	5.0	6.7		0.12±0.01	0.10±0.01
	15.0			0.52±0.02	0.41±0.03
	25.0			1.99±0.05	2.4±0.4
	35.0			6.9±0.3	7.6±0.3

Table 6.2.1 continued

Parameter	Temp. / °C	Using equation	351 nm Value	351 nm Average	362.5 nm Value
k_4 / s^{-1}	5.0	6.7	0.61±0.02	0.63±0.03	0.65±0.02
		6.2.2	0.66±0.03		
		6.2.4	0.62±0.08		
	15.0	6.7	2.4±0.1	2.5±0.1	2.58±0.08
		6.2.2	2.6±0.1		
		6.2.4	2.5±0.3		
	25.0	6.7	7.0±0.2	7.1±0.1	7.1±0.4
		6.2.2	7.1±0.3		
		6.2.4	7.2±0.5		
	35.0	6.7	20.2±0.9	21.2±1.4	14.2±1.2
		6.2.2	22.2±1.3		
		6.2.4	(18.2±7.3)		

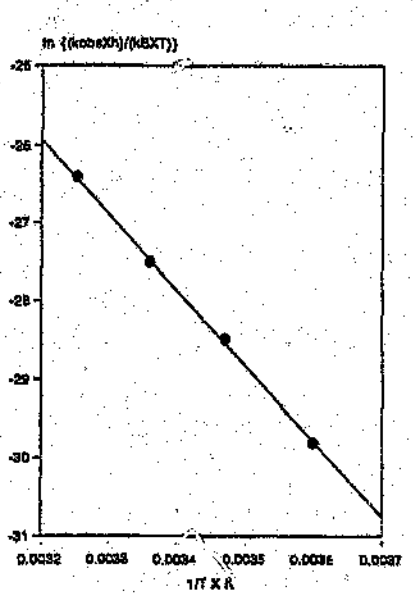
Table 6.2.2 Rate and equilibrium constants for the coordination of the ligand, L, by aquocobalamin.

Ligand	Temp / °C	Parameter K / $dm^3\ mol^{-1}$	k_4 / s^{-1}	k_{-4} / s^{-1}
hydroxylamine	5.4	0.066	35	
	15.0	0.14 ± 0.01	53 ± 4	
	25.0	0.25 ± 0.03	87 ± 3	
	36.2	0.62 ± 0.09	101 ± 8	
methyl glycinate	19.7	2.0 ± 0.4	0.61 ± 0.02	
	25.2	1.7 ± 0.2	1.03 ± 0.04	
	35.1	1.8 ± 0.2	2.6 ± 0.2	
	50.1	2.9 ± 0.3	6.9 ± 0.3	
4-methyl-pyridine	5.7	2.8 ± 0.1	0.61 ± 0.02	0.025 ± 0.005
	15.3	2.9 ± 0.1	2.24 ± 0.04	0.11 ± 0.02
	25.0	3.3 ± 0.1	6.4 ± 0.2	0.44 ± 0.08
	35.0	3.6 ± 0.3	15.9 ± 0.5	1.46 ± 0.2
imidazole	5.7	0.93 ± 0.01	4.5 ± 0.3	
	15.8	0.63 ± 0.04	14.9 ± 0.5	
	25.0	0.65 ± 0.07	43.3 ± 0.9	
	45.0	0.42 ± 0.14	209 ± 9	
histamine	9.2	1.0 ± 0.6	0.19 ± 0.05	
	15.6	0.65 ± 0.10	0.58 ± 0.04	
	20.0	0.59 ± 0.09	1.2 ± 0.1	
	24.2	0.49 ± 0.15	2.0 ± 0.2	
	35.0	0.33 ± 0.04	8.5 ± 0.7	

From the temperature dependence of k_4 and (where applicable) k_{-4}, the activation parameters of the reactions were determined by plotting $\ln\{k_i h/k_B T\}$, i = 4 or -4, against T^{-1}. Figure 6.2.5 shows the plots for pyridine. The activation parameters thus obtained are given in table 6.2.3. There is considerable uncertainty in the values of the pre-equilibrium constant, K. It was assumed that a plot of ln K against T^{-1} was linear and ΔH° and ΔS° values were determined from the slopes and intercepts. These values are also listed in table 6.2.3.

Figure 6.2.5 Temperature dependence of (a) k_4 and (b) k_{-4}, for the reaction of pyridine with aquocobalamin.

(a)



(b)

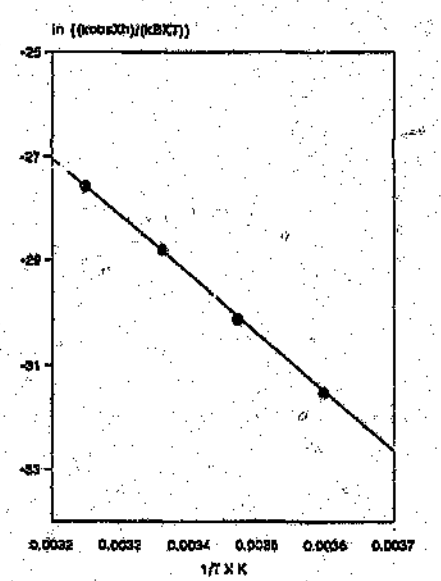


Table 6.2.3 Rate and thermodynamic parameters for the reaction of aquocobalamin with the ligand, L (1 hydroxylamine, 2 methyl glycinate, 3 pyridine, 4 4-methylpyridine, 5 imidazole, 6 histamine).

L	k_4		k_{-4}		K	
	$\Delta H^{\ddagger}$ / kJ mol^{-1}	$\Delta S^{\ddagger}$ / $JK^{-1}mol^{-1}$	$\Delta H^{\ddagger}$ / kJ mol^{-1}	$\Delta S^{\ddagger}$ / $JK^{-1}mol^{-1}$	ΔH° / kJ mol^{-1}	ΔS° / $JK^{-1}mol^{-1}$
1	23 ± 4	-131 ± 12			45 ± 7	139 ± 24
2	60 ± 3	-43 ± 10			10 ± 7	40 ± 22
3	80 ± 2	41 ± 1	95 ± 1	79 ± 3	7 ± 5	33 ± 19
4	78 ± 3	32 ± 9	99 ± 1	81 ± 4	6 ± 1	31 ± 4
5	70 ± 4	19 ± 12			-14 ± 3	-51 ± 9
6	101 ± 4	101 ± 14			-30 ± 2	-106 ± 8

6.3 DISCUSSION

The classical reaction scheme for the ligand substitution reactions of transition metal ions, given in equations 6.1 and 6.2 or 6.5 and 6.6,[9] are challenged by the results observed for the ligand substitution reactions of aquacobalamin with pyridine. The absorbance time traces followed at 362.5 nm were best fitted by a two-exponential expression, in contrast to those traces measured at 351 nm which were best fitted with a single exponential trace. This suggests that at least two kinetically-distinguishable processes are occuring. The faster phase was about three times as fast as the slower phase and usually accounted for about 15% of the total observed signal change. The rate of the slow phase corresponded well with the single rate observed at 351 nm. No analogous effects were

reported for the other five ligands investigated, though here the reactions were only investigated at a single wavelength and thus an analogous effect could have been overlooked.

It is mathematically impossible to distinguish between parallel and consecutive processes;[48] and it is thus possible that we are observing the "slow" formation of some unstable intermediate which then rapidly rearranges to the final equilibrium product. It is also possible that we are observing a parallel process where the approach of the ligand to the metal atom follows at least two kinetically-distinguishable trajectories. Why this process is observable at one wavelength but not another is not clear, but is not particularly surprising since there is a possibility that two closely related compounds could produce UV/VIS spectra which are identical in some regions and distinguishable in others. The ligand substitution reactions of B_{12a} may be more complex than was originally assumed, and the reaction schemes given in equations 6.1 and 6.2 or 6.5 and 6.6 may be, at best, approximations of the events occuring at the molecular level. Further work is required before any real conclusions can be drawn concerning this particular observation.

In any event, the focus of this chapter, to determine whether saturation kinetics can be used to distinguish between a D and an I_D mechanism, can be addressed. For convenience the saturating rate constants for the six ligands investigated were recalculated using the activation parameters in table 6.2.3 and normalised to 25°C in table 6.3.1. It is clear that k_{sat}, and the activation parameters associated with this microscopic rate constant, depend on the identity of L, and thus an I_D mechanism, in which there is nucleophilic participation of the incoming ligand in the transition state, is operable.

Table 6.3.1 Saturating rate constants (k_4) for the reaction of aquocobalamin with the ligand, L, at 25°C; calculated using the activation parameters given in table 6.2.3.

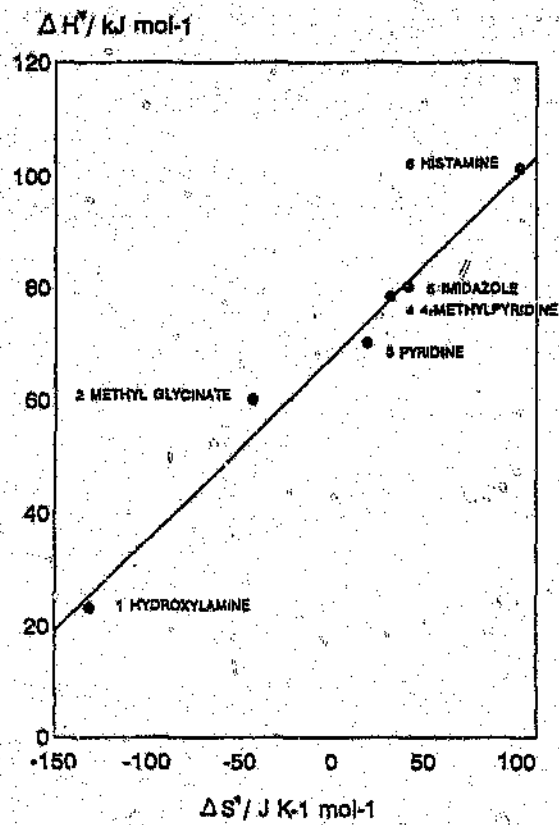
Ligand	k_4 / s^{-1}
methyl glycinate	1
histamine	2.3
4-methylpyridine	6.2
pyridine	8.2
imidazole	33
hydroxylamine	83

Figure 6.3.1 shows that a plot of $\Delta H^{\ddagger}$ against ΔS^{*} for k_4 is a straight line. A similar correlation has been noted for these two quantities for the reaction of aquocobalamin with primary amines[39,40] and thus a compensation effect between the entropy and enthalpy of activation may be a general feature of the ligand substitution reactions of aquocobalamin. This feature has led to the erroneous conclusion that similar rates of reaction are indicative of a D mechanism.

Marques *et al.*[27] showed that the steric bulk of the ligands could be used to explain the increasing order of the saturating rate constants given in table 6.3.1. A reasonable correlation between ΔH^{*} and the ligand cone angle, and ΔH and the molecular volume of the incoming ligand was found. This is not surprising since the β-face of the corrin ring is sterically crowded with the b and c acetamide side-chains of rings A and B, respectively, and the methyl groups at positions 12 and 17 in the C and D rings, respectively, placing four steric pickets in the pathway of a ligand approaching the metal atom. The correlation between steric

bulk and saturating rate constant is further evidence for an I_D mechanism since for a D mechanism the steric bulk of the ligand should have no effect whatsoever on k_{sat}.

Figure 6.3.1 Relationship between $\Delta H^{\ddagger}$ and $\Delta S^{\ddagger}$ for k_4 : 1 hydroxylamine, 2 methyl glycinate, 3 pyridine, 4 4-methylpyridine, 5 imidazole, 6 histamine.



6.4 CONCLUSIONS

The work discussed in this chapter confirms that saturation kinetics can be used to distinguish between a D and an I_D substitution mechanism. It is clear that k_{sat}, and the activation parameters associated with this microscopic rate constant, depend on the identity of L, and thus an I_D mechanism, in which there is nucleophilic participation of the incoming ligand in the transition state, is operable.

7 SATURATION KINETICS TO DISTINGUISH BETWEEN AN I_D AND A D MECHANISM FOR THE SUBSTITUTION OF THE AXIAL WATER MOLECULE IN AQUOHYDROXOCOBINAMIDE BY FIVE LIGANDS

In chapter 6 it was shown that extensive research has been done into the determination of the mechanism by which the axial water molecule in aquocobalamin is substituted by an incoming ligand. Relatively little work has been done on the kinetics of the substitution reactions of DAC/AHC[1,3], despite the obvious similarities between the two systems, and thus the question of whether the substitution of the axial water molecule(s) in DAC/AHC proceeds via a D or an I_D mechanism has still to be broached. Of the few kinetic investigations available in the literature, no mention could be found of the observation of saturation kinetics. The use of saturation kinetics to confirm the I_D mechanism of substitution in aquocobalamin[27] (chapter 6) has indicated that saturation kinetics is a useful tool in mechanistic determinations. In this work, it was hoped that saturation kinetics would be observed in similar reactions with AHC, and that the value of k_{sat}, and its associated activation parameters, thus obtained could be used to differentiate between a D and an I_D mechanism.

7.1 EXPERIMENTAL PROCEDURES

The substitution of a water molecule in AHC by 5 ligands, *viz.*, cyanide, azide, pyridine, N-methylimidazole, and 3-amino-1-propanol, were followed at four temperatures at a single pH. All reactions were studied under pseudo first-order conditions at pH 12.00. As explained in chapter 4, a high pH was used in kinetic and preliminary thermodynamic determinations in order to limit the number of possible labile corrin species in solution. At pH 12.00, the cobinamide is present as DHC or AHC. Only AHC is labile, though the

possibility of biphasic kinetics as a result of the two structural isomers was nevertheless still anticipated. Cobinamide solutions, [AHC] + [DHC] = $2X10^{-5}$ mol dm^{-3}, were buffered with phosphate (0.1 mol dm^{-3}) and adjusted to pH 12.00 at 25.0°C using either NaOH or HCl, where appropriate, and then adjusted to a total ionic strength of 1.00 mol dm^{-3} with KCl for reactions with the neutral ligands, and 2.00 mol dm^{-3} for reactions with the anionic ligands. Ligand solutions (between 7 and 13) varying in concentration between 2 mmol dm^{-3} to 1.0 mol dm^{-3}, were similarly prepared. Reactions, monitored at the same wavelengths as used for the binding constant determination (chapter 4), were followed by mixing equal volumes (100 μ dm^3) of the two solutions using a Hi-Tech Scientific SF-51 stopped flow spectometer (cell pathlength 1.00 cm) interfaced through a DAS-50 A/D board with an IBM-type PC. The experimentally determined rate constants, k'_{obs}, were found by fitting the absorbance/time trace to an equation of the form $A_1\exp(-k'_{obs}t) + A_2$ using a non-linear least squares technique employing a Newton-Raphson procedure. The temperature of the system was maintained (±0.1°C) with a circulating water bath. Subsequent data analysis was by means of either a non-linear least squares technique employing a Newton-Raphson procedure and Marquardt's algorithm, or by standard linear least squares methods.

7.2 RESULTS

In chapter 5 the dependence on pH of the experimentally determined pseudo first-order rate constants, k'_{obs}, for the ligand substitution reaction of AHC with azide was established. Dihydroxocobinamide was confirmed to be inert to substitution. The pH-dependent rate constants can be converted to pH independent rate constants using equation 7.2.1. Table 7.2.1 gives the values of pK_L , the acid dissociation

constants for the ligands used in this work. It is thus clear that at pH 12.00, all ligands are unprotonated. Values of pK_{a2} were determined in chapter 3 (ΔH° = 27 kJ mol^{-1}, ΔS° = -109 J K^{-1} mol^{-1})[31].

$$k_{obs} = k'_{obs}\,(1 + [H^+]/K_L)(1 + K_{a2}/[H^+]) - k'_{obs}\,(1 + K_{a2}/[H^+]) \qquad 7.2.1$$

Table 7.2.1 gives the values of $1 + [H^+]/K_L$, at pH 12.00, for the five ligands investigated. In all cases $1 + [H^+]/K_L$ = 1.00, and hence the approximated version of equation 7.2.1 could be used to convert pH-dependent, k'_{obs}, to pH-independent, k_{obs}, rate constants. Tables 11.5.1 - 11.5.5 in the appendix give the values of k'_{obs} and k_{obs} for the five ligands investigated at each of four different temperatures.

Table 7.2.1 Values of pK_L, the acid dissociation constants of the ligands used in this work, and the calculated values of $1 + [H^+]/K_L$ at pH 12.00.

Ligand	pK_L (25°C)	Ref.	$1 + [H^+]/K_L$
Cyanide	9.04	42	1.001
Azide	4.54	39	1.000
Pyridine	5.25	27	1.000
N-methylimidazole	7.209	43	1.000
3-amino-1-propanol	10.435	41	1.027

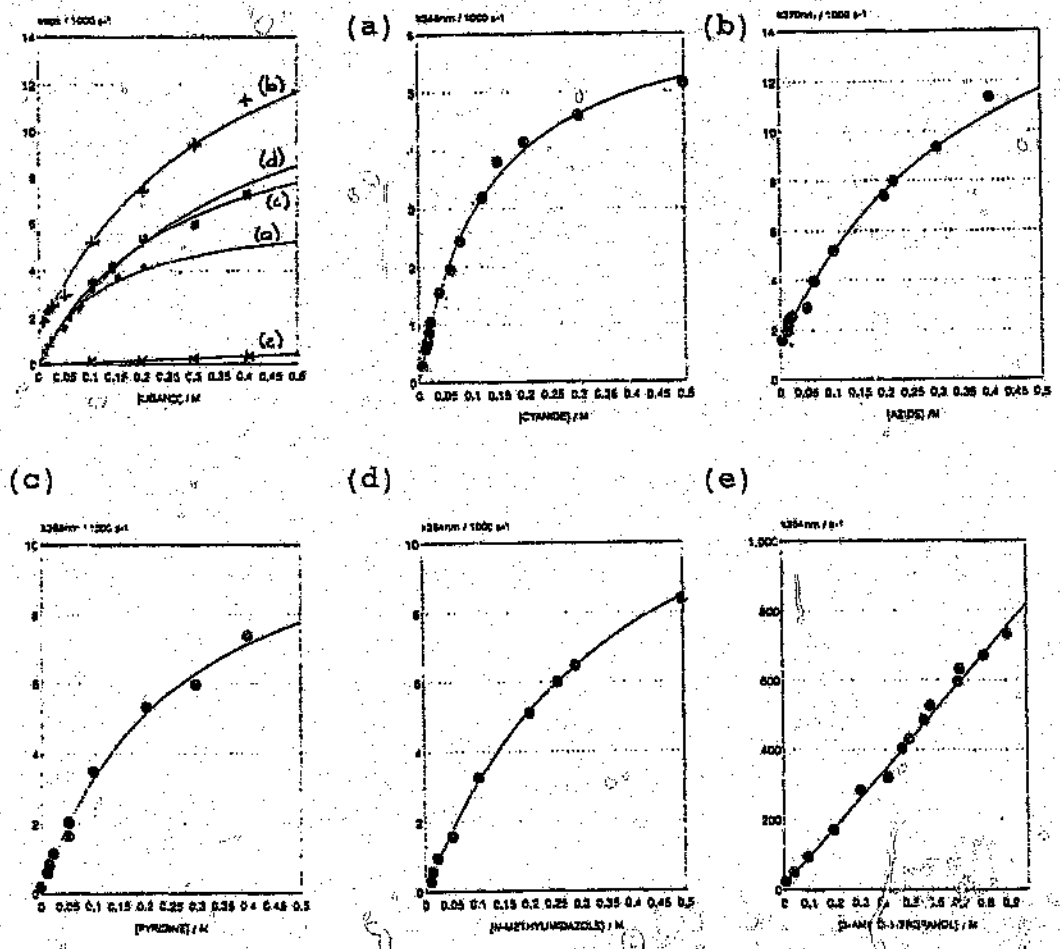
Values of k_{obs}(25°C) for the five ligands investigated are plotted as a function of ligand concentration in figure 7.2.1. Significant curvature is seen for the reactions with cyanide and azide, slight curvature is seen for the reactions with pyridine and N-methylimidazole, and no curvature is seen for the reaction with 3-amino-1-propanol. As was seen for the

reactions with aquocobalamin (chapter 6) the values of k_{sat} appear dependent on the nature of the incoming ligand and thus an I_D mechanism is suggested. The relevant mechanism is then,

$$HO\text{-}Co\text{-}H_2O + L \underset{}{\overset{K}{\rightleftharpoons}} \{\ H_2O\ldots\overset{OH}{\overset{|}{Co}}\ldots L\ \} \qquad (7.2.2)$$

$$\{\ H_2O\ldots\overset{OH}{\overset{|}{Co}}\ldots L\ \} \underset{k_{-4}}{\overset{k_4}{\rightleftharpoons}} HO\text{-}Co\text{-}L + H_2O \qquad (7.2.3)$$

Figure 7.2.1 Plots of k_{obs}(25°C) as a function of ligand concentration for, (a) cyanide, (b) azide, (c) pyridine, (d) N-methylimidazole and (e) 3-amino-1-propanol.



It is clear from figure 7.2.1 that complete saturation is not attainable in the ligand concentration range studied, so that reliable values for the saturating rate constants are difficult to obtain. Higher ligand concentrations could not generally be used. In the case of pyridine and N-methylimidazole, a large signal change was seen to occur on first mixing, an analogous effect having been noted for the reactions of pyridine, 4-methylpyridine and histamine with aquocobalamin in chapter 6. The size of this initial signal increased with ligand concentration. Since the rate of the reaction also increases with ligand concentration, this effect results in the loss of valuable kinetic data for the more concentrated ligand solutions. The origin of this mixing effect is believed to be in the very different refractive indices of the mixed solutions. In the case of cyanide and azide, the rates of the reactions became so fast that the detection limit of the stopped-flow spectrometer (2 ms dead time) was exceeded and meaningful data could no longer be obtained. In the case of 3-amino-1-propanol, a 2 mol dm^{-3} solution (which on mixing leads to a solution 1 mol dm^{-3} in ligand) is close to the solubility limit of the ligand.

As was shown in chapter 6, the microscopic rate constants for this proposed mechanism can be related to k_{obs} using equations 7.2.4 and 7.2.5.

$$k_{obs} = \frac{k_4K[L]}{1 + K[L]} + k_{-4} \qquad (7.2.4)$$

$$k_{obs} = \frac{k_4K[L]}{1 + K[L]} \qquad (7.2.5)$$

For all ligands <u>except</u> azide, fitting equation 7.2.4 to the data resulted in values for the y-axis intercept that were within two standard deviations of the origin, which means that the reverse rate constants (k_{-4}) are very small and equation 7.2.5 is adequate to describe the observed relationship between k_{obs} and the ligand concentrations. For azide, the rate constant for dissociation of the ligand from Co(III) is significant, and hence equation 7.2.4 was used.

The linear plots used to determine the value of k_{sat} in chapter 6 were also used on this data. The relevant equations are,

$$\frac{1}{k_{obs} - k_{-4}} = \frac{1}{k_4 K[L]} + \frac{1}{k_4} \qquad (7.2.6)$$

$$\frac{1}{k_{obs}} = \frac{1}{k_4 K[L]} + \frac{1}{k_4} \qquad (7.2.7)$$

$$\frac{k_{obs} - k_{-4}}{[L]} = -k_{obs}K + (k_4 + k_{-4})K \qquad (7.2.8)$$

$$\frac{k_{obs}}{[L]} = -k_{obs}K + k_4 K \qquad (7.2.9)$$

Again, to prevent small errors in the measurements made at low ligand concentrations skewing the fits of equations 7.2.6 and 7.2.7, only the last 5 - 8 points of each data set (corresponding to the higher ligand concentrations) were used for obtaining values of k_4, whilst the complete data set was used for obtaining the values of K. Equations 7.2.8 and 7.2.9 were fitted to the complete data sets, though the fits

obtained were not generally very good. For the case of azide, the value of k_{-4} obtained from fitting equation 7.2.4 to the data, was substituted into equations 7.2.6 and 7.2.8 in order to obtain alternative values of k_4 and K. Figures 7.2.2 and 7.2.3 below indicate the kind of fits obtained. The values of k_4, k_{-4} and K obtained from these various plots, and their averages, are listed in table 7.2.2

Figure 7.2.2 Plot of k_{obs}^{-1} against $[L]^{-1}$ for the reaction of (a) CN^-, (b) N_3^-, (c) pyridine, (d) N-methylimidazole, and (e) 3-amino-1-propanol with aquohydrokocobinamide at 25°C.

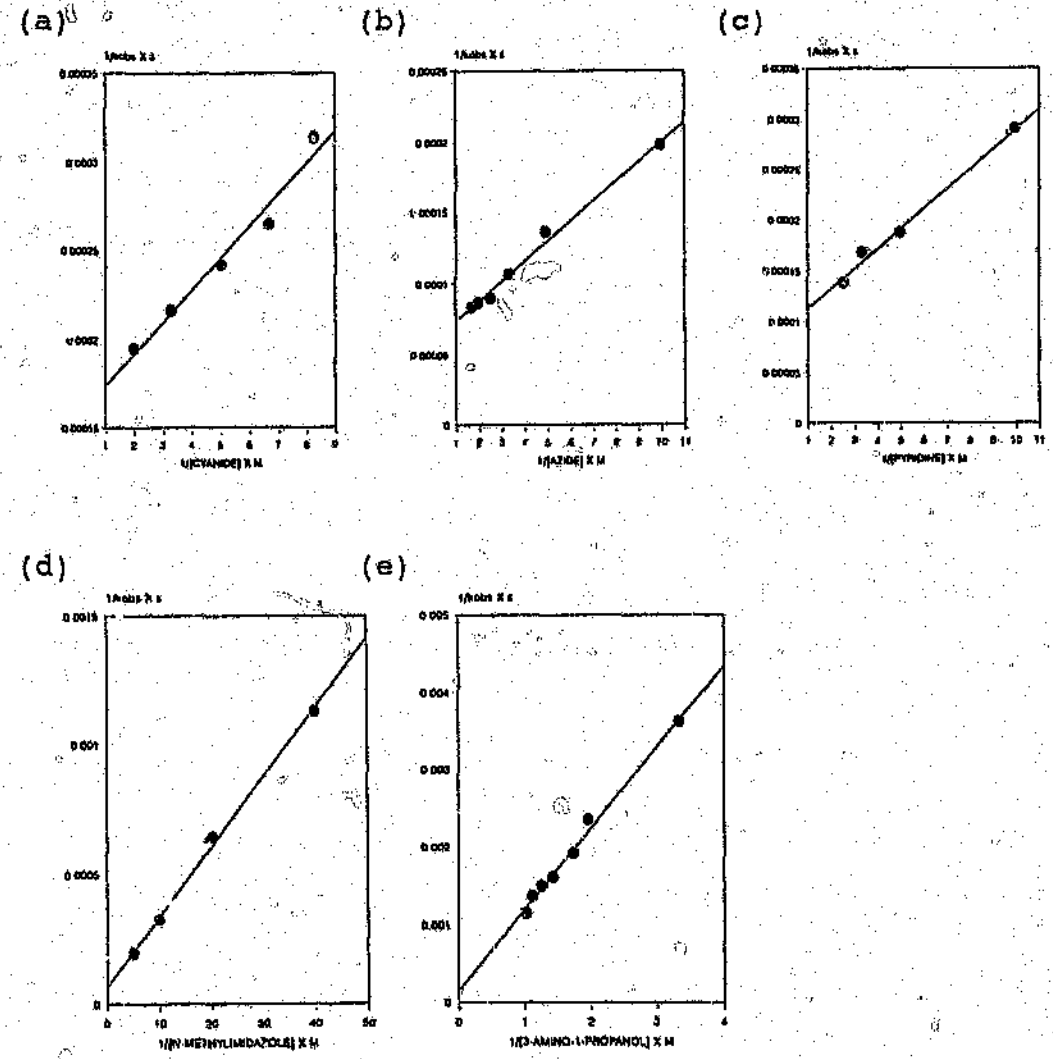


Figure 7.2.3 Plot of $k_{obs}/[L]$ against k_{obs}^{-1} for the reaction of (a) CN^-, (b) N_3^-, (c) pyridine, and (d) N-methylimidazole with aquohydroxocobinamide at 25°C.

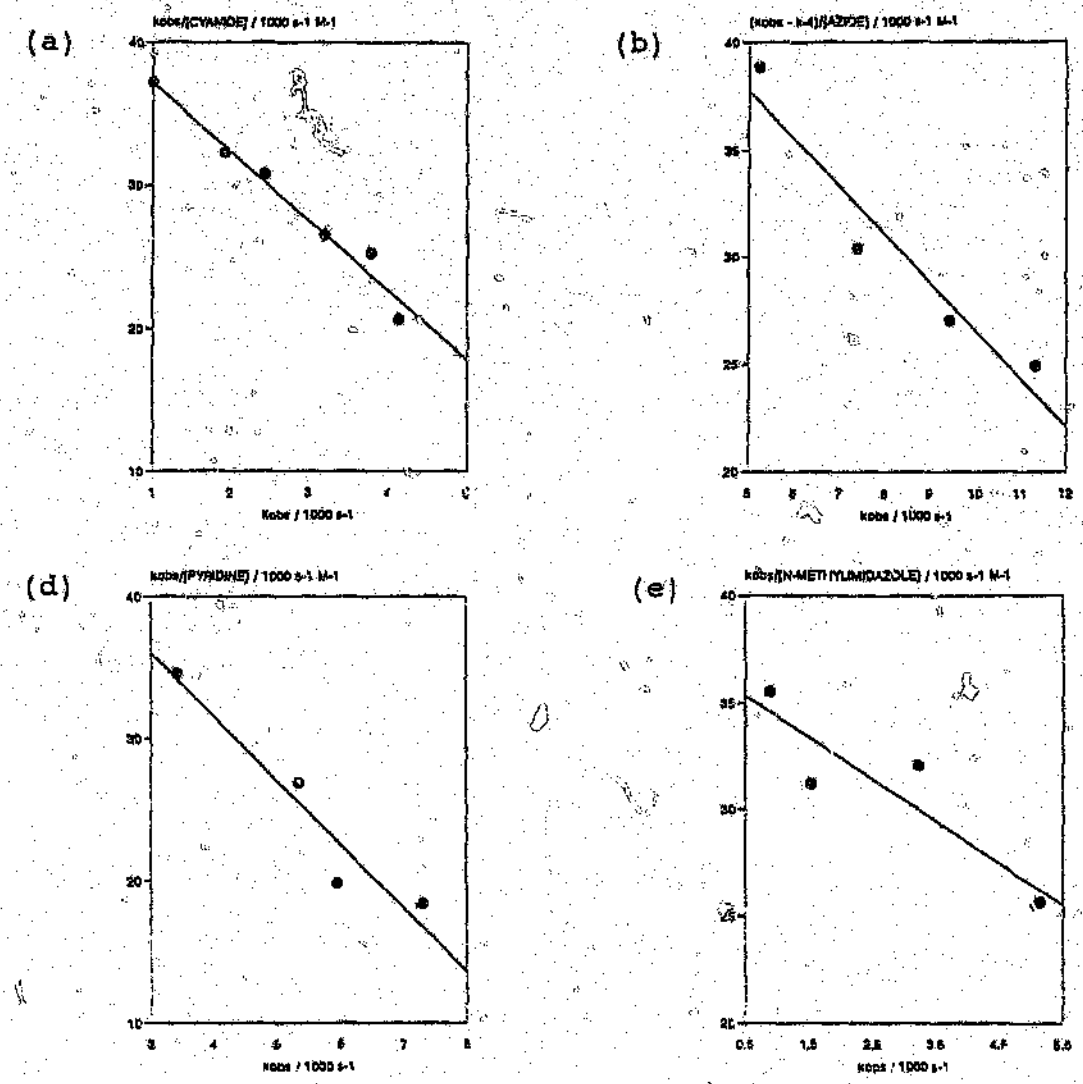


Table 7.2.2 Rate and Equilibrium constants for the coordination of the ligand, L, by aquohydroxocobinamide.

Ligand	Parameter	Temp. / °C	Using Equation	Value	Average
Cyanide	K / $dm^3\ mol^{-1}$	25.0	7.2.5	7.8±0.5	8.9
			7.2.7	9.9±0.3	
			7.2.8	9.1±0.9	
		18.0	7.2.5	7.8±0.4	7.2
			7.2.7	7.6±0.3	
			7.2.8	6.1±1.1	
		12.0	7.2.5	5.9±0.8	4.7
			7.2.7	3.1±0.2	
			7.2.8	5.2±1.2	
		5.0	7.2.5	5.5±0.6	3.9
			7.2.7	1.7±0.3	
			7.2.8	4.4±1.2	
	k_4 X 10^3 / s^{-1}	25.0	7.2.5	6.6±0.2	6.6
			7.2.7	6.9±0.4	
			7.2.8	6.2±0.6	
		18.0	7.2.5	3.9±0.1	5.0
			7.2.7	5.8±0.7	
			7.2.8	5.2±0.4	
		12.0	7.2.5	2.9±0.2	2.9
			7.2.7	2.8±0.3	
			7.2.8	3.1±0.3	
		5.0	7.2.5	1.8±0.2	2.6
			7.2.7	3.4±0.6	
			7.2.8	2.5±0.2	

Table 7.2.2 continued

Ligand	Parameter	Temp. / °C	Using Equation	Value	Average
Azide	K / $dm^3\ mol^{-1}$	25.0	7.2.4	2.7±0.6	3.2
			7.2.6	3.8±0.3	
			7.2.8	3.0±0.6	
		18.0	7.2.4	3.7±1.1	2.8
			7.2.6	2.8±0.4	
			7.2.8	1.8±1.6	
		12.0	7.2.4	6.4±1.8	(5.9)
			7.2.6	5.5±0.5	
			7.2.8	5.8±1.5	
		5.0	7.2.4	1.9±0.5	2.3
			7.2.6	3.4±0.1	
			7.2.8	1.5±0.2	
	k_4 X 10^4 / s^{-1}	25.0	7.2.4	1.8±0.2	1.6
			7.2.6	1.4±0.8	
			7.2.8	1.7±0.1	
		18.0	7.2.4	1.5±0.2	1.3
			7.2.6	1.0±0.8	
			7.2.8	(2.3±0.5)	
		12.0	7.2.4	0.61±0.6	(0.61)
			7.2.6	0.58±0.4	
			7.2.8	0.64±0.7	
		5.0	7.2.4	0.79±0.12	0.75
			7.2.6	0.45±0.4	
			7.2.8	1.0±0.1	
	k_{-4} X 10^2 / s^{-1}	25.0	7.2.4	13.4±2.4	13.4
		18.0	7.2.4	7.1±3.2	7.1
		12.0	7.2.4	2.0±1.5	2.0
		5.0	7.2.4	1.9±0.4	1.9

Table 7.2.2 continued

Ligand	Parameter	Temp. / °C	Using Equation	Value	Average
Pyridine	K / $dm^3\ mol^{-1}$	25.0	7.2.5	4.1±0.6	5.0
			7.2.7	6.1±0.3	
			7.2.8	4.9±0.8	
		18.0	7.2.5	2.3±0.7	4.4
			7.2.7	6.4±0.6	
			7.2.8	4.5±1.4	
		12.0	7.2.5	2.2±0.6	4.0
			7.2.7	5.8±0.5	
			7.2.8	4.1±1.3	
		5.0	7.2.5	3.4±0.6	3.7
			7.2.7	5.4±0.6	
			7.2.8	2.4±0.8	
	k_4 X 10^3 / s^{-1}	25.0	7.2.5	11.5±0.9	10.4
			7.2.7	9.3±2.2	
			7.2.8	10.4±6.0	
		18.0	7.2.5	8.4±1.6	6.4
			7.2.7	4.9±1.6	
			7.2.8	5.8±0.6	
		12.0	7.2.5	6.6±1.0	5.1
			7.2.7	3.9±1.3	
			7.2.8	4.7±0.5	
		5.0	7.2.5	2.1±0.2	1.8
			7.2.7	1.5±0.5	
			7.2.8	1.8±0.2	

Table 7.2.2 continued

Ligand	Parameter	Temp. / °C	Using Equation	Value	Average
N-methyl-imidazole	K / dm^3 mol^{-1}	25.0	7.2.5	2.4±0.5	2.1
			7.2.7	1.7±0.1	
			7.2.8	2.2±0.6	
		18.0	7.2.5	0.91±0.16	(1.0)
			7.2.7	0.92±0.03	
			7.2.8	1.3±0.4	
		12.0	7.2.5	2.1±1.0	1.7
			7.2.7	1.3±0.1	
			7.2.8	(5.4±10.1)	
		5.0	7.2.5	2.0±0.2	1.8
			7.2.7	2.1±0.1	
			7.2.8	1.4±0.5	
	k_4 X 10^3 / s^{-1}	25.0	7.2.5	15.9±2.2	16.6
			7.2.7	(21.8±8.4)	
			7.2.8	17.3±0.7	
		18.0	7.2.5	(23.0±3.5)	(16.8)
			7.2.7	(24.1±11.2)	
			7.2.8	16.8±0.5	
		12.0	7.2.5	5.6±2.5	6.9
			7.2.7	8.1±4.8	
			7.2.8	(2.0±0.6)	
		5.0	7.2.5	3.6±0.3	3.9
			7.2.7	3.1±0.5	
			7.2.8	5.0±0.2	

The plots of k_{obs} versus [3-amino-1-propanol] (Figure 7.2.1) are linear at all temperatures investigated. The slope of this line, if an I_D mechanism is operable, corresponds to k_4K. Table 7.2.3 gives the values of this composite constant, calculated by fitting a straight line to the four data sets.

Table 7.2.3 Values of the composite function, k_4K, for the reaction of 3-amino-1-propanol with aquohydroxocobinamide.

Temperature / °C	k_4K / $dm^3\ mol^{-1}\ s^{-1}$
25.0 ± 0.1	854 (18)
18.0 ± 0.1	501 (9)
12.0 ± 0.1	311 (13)
5.0 ± 0.1	172 (6)

From the temperature dependence of k_4 and (where applicable) k_{-4}, the activation parameters of the reactions were determined by plotting ln $\{k_i h/k_B T\}$, i = 4 or -4, against T^{-1}. The graphs in figure 7.2.4 show these plots and the activation parameters thus determined are listed in Table 7.2.4.

Figure 7.2.4 Plot of ln $\{k_4 h/k_B T\}$ versus T^{-1} for the substitution of a water molecule in AHC by (a) CN^-, (b) N_3^-, (c) pyridine, and (d) N-methylimidazole.

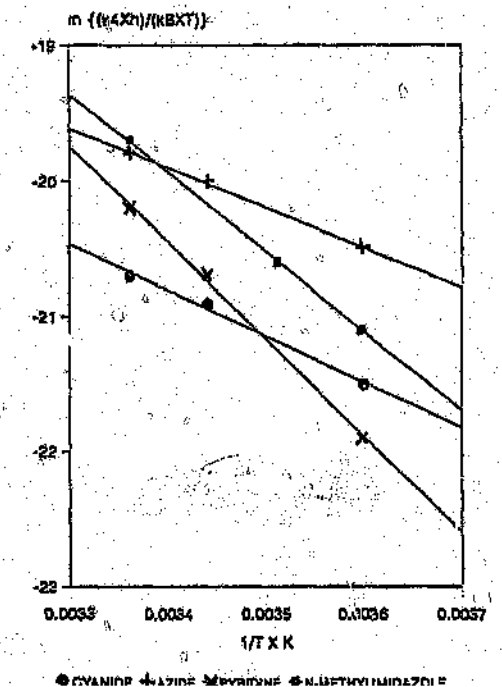


Table 7.2.4 Rate and thermodynamic parameters for the reaction of aquohydroxocobinamide with the ligand, L; 1 cyanide, 2 azide, 3 pyridine, 4 N-methylimidazole, 5 3-amino-1-propanol.

L	Parameter	$\Delta H^{\ddagger}$ / kJ mol^{-1}	$\Delta S^{\ddagger}$ /J K^{-1} mol^{-1}	ΔH° / kJ mol^{-1}	ΔS° /J K^{-1} mol^{-1}
1	k_4	30 (6)	-71 (22)		
	K			26 (5)	-140 (17)
2	k_4	25 (1)	-82 (4)		
	k_{-4}	62 (0)	24 (34)		
	K			10.6 (0.3)	-200 (1)
3	k_4	56 (10)	22 (34)		
	K			8 (1)	-205 (4)
4	k_4	48 (1)	-0.4 (3.4)		
	K			4 (5)	-224 (19)
5	k_4K	52 (2)	12 (6)		

7.3 DISCUSSION

When determining the equilibrium constants for the reaction of azide, pyridine, N-methylimidazole and 3-amino-1-propanol with AHC (chapter 4) only one ligand was found to coordinate to the cobalt atom. In the case of cyanide however, two ligands bound to the cobalt atom to form dicyanocobinamide. The process whose kinetics were measured for all ligands, L, other than CN^-, is thus the replacement of H_2O in AHC by L. This may not be the case for CN^- however. The absorbance/time traces for the substitution of H_2O in AHC by all five ligands investigated could all be fitted using a single exponential function, indicating that only one kinetically distinguishable

process was being followed. It is likely that the two AHC stereoisomers interconvert rapidly and react with the incoming ligands at approximately the same rates. Furthermore, for the case of cyanide, either the second substitution reaction must occur faster than the first so that the rate limiting step in the reaction is the first substitution, or the first substitution is faster than the dead time of the stopped-flow instrument (c. 2 ms). Reenstra and Jencks[49] determined the rate constants for the reaction of CN^- with the two isomers of aquocyanocobinamide. At pH 12.0 Marques[51] determined that the apparent second-order rate constants would then be 2.4×10^5 (α-cyano-β-aquo) and 1.7×10^5 (β-cyano-α-aquo) $dm^3\ mol^{-1}\ s^{-1}$. At pH 12.0 the apparent second-order rate constant for the reaction of AHC is $1.4 \times 10^3\ dm^3\ mol^{-1}\ s^{-1}$. The reaction to produce the intermediate aquocyanocobinamide is thus clearly rate limiting. This is not unexpected since CN^- has a greater thermodynamic *trans*-effect than OH^-,[1] and there is a direct correlation between the thermodynamic and the kinetic *trans*-effects.[14]

Baldwin *et al*[3] found that, in contrast to these observations, kinetic traces of the substitution of H_2O in DAC/AHC by CN^- and $[Co(CN)_6]^{3-}$ were distinctly bi- or even tri-phasic over the whole pH range investigated (4.50 - 12.01 for CN^-, 1.00 - 11.98 for $[Co(CN)_6]^{3-}$). They developed a theory involving the classification and description of equilibrium events into major and minor equilibria. Major equilibria were defined to involve changes in the nature of the axial ligands and their relative orientations, whilst minor equilibria were defined to involve steric, hydrogen bonding and hydrophobic interactions of the corrin and the axial ligands. DAC and AHC were postulated to exist in solution as pH-independent mixtures of 2 or 3 "isomers" and the rate of interconversion between these "isomers" was seen to be small compared to the rate of

reaction with the incoming ligand (and the rate of loss or gain of a proton). These different "isomers" were then the result of different hydrogen bonds between the axial ligand(s) and different side chains or combination of side chains. The slow interconversion of the "isomers" would be due to the slow conformational changes of one or more of the side chains. The isomers were shown to exhibit only slight differences in spectra, pK values and rate constants.

No other record of these "isomers" has been reported. In the determination of binding constants and acid dissociation constants of DAC/AHC (chapter 3,4) no indications of isomers were found, probably because the spectral differences between the various isomers are expected to be very small. Baldwin's[13] observations are similar to those recorded earlier regarding the substitution reactions of aquocobalamin (chapter 6) by pyridine. Changing the wavelength at which the reaction was followed was seen to produce different kinetic traces, with those followed at 351 nm being monophasic, and those at 362.5 nm being biphasic. The ligand substitution reactions of AHC and aquocobalamin thus may well be more complicated than suggested in the reaction scheme above (equations 7.2.2 and 7.2.3). It is nevertheless possible to draw conclusions from the kinetic data concerning the mechanism of these reactions.

No general isokinetic relationship between the values of k_4 for the ligands studied exists, since plots of ln k_4 against T^{-1} (figure 7.3.1) do not intersect at a common point. Although no generally accepted explanation for the origin of isokinetic relationships appears yet to have been advanced they have been taken as indicative of the operation of a single reaction mechanism.[27] The absence of such a relationship may then be further indication of the complexity of these apparently simple reactions.

Figure 7.3.1 Plots of ln k_4 against T^{-1} for the four ligands which showed saturating behaviour in the substitution of H_2O in AHC.

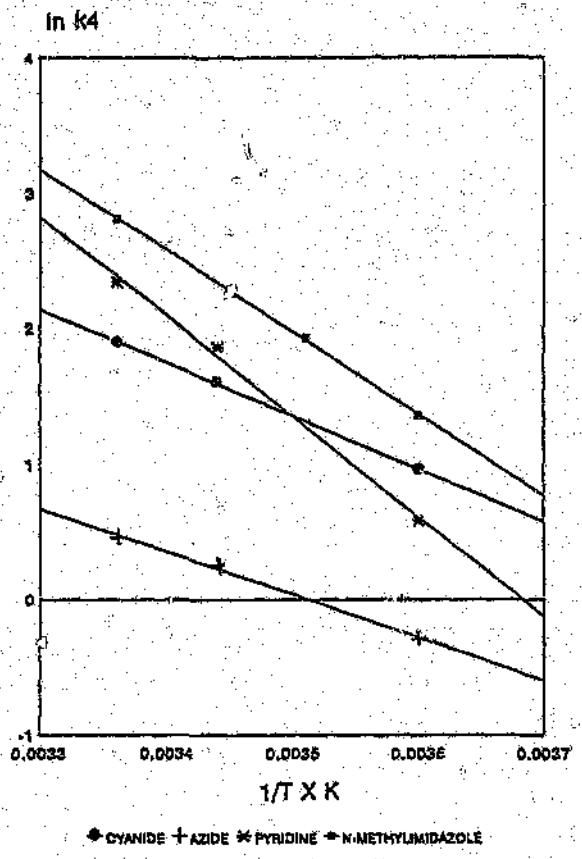


Table 7.3.1 gives the averaged saturating rate constants (25 °C) and activation parameters for the saturating rate constants for the four ligands which exhibited saturating behaviour. Considerable error is associated with the optimised values of k_{sat} because saturation effects were only observed at high ligand concentrations where measurement of the observed rate constant, as explained above, was very difficult. Comparisons between the saturating rate constants of the four ligands certainly does not seem to conclusively point to an I_D mechanism. Comparisons between the activation parameters are

more useful in this case. Real differences in activation parameters for the four ligands are evident, which supports the proposed I_D mechanism.

Table 7.3.1 Averaged saturating rate constants (25°C) and activation parameters for the saturating rate constants for the four ligands which exhibited saturating behaviour.

Ligand	k_{sat} / s^{-1}	$\Delta H^{\neq}$ / kJ mol^{-1}	$\Delta S^{\neq}$ / J K^{-1} mol^{-1}
Cyanide	6.6 X 10^3	30 (6)	-71 (22)
Azide	1.6 X 10^4	25 (1)	-82 (4)
pyridine	1.0 X 10^4	56 (10)	22 (34)
N-methylimidazole	1.7 X 10^4	48 (1)	-0.4 (3.4)

Figure 7.3.2 below shows the existence of a linear relationship between the activation parameters for the different ligands investigated. It should however be borne in mind that a compensation effect, observed in similar kinetic determinations of aquocobalamin[27,41], is not necessarily statistically significant since both quantities are derived from the same data set and are thus not independent.[41] Although there may be other interpretations possible for the compensation effect, we believe that these parameters are a measure of the extent of involvement of the incoming ligand in the transition state of the reaction.

The activation parameters for an I_D mechanism will be critically affected by any nucleophilic participation, however small, of the incoming ligand in the transition state. Such participation is expected to increase with the increasing donor power of the incoming ligand which should manifest as a decrease in $\Delta H^{\neq}$ (as Co-L bond formation compensates for Co-O bond breaking) and a parallel decrease in $\Delta S^{\neq}$ (due to loss of

freedom of motion of the ligand). Considerable bond formation between L and Co thus compensates for the bond breaking between Co and water. This compensation effect thus masks the dependence of k_{sat} on L[27], which could be one of the reasons for the apparent insensitivity of k_4 to L (table 7.3.1).

Figure 7.3.2 Plot of ΔH^* versus ΔS^* for the substitution of H_2O in AHC by the four ligands which exhibited saturating behaviour.

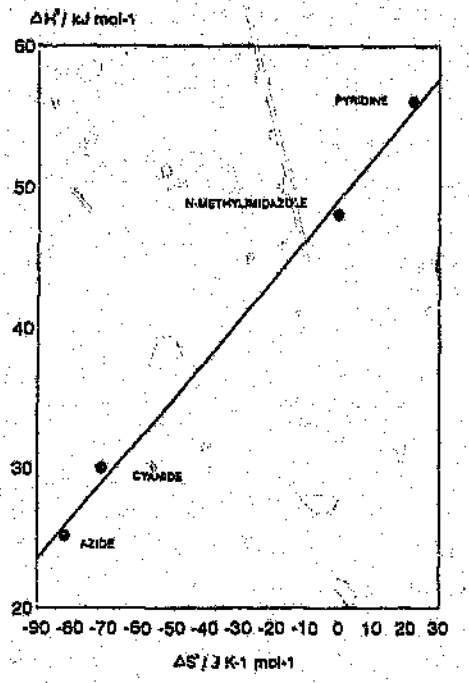


Figure 7.3.2 shows that the four ligands can be divided into two groups, small anionic ligands and aromatics. This suggests that the nature of the incoming ligand is important in determining the magnitude of the saturating rate constant, which indicates that an I_D mechanism is operable. Independence of the activation parameters on the nature of the incoming ligand would be a prerequisite for a D mechanism. The small anionic ligands have smaller activation parameters (i.e. less positive ΔH^* and more negative ΔS^*) than the aromatics,

indicating that their nucleophilic participation in the transition state is greater. The primary amines, represented in this study by the ligand 3-amino-1-propanol, would then constitute a third group which, if the activation parameters for the saturating rate constant could be determined, would presumably be characterised by much larger activation parameters.

Both electronic and steric effects contribute to the success of a ligand as a nucleophile. Marques noted that for the ligand substitution reactions of primary amines with aquocobalamin, a linear relationship between the pK_a of the incoming ligand and the activation parameters of the pH-independent second order rate constant existed.[41] Table 7.3.2 gives a comparison between $\Delta H^{\ddagger}$ of the saturating rate constant and the pK_a of the incoming ligand. Clearly no direct correlation is possible in this case, presumably because two classes of ligands are under investigation here, whereas Marques restricted his analysis to a single class.[41] An analogous inability to draw any conclusions regarding the importance of the role of electronic effects in the similar reactions with aquocobalamin (chapter 6) was noted.

Table 7.3.2 Comparison between the acid dissociation constants of the incoming ligands, here shown as the pK_a, and the ΔH^* for the saturating rate constant for the substitution of water in AHC by this ligand.

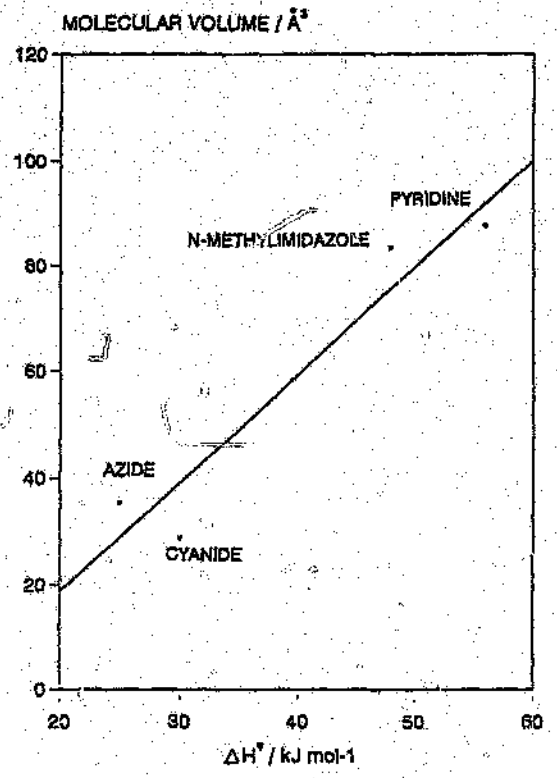
Ligand	pK_a	ΔH^* / kJ mol^{-1}
azide	4.1	25
pyridine	5.25	56
N-methylimidazole	7.21	48
cyanide	9.31	30

The influence of steric effects can be determined by comparing the molecular areas and volumes of the incoming ligands (calculated in chapter 4) with the activation parameters. The results shown in Table 7.3.3 indicate that a fairly good correlation exists between molecular volume and the activation parameters, with a large ΔH^* being associated with the larger ligands and vice versa (figure 7.3.3). A similar correlation was found in the analogous aquocobalamin reactions (chapter 6).

Table 7.3.3 Comparison between the molecular area and volume of the incoming ligands and the ΔH^* for the saturating rate constant for the substitution of H_2O in AHC by this ligand.

Ligand	Molecular area / $Å^2$	Molecular volume / $Å^3$	ΔH^* / kJ mol^{-1}
cyanide	46.3	29.0	30
azide	59.4	35.4	25
N-methylimidazole	112.2	83.4	48
pyridine	110.1	87.5	56

Figure 7.3.3 Plot of molecular volume versus $\Delta H^{\ddagger}$ for the reactions of AHC with the four ligands which exhibited saturating behaviour.



Although steric factors appear to be of considerable importance, an explanation of the observed nucleophilic order is likely to be found in a combination of steric and electronic factors.

7.4 CONCLUSIONS

Problems in acquiring meaningful data at higher ligand concentrations have made the observation of saturation kinetics and comparison between the saturating rate constants of different ligands quite difficult. The manifestation of a

compensation effect between activation parameters results in an apparent only weak dependence of the saturating rate constant on the nature of the incoming ligand, and prevents firm conclusions on the intimate nature of the reaction mechanism being drawn from a simple comparison of rate constants. The significant differences between activation parameters of the saturating rate constants for the various ligands does however argue strongly in favour of an I_D mechanism. Activation parameters were seen to decrease (i.e. less positive ΔH^* and more negative ΔS^*) as the degree of nucleophilic participation by the incoming ligands in the transition state increased. Nucleophilicity is known to be dependent on both steric and electronic factors. Substitution of a water molecule axially bonded to the Co(III) atom of the AHC is thus facilitated when the incoming ligand is negatively charged. The amide side chains on the upper face of the corrin ring, and the propionamide side chains on the lower face, provide some steric hindrance to approaching ligands, and are thus probably responsible for the close relationship between molecular volume of the incoming ligand and the activation parameters.

Both aquocobalamin (chapter 6) and aquohydroxocobinamide are thus seen to undergo substitution reactions via an I_D mechanism. Reensta and Jencks[49] state that the addition of ligands to octahedral metal complexes in aqueous solution proceed predominantly through an I_D mechanism, and thus the results obtained here fulfil these expectations.

Reensta and Jencks[49] indicate that rather special requirements must be met for a second-order type D reaction for cobalamins in aqueous solution. The following reactions apply for a purely D mechanism,

$$HO\text{-}Co\text{-}H_2O \underset{k_{-1}}{\overset{k_1}{\rightleftharpoons}} HO\text{-}Co + H_2O$$

$$HO\text{-}Co + L \underset{k_{-2}}{\overset{k_2}{\rightleftharpoons}} HO\text{-}Co\text{-}L$$

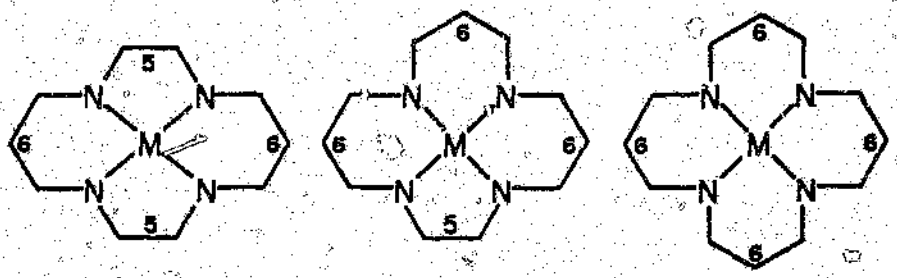
In order for the D mechanism to be favoured over the I_D mechanism the addition of H_2O to the pentacoordinate intermediate (k_{-1}) must be slow compared with the rate of diffusion of the leaving ligand, L, away from the metal's outer coordination sphere(k_{-2}). However, for the reaction to be second order, with rate-limiting addition of the ligand, the addition of H_2O must be fast compared with addition of the incoming ligand. This mechanism will not be common, because water is not an exceptionally reactive ligand towards most metal ions.

8 SYNTHESIS OF MODEL CORRINOID MACROCYCLES

In the introduction to this thesis (chapter 1) it was shown that the cobalt corrinoids exhibit surprising kinetic lability compared to other Co(III) octahedral complexes. The strong *cis*-labilising effect of the corrin macrocycle, a consequence of the delocalised π electrons of the unsaturated conjugated corrin ring, is expected to be largely responsible for this observed lability.[1,7,20] Quantification of this kinetic *cis*-effect requires the comparison of the rates of reaction of a number of sterically similar ligands, which differ only in their degree of unsaturation.

Inorganic synthetic chemists have devised various methods for generating tetraaza macrocycles by the fusion of four-, five-, and/or six-membered chelate rings. Three of the more common ring-size patterns so generated are shown in figure 8.1 below. The 6-5-6-6 and 6-6-6-6 patterns correspond to those of naturally occuring macrocycles, the corrin and porphyrin rings respectively. The large majority of saturated and unsaturated macrocycles with these ring-size patterns have been prepared by metal template reactions in which the metal ion acts as an organising centre around which the ring closure occurs.[10] A disadvantage of this method is that the encycled metal ions are frequently difficult to remove or cannot be removed without the destruction of the macrocyclic ligand.[10] In addition, template cyclizations with aliphatic diamines are dependent on the presence of an activating group (COR or COOR),[52,53] which is undesirable in subsequent oxidative dehydrogenation reactions of the macrocyclic complexes.[53,54] Whilst some nondestructive demetalation reactions for certain macrocycles have been achieved[55,56], a more desirable procedure is the direct synthesis of the desired macrocycle by a nonmetal ion template route.

Figure 8.1 Schematic representation of the 6-5-6-5, 6-5-6-6, and 6-6-6-6 ring size patterns.

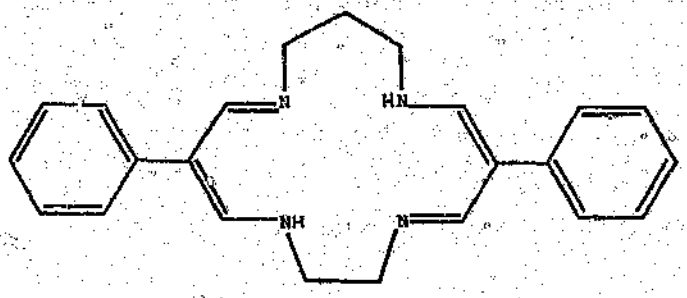


Holm et.al. have done substantial work into the development of a synthetic procedure affording 12-π macrocycles in a form such that the desired metal complexes can be prepared and subjected to oxidative dehydrogenation reactions affording 14-π to 16-π species.[10,11] Two such macrocycles, shown in figure 8.2 below, were of interest to this research group. Both macrocycles have a [15]aneN$_4$ ring structure, with the second macrocycle (b) mimicing the 14-π corrin ring nucleus, though both models are devoid of the supporting pyrroline rings found in vitamin B$_{12}$.

Figure 8.3 below compares the UV/VIS spectra of [Co(Ph$_2$[15]hexaenatoN$_4$)(CN)$_2$] and dicyanocobalamin in a common solvent. The spectra exhibit a near band-for-band correspondence, with the three features in the α - β spectral region strikingly similar in band contours and intensities, which supports the existence of a chromophore of the corrinoid type in this model compound.

Figure 8.2 Model corrinoid macrocycles for invesigation of the corrin *cis*-effect.

(a) Ph_2[15]tetraenatoN_4



(b) Ph_2[15]hexaenatoN_4

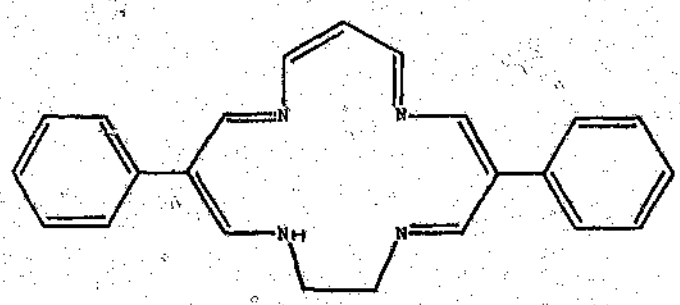
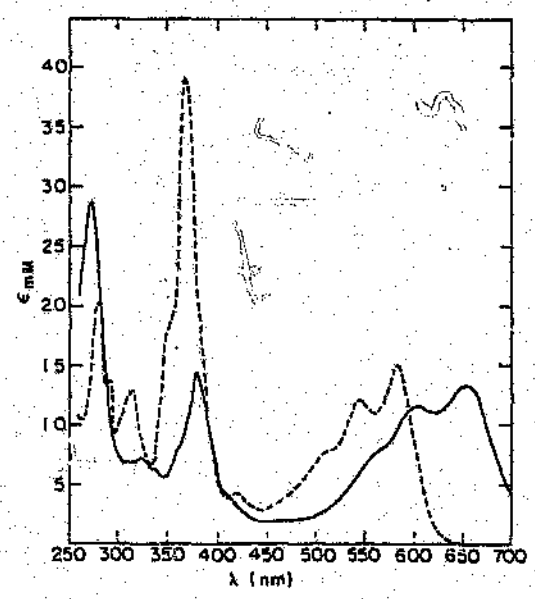


Figure 8.3 Electronic spectra of [Co(Ph_2[15]hexaenatoN_4)$(CN)_2$], ——, and dicyanocobalamin, ---, in 9:1 v/v DMSO-H_2O.[11]

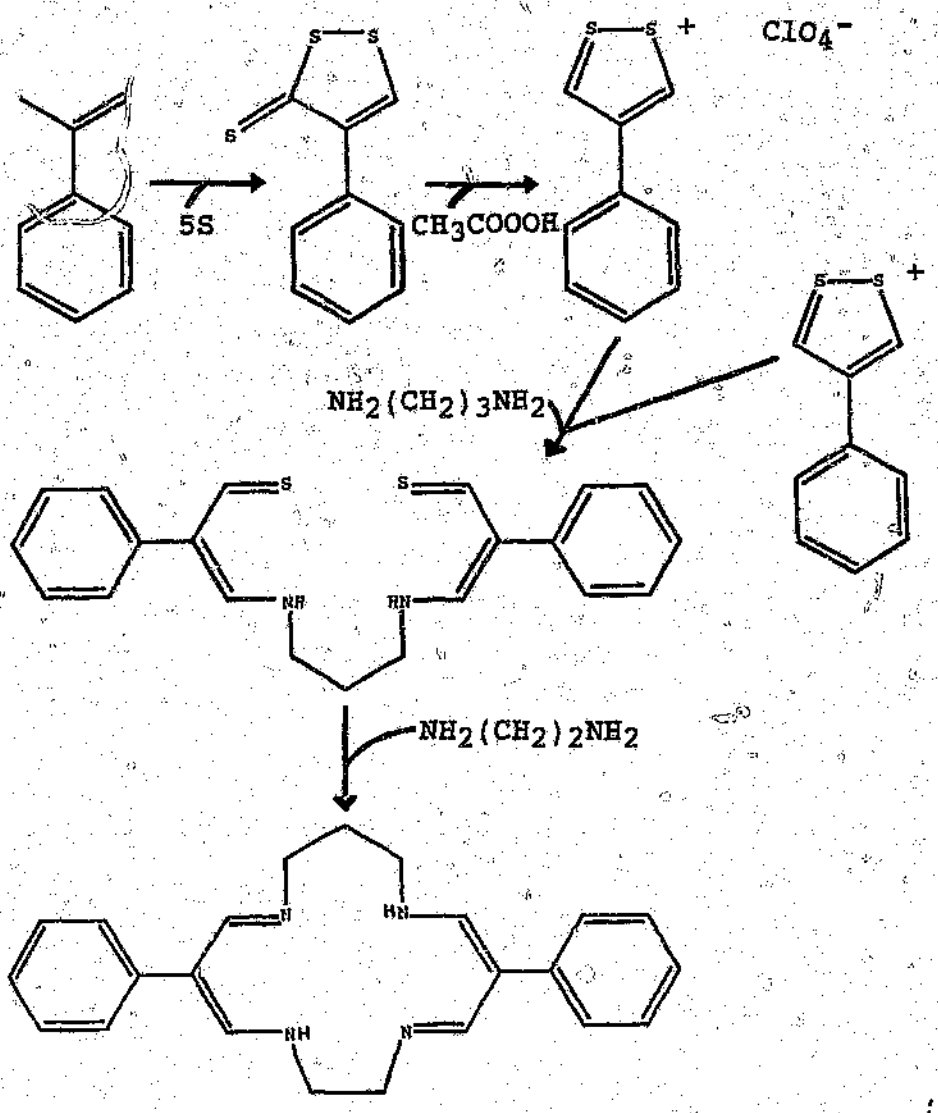


This chapter describes the use of Holm's nonmetal ion template synthesis[10,11] to prepare the the two model macrocycles indicated above in figure 8.2. It was intended that these model macrocycles would be used in an investigation of the importance of the degree of π-unsaturation of the macrocycle on the lability of the Co(III) macrocycles. The rate of substitution of water in these Co(III) complexes by a probe ligand would be compared with those values already obtained for the same reaction with AHC. Both macrocycles have the [15]aneN_4 skeleton, typical of the corrin family of molecules, but they differ in the degree of unsaturation of the macrocycle, and hence were assumed to be good probes for a study of the *cis*-effect.

8.1 SYNTHESIS OF Co(III) 6,14-diphenyl-1,4,8,12-tetraaza-cyclopentadeca-4,6,12,14-tetraene, $[Co(Ph_2[15]tetraenatoN_4)]^+$.[10,11]

Figure 8.1.1 below indicates the route by which the synthesis of Ph_2[15]tetraenatoN_4, by Holm's[10,11] nonmetal ion template synthesis, was achieved. This method exploits the electrophilic reactivity of the 1,2-dithiolium cation and vinylogous β-amino thiones with primary amines. The reaction of the 4-phenyl-1,2-dithiolium cation with trimethylenediamine yields the precursor bis(β-aminothione). This compound is then cyclized by a second equivalent of diamine, ethylenediamine this time, giving the 15-membered macrocycle, Ph_2[15]tetraenatoN_4, in low yields.

Figure 8.1.1 Representation of the synthetic route by which Ph_2[15]tetraenatoN_4 was synthesised.



Synthesis of 4-phenyl-1,2-dithiole-3-thione. (I)[46]

Fields reported that cumenes react with sulphur at atmospheric pressure in the presence of catalytic amounts of base to give good yields of 4-aryl-1,2-dithiole-3-thiones.[46] The postulated mechanism of this reaction involves the conversion of cumenes to α-methylstyrenes, which in turn react rapidly with sulphur to give dithiolethiones. The dithiolethione required here was thus prepared directly from α-methylstyrene.[47] Flowers of sulphur, 19.1708 g (0.598 mol) (BDH), and 0.4009 g (1.65 mmol) di-o-tolylguanidine (Aldrich) were dissolved in 90 ml freshly distilled mesitylene and refluxed at ~165°C. α-Methylstyrene, 50.00 ml (0.385 mol) (Aldrich) was added dropwise to the refluxing solution over 8 hours. Hydrogen sulphide was steadily evolved during this reaction. The solution was left to reflux for a further 13 hours. The flask was plunged into an ice bath, whereupon crystals could be seen forming from the deep red viscous, pungent mother liquor. After the mixture was kept chilled for several hours, the red crystals were filtered off, and recrystallised twice from a solution containing 60 ml benzene / 40 ml hexane. A 55% yield, based on sulphur, of the recrystallised product, 13.8333 g (0.0659 mol), was obtained. The red crystals were characterised by NMR (appendix 11.6), assignments in table 8.1.1 below. Their melting point was measured to be between 122-123°C, which compares well with the reported value of 122°C.[46]

Table 8.1.1 Assignments for the peaks in the NMR spectrum of 4-phenyl-1,2-dithiole-3-thione in deuterated acetone.

Proton	Chemical Shift / ppm	Splitting
phenyl protons	7.4121 - 7.4719 7.5875 - 7.6363	two multiplets
heterocyclic proton	9.0056	singlet

Synthesis of 4-phenyl-1,2-dithiolium hydrogen sulphate. (II)[47]

4-Phenyl-1,2-dithiolium salts can be prepared by peracetic acid oxidation of the corresponding 4-phenyl-1,2-dithiole-3-thione.[47] When an acetone solution of 4-phenyl-1,2-dithiole-3-thione is treated with three mole equivalents of peracetic acid, an 85 - 90% yield of the acid sulphate of the corresponding 4-phenyl-1,2-dithiolium salt is reported to rapidly crystallize out of solution. The success of the reaction depends upon the insolubility of dithiolium sulphates in acetone, since the dithiolethione system is known to be destroyed by hydrogen peroxide oxidation. Whilst the acid sulphates are freely soluble in water, the perchlorate salt is water insoluble.

The explosive nature of peracetic acid makes its transport, and hence ready availability, difficult. Peracetic acid was thus prepared[48] *in situ* by mixing a vigorously stirred solution of 5.0 ml 30% H_2C_2 (Saarchem) and 23.0 ml acetic anhydride (Merck) in a beaker maintained at 40°C for 4 hours.

The solution was then stored at 5°C. The concentration of peracetic acid was not determined, but was assumed to be about 1 mol dm^{-3}.[18]

The dithiolium cation (I), 9.0178 g (0.0429 mol), was dissolved in 200 ml freshly distilled acetone using gentle warming. The solution was stirred in an ice-bath while 130 ml of freshly prepared peracetic acid was added over 15 minutes. (In order to prevent crystallization of the starting material, the addition of peracetic acid was begun before the solution was thoroughly chilled.) The product, which is insoluble in acetone, separated out as fine yellow crystals. The mixture was stirred for a further 10 minutes in the ice bath, filtered and washed with a little cold acetone. A 50 % yield of the hydrogen sulphate product, 5.8884 g (0.0213 mol), was obtained. Addition of more peracetic acid to the chilled supernatant yielded a further 2.0361 g (7.37 mmol) product, indicating that the peracetic acid prepared was less concentrated than that which was predicted.

The 1,2-dithiolium cation may be regarded as a resonance hybrid of two equivalent sulphonium ions. An NMR spectrum (appendix 11.6), assignments in table 8.1.2 below, of the product has two peaks in the ratio 2:5, which shows the equivalence of the two hetero ring protons against the phenyl protons. This indicates that the two resonance hybrids of the 1,2-dithiolium cation are equivalent. The crystals' melting point was measured to be between 231-232°C, which compares well with the literature value of between 230-232°C.

Table 8.1.2 Assignments for the peaks in the NMR spectrum of 4-phenyl-1,2-dithiolium hydrogen sulphate in D_2O.

Proton	Chemical Shift / ppm	Splitting
phenyl protons	7.5741 - 7.7806 7.7933 - 7.8110	two multiplets
heterocyclic protons	10.5818	singlet

The pale yellow hydrogen sulphate salt was dissolved in 100 ml deionised water. Excess ammonium perchlorate, ~ 6 g (Aldrich) was added. A burnt orange crystal, the perchlorate salt of the dithiolium product, crystallized out instantly in quantitative yields.

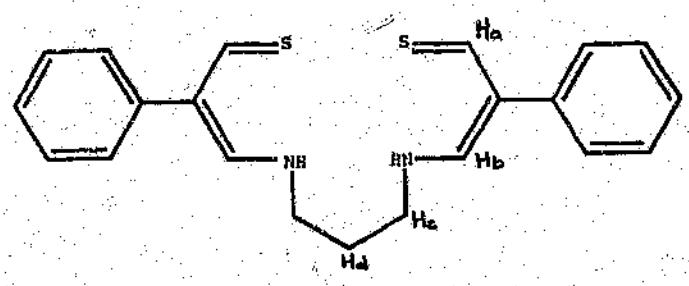
Synthesis of N,N'-Bis(2-thioformyl-2-phenylvinyl)trimethylenediamine. H_2[SHPhHtn] (III)[10]

The electrophilic reactivity of the 1,2-dithiolium cation is exploited in this synthesis.[10,11,47] The dithiolium perchlorate (II), 5.4242 g (0.0195 mol), was suspended in 65 ml benzene at room temperature. Trimethylenediamine, 1.80 ml (0.036 mol) (Aldrich), dissolved in 10 ml benzene, was added dropwise over 20 minutes with vigorous stirring. The suspension was warmed to 70°C. The red-orange solution was decanted from the dark red oil residue and allowed to cool. Approximately 2/3 of the solvent was removed by rotary evaporation and the flask was left overnight at 5°C. The yellow crystals which had formed overnight were filtered off, washed with anhydrous ether, and recrystallised twice from benzene. A 17% yield based on the dithiolium, 0.6380 g (1.70

mmol), was achieved. An NMR spectrum (appendix 11.6) of the product, assignments in table 8.1.3 below, confirmed its identity. Microanalysis of the product indicated : [Element, Experimental (Theoretical)] %C, 68.49 (68.81); %N, 7.57 (7.64); %H, 5.99 (6.05).

Table 8.1.3 Assignments for the peaks in the NMR of H_2[SHPhHtn] in deuterated acetone. The positions of the protons (a-d) in the H_2[SHPhHtn] molecule are shown in a schematic representation of the molecule below the table. The signal due to the amine proton is expected at a chemical shift > 10.5.[10]

Proton	Chemical Shift / ppm	Splitting
phenyl protons	7.1744 - 7.2994 7.3115 - 7.3554	two multiplets
H_a	7.9717 - 8.0539	doublet of doublets
H_b	10.1197 - 10.1354	doublet
H_c	3.8155 - 3.8814	doublet of triplets (apparent quartet)
H_d	2.1861 - 2.3233	quintet

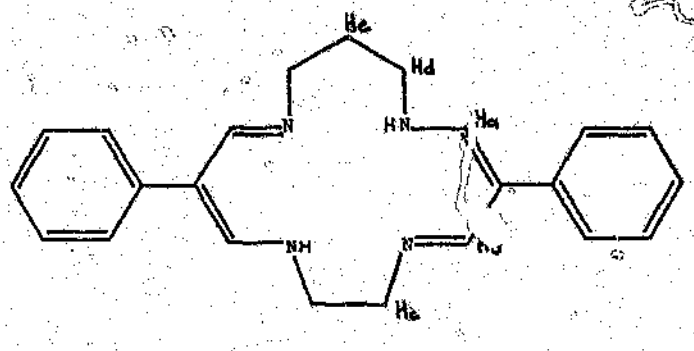


Synthesis of 6,14-Diphenyl-1,4,8,12-tetraazacyclopentadeca-4,6,12,14-tetraene. Ph_2[15]tetraenatoN_4 (IV)[10]

H_2[SHPhHtn], 0.1410 g (0.385 mmol), was dissolved in 10 ml vigorously stirred benzene at 45°C. Ethylenediamine, 26μl (Aldrich), dissolved in 2 ml benzene, was added drpowise over 1 hour. The solution was decanted from the remaining solid residue and evaporated down to dryness. The yellow crystals were recrystallised twice from a 1:1 mixture of chloroform/methanol. A 10% yield, based on H_2[SHPhHtn], 0.0138g (0.039 mmol), was achieved. An NMR spectrum of the product (appendix 11.6), assignments in table 8.1.4 below, confirmed its identity. Holm *et al*[10] indicated that they obtained a mixture of products, Ph_2[15]tetraenatoN_4 and Ph_2[14]tetraenatoN_4. These molecules were separated using fractional recrystallisation from chloroform/methanol. In this synthesis the quantities of product obtained precluded such an operation. It is thus probable that the yellow crystals obtained represent a mixture of these two compounds. Microanalysis of the product indicated : [Element, Experimental (Theoretical)] %C, 77.35 (77.06); %N, 15.51 (15.63); %H, 7.14 (7.31).

Table 8.1.4 Assignments for the peaks in the NMR of H_2[HPhH(en)(tn)] in deuterated acetone. The positions of the protons (a-d) in the Ph_2[15]tetraenatoN_4 molecule are shown in a schematic representation of the molecule below the table. The signal due to the amine proton is expected at a chemical shift > 9.0.[10]

Proton	Chemical Shift / ppm	Splitting
phenyl protons	7.0580 - 7.0885 7.2472 - 7.2828	two multiplets
H_a , H_b	7.7032 - 7.7926	doublet of doublets
H_c	3.5867	singlet
H_d	3.6470 - 3.7015	multiplet
H_e	1.9573 - 1.9745	multiplet



Insertion of the Cobalt(II) Metal Ion. Co(Ph_2[15]tetraenatoN_4) (V)[10]

Ph_2[15]tetraenatoN_4, 0.0069g (0.019 mmol), was dissolved in 3 ml DMF. The vigorousy stirred solution was heated to 80°C under nitrogen for 0.5 hours. Cobaltous actetate, 0.0048g (41 μmol) (Saarchem), was added to the solution. The solution was left stirring at 80°C under nitrogen for another 0.5 hours. During this time the pale yellow solution turned red/pink. The flask was stored in the fridge overnight during which time the solution turned orange. Opening the flask to the air accelerated this colour change. It was hoped that this represented a change in the oxidation state of the cobalt atoms from II to III. A UV/VIS spectrum of the solution, however, indicated that the primary change was a degradation of the macrocycle. Holm *et al*[15] similarly reported that the Co(II) macrocycle was unstable in solution in air.

8.2 SYNTHESIS OF Co(III) 6,14-diphenyl-1,4,8,12-tetraazacyclopentadeca-4,6,8,10,12,14-hexaene, Co(Ph_2[15]hexaenatoN_4)$^{2+}$.[11]

Holm *et al*[19] reported that Cu(II), Ni(II), and Co(II) complexes of 14-, 15-, and 16-membered macrocyclic rings undergo oxidative dehydrogenation reactions with 2,3-dichloro-5,6-dicyano-*p*-benzoquinone (DDQ) affording complexes with increased π-unsaturation. It was intended to use this method to produce a more unsaturated form of (IV) (see figure 8.2 (b)). Since the synthesis of Co(Ph_2[15]tetraenatoN_4) was unsuccessful however, this synthesis could not be attempted.

8.3 DISCUSSION

Tang and Holm[11] reported their interest in producing a 14-π 15-membered tetraaza macrocyclic system similar to that present in the basic corrin unit. They were able to produce the Cu(II), Ni(II), and Co(II) complexes of the Ph_2[15]tetraenatoN_4 macrocycle, and the Cu(II) and Ni(II) complexes of the Ph_2[15]hexaenatoN_4 macrocycle. The Co(II) Ph_2[15]tetraenatoN_4 macrocycle was however reported to be unstable in air. It was hoped that the instability referred to was simply a change in oxidation state of the Co(II) to Co(III). However, when this instability was similarly noted in this work, UV/VIS analysis made it clear that the ligand itself decomposed rapidly in air.

Tang and Holm[11] reported that the low-spin Co(II) complex of Ph_2[15]tetraenatoN_4 is readily oxidized by iodine in the presence of pyridine to afford in good yields the corresponding transdipyridine Co(III) complex, isolated as an iodide salt. Reaction of Co(Ph_2[15]tetraenatoN_4) with DDQ in benzene followed by addition of aqueous sodium cyanide to an ethanol solution of the isolated reaction product afforded the neutral red crystalline dicyano complex [Co(Ph_2[15]hexaenatoN_4)(CN_2] in moderate yields. A similar reaction of Co(Ph_2[15]pentaenatoN_4) with excess DDQ in benzene followed by treatment with pyridine and $NaPF_6$ in ethanol produced the $[Co(Ph_2[15]hexaenatoN_4)(py)_2]^{2+}$ cation. The synthesis of both [Co(Ph_2[15]hexaenatoN_4)(CN_2] and $[Co(Ph_2[15]hexaenatoN_4)(py)_2]^{2+}$ were performed under anaerobic conditions. The quinone thus appears to effect both 12π to 14π ligand oxidative dehydrogenation and Co(II) to Co(III) oxidation in the presence of ligands (*i.e.* py, CN^-) capable of stabilizing the higher metal oxidation state.

These results suggest that with suitable variation of the axial ligands and the cobalt atom's oxidation state, the cobalt model complexes could still serve as useful vehicles in B_{12} model systems. These observations were not however pursued here, since the overall aim of this synthetic work, to produce model macrocycles for comparative kinetic determinations, requires the production of the relevant diaquo-complexes. Comparitive studies between dicyanocobinamide and the model dicyano-complex could nevertheless still yield some interesting results.

8.4 CONCLUSIONS

Whilst the synthesis of the Ph_2[15]tetraenatoN$_4$ macrocycle was succesful, the insertion of the metal into the macrocycle was not, and hence the subsequent oxidative dehydrogenation to Co(Ph_2[15]hexaenatoN$_4$) could not be attempted. The aim of this synthetic work was hence not achieved, and Holm's[10,11] model compounds were proven unsuitable for the applications we required. Alternative model compounds are thus required for this work.

9 CONCLUSIONS

In chapter 1 the primary aims of this project were defined as,

(1) to elaborate on the data supporting a kinetic and thermodynamic *trans*-effect in the cobalt corrinoids, with particular reference to DAC/AHC,
(2) to determine the relationship between the degree of macrocyclic unsaturation and the kinetic *cis*-effect.

In order to realise these primary aims a list of secondary aims can be also compiled,

(1) to synthesise DAC,
(2) to determine the thermodynamic parameters for the two deprotonation equilibria of DAC,
(3) to determine the mechanism by which an axial water molecule of DAC/AHC is substituted by an incoming ligand,
(4) to synthesise model compounds suitable for a subsequent investigation of the macrocyclic *cis*-effect

Of these four secondary aims, only the first three were achieved. The instability of the synthesised model compounds[10,11] in air made them unsuitable for use in the investigation of the macrocyclic *cis*-effect, and hence prevented realisation of the second of the primary aims of this thesis. Alternative model macrocycles are thus required. Achievement of the first primary goal, elaborated on below, was however successful.

DAC was successfuly synthesised from cyanocobalamin via the intermediate Factor B using Brown's unpublished method.[29] At best, using HPLC peak integration, a yield of 93% was recorded, and at worst a yield of 75%. Stable yellow corrinoid production during and after the synthesis appears to be unavoidable, though degradation can be minimised by freezing DAC samples under an inert atmosphere in containers shielded from light.[3,5,29] Brown's

method appears to be superior to the other two reported methods. Photolysis of Factor B produces DAC in 85% yields,[29] whilst photolysis of methylcobinamide produces DAC in only 70% yields.[3] Since DAC is known to be susceptible to radiation degradation, it is not surprising that a synthetic method which does not require sample irradiation should be superior to techniques which do.

In-cell spectrophotometric titrations of DAC at two different wavelengths were used to determine the thermodynamic parameters for the two deprotonation equilibria of DAC. Thermodynamic parameters for the first equilibrium (DAC $\rightleftharpoons$ AHC + H^+) were calculated to be, ΔH° = 44 kJ mol^{-1} and ΔS° = -35 J K^{-1} mol^{-1}. The value for pK_{a1} at 25°C, calculated from these thermodynamic parameters, compares well with other published results.[5,3] The value of pK_{a2} at 25°C, calculated from the thermodynamic parameters for the second equilibrium (AHC = DHC + H^+), does not however compare well with other published results[5,3] or with results obtained by other members of this research group.[31] The most likely cause for the discrepencies in the pK_{a2} values is experimental error associated with the pH measurements during these titrations. Thermodynamic parameters for the second equilibrium were then obtained from Marques[31] : ΔH° = 27 kJ mol^{-1} and ΔS° = -109 J K^{-1} mol^{-1}.

Binding constants of AHC (pH 12.00) with five selected ligands : cyanide, azide, pyridine, N-methylimidazole and 3-amino-1-propanol were determined by in-cell spectrophotometric titrations at 25°C. Comparison of the calculated unconditional binding constants with available data on DAC, aquocobalamin and Factor B (*i.e.* the *trans*-ligands H_2O, dmbzm and CN^-) confirmed the *trans*-effect order, H_2O < dmbzm < OH^- < CN^-.[1,14] A combination of both steric and electronic effects were considered

in an attempt to rationalise the observed order of binding constants of the ligands to AHC : azide < pyridine < 3-amino-1-propanol < N-methylimidazole < cyanide.

A controversy concerning the intimate mechanism of the substitution reactions of aquocobalamin has existed for some time.[14,22-26] Marques *et al.* observed that saturation kinetics could be used to distinguish between a D and an I_D mechanism when a series of ligands showing saturating behaviour are compared.[27] The dependence of k_{sat} and its activation parameters on the nature of the incoming ligand confirmed that an I_D mechanism is in fact operable.

The same approach was then used in an analogous study using AHC (pH 12.00). Preliminary data on the relationship between pH and the observed second order rate constants for the substitution of H_2O by HN_3/N_3^- confimed that DHC is substitutionaly inert.[3] The equation derived to explain this relationship fitted the high pH data well, but not the low pH data. The values of pK_{azide} and pK_{a1} were elevated substantialy in order to achieve a good fit of the derived equation to the data. No reason for such an elevation could be found and no precedent exists in the literature. The low-pH data certainly requires further investigation.

Saturation kinetics were observed for the substitution of water in AHC (pH 12) by four of the five selected ligands : cyanide, azide, pyridine, and N-methylimidazole. No saturation kinetics were observed for the ligand 3-amino-1-propanol over the ligand concentration range (up to 1.0 mol dm^{-3}) investigated. Problems in acquiring meaningful data at higher ligand concentrations made the observation of saturation kinetics and comparison between the saturating rate constants of different ligands quite difficult. Furthermore, the manifestation of a compensation effect between the activation parameters results in an apparent only weak dependence of k_{sat} on the nature of the incoming ligand, and

prevents firm conclusions on the intimate nature of the reaction mechanism being drawn from a simple comparison of saturating rate constants. Significant differences between the activation parameters of k_{sat} for the various ligands does however argue strongly in favour of an I_D mechanism. Activation parameters were seen to decrease (*i.e.* less positive ΔH^* and more negative ΔS^*) as the dgree of nucleophilic participation by the incoming ligands in the transition state increased. Both electronic and steric factors were shown to be important in determining the nucleophilicity of the incoming ligand.

10 REFERENCES

10.1 J.M.PRATT, *Inorganic Chemistry of Vitamin B_{12}*, Academic Press, London, 1972

10.2 R.A.FIRTH, H.A.O.HILL, J.M.PRATT, and R.G.THORP, *J.Chem.Soc.(A)*, 1968, 453.

10.3 D.A.BALDWIN, E.A.BETTERTON, and J.M.PRATT, *J.Chem.Soc.Dalton Trans.*, 1983, 217.

10.4 R.A.FIRTH, H.A.O.HILL, J.M.PRATT, R.G.THORP, and R.J.P.WILLIAMS, *J.Chem.Soc.(A)*, 1968, 2428.

10.5 S.H.FORD, A.NICHOLS, and M.SHAMBEE, *J.Inorg.Biochem.*, 1991, **41**, 235.

10.6 W.H.PAILES, and H.P.C.HOGENKAMP, *Biochem.*, 1968, **7**, 1160.

10.7 E.B.FLEISCHER, S.JACOBS, and L.MESTICHELLI, *J.Am.Chem.Soc.*, 1968, **90**, 2527.

10.8 G.N.SCHRAUZER, *Acc.Chem.Res.*, 1968, **1**, 97.

10.9 C.K.POON, *Coord.Chem.Rev.*, 1973, **10**,1.

10.10 S.C.TANG, S.KOCH, G.N.WEINSTEIN, R.W.LANE, and R.H.HOLM, *Inorg.Chem.*, 1973, **12**, 2589.

10.11 S.C.TANG, and R.H.HOLM, *J.Am.Chem.Soc.*, 1975, **97**, 3359.

10.12 J.M.PRATT, and R.G.THORP, *Adv.Inorg.Chem.Radiochem.*, 1969, **12**, 375.

10.13 M.L.TOBE, *Acc.Chem.Res.*, 1970, **3**, 377.

10.14 D.A.BALDWIN, E.A.BETTERTON, and J.M.PRATT, *S.Afr.J.Chem.*, 1982, **35**, 173.

10.15 D.P.RILLEMA, J.F.ENDICOTT, and J.R.BARBER, *J.Am.Chem.Soc.*, 1973, **95**, 6987.

10.16 C.K.POON, and C.L.WONG, *Inorg.Chem.*, 1976, **15**, 1573.

10.17 R.F.PASTERNACK, and G.R.PARR, *Inorg.Chem.*, 1976, **15**, 3087.

10.18 K.RASHLEY, and S.AU-YOUNG, *Inorg.Chem.*, 1976, **15**, 1937.

10.19 N.K.KILDAHL, and G.ANTONOPOULOS, *J.Coord.Chem.*, 1986, **14**, 293.

10.20 J.A.KERNOHAN, and J.F.ENDICOTT, *Inorg.Chem.*, 1970, **6**, 1504.

10.21 E.B.FLEISCHER and M.KRISHNAMURTHY, *J.Am.Chem.Soc.*, 1971, **93**, 3785.

10.22 D.THUSIUS, *J.Am.Chem.Soc.*, 1971, **93**, 2629.

10.23 F.NOME, and J.H.FENDLER, *J.Chem.Soc.,Dalton Trans.*, 1976, 1212.

10.24 G.STOCHEL, R.VAN ELDIK, H.KUNKLEY, and A.VOGLER, *Inorg. Chem.*, 1989, **28**, 4314.

10.25 G.STOCHEL, and R.VAN ELDIK, *Inorg.Chem.*, 1990, **29**, 2075.

10.26 W.C.RANDALL, and R.A.ALBERTY, *Biochemistry*, 1967, **6**, 1520.

10.27 L.M.MARQUES, J.C.BRADLEY, and L.A.CAMPBELL, *J.Chem.Soc.,Dalton Trans.*, 19 , 2019.

10.28 G.C.HAYWARD, H.A.O.HILL, J.M.PRATT, N.J.VANSTON, and R.J.P.WILLIAMS, *J.Chem.Soc.*, 1965, 6485.

10.29 K.L.BROWN, and H.BROOKS, personal communication.

10.30 P.REUZ, *Methods Enzymol.*, 1971, **18**, 82.

10.31 H.H.MARQUES, Unpublished results

10.32 R.A.FIRTH, H.A.O.HILL, J.M.PRATT, R.G.THORP, and R.J.P.WILLIAMS, *J.Chem.Soc.(A)*, 1969, 381.

10.33 G.C.HAYWARD, H.A.O.HILL, J.M.PRATT, and R.J.P.WILLIAMS, *J.Chem.Soc.(A).*, 1971, 196.

10.34 F.A.COTTON, and G.WILKINSON, *Advanced Inorgancic Chemistry*, 4th Ed., Wiley & Sons, New York, 1980.

10.35 G.M.SMITH, *MOLSV: A computer program for the calculation of molecular volume and surface area*, Quantum Chemistry Exchange Program No. 509, 1985. Modified by P.W.Wade, University of the Witwatersrand, 1991.

10.36 ALCHEMY II Molecular Modelling Software (1989), Tripos Associates, 6548 Clayton Road, St. Louis, Missouri, 63117, U.S.A.

10.37 R.A.FIRTH, H.A.O.HILL, B.E.MANN, J.M.PRATT, R.G.THORP, and R.J.P.WILLIAMS, *J.Chem.Soc.(A)*, 1968, 2419.

10.38 K.TSUKAHARA, H.OSHITA, Y.EMOTO, and Y.YAMAMOTO, *Bull.Chem.Soc.Jpn.*, 1982, **55**, 2107.

10.39 H.M.MARQUES, *J.Chem.Soc., Dalton Trans.*, 1991, 1437.

10.40 H.M.MARQUES, *S.Afr.J.Chem.*, 1991, **44**, 114.

10.41 H.M.MARQUES, *J.Chem.Soc., Dalton Trans.*, 1991, 339.

10.42 H.M.MARQUES, K.L.BROWN, and D.W.JACOBSEN, *J.Biol.Chem.*, 1988, **263**, 12378.

10.43 H.M.MARQUES, T.J.EGAN, J.H.MARSH, J.R.MELLOR, and O.Q.MUNRO, *Inorg.Chim.Acta.*, 1989, **166**, 249.

10.44 R.F.PASTERNACK, M.A.COBB, and N.SUTIN, *Inorg.Chem.*, 1975, **14**, 866.

10.45 H.M.MARQUES, E.L.J.BREET, and F.F.PRINSLOO, *J.Chem.Soc., Dalton Trans.*, 1991, 2941.

10.46 E.K.FIELDS, *J.Am.Chem.Soc.*, 1955, **77**, 4255.

10.47 E.KLINGSBERG, *J.Am.Chem.Soc.*, 1961, **83**, 2934.

10.48 T.W.FINDLEY, D.SWERN, and J.T.SCANLAN, *J.Am.Chem.Soc.*, 1945, **67**, 412.

10.49 W.W.REENSTRA, and W.P.JENCKS, *J.Am.Chem.Soc.*, 1979, **101**, 5780.

10.50 K.L.BROWN, and J.H.HAKIMI, *Inorg.Chem.*, 1984, **23**, 1756.

10.51 H.M.MARQUES, in press.

10.52 P.RAMFIELD, *J.Chem.Soc.A*, 1969, 2021.

10.53 T.J.TRUEX, and R.H.HOLM, *J.Am.Chem.Soc.*, 1972, **94**, 4529.

10.54 S.C.TANG, G.N.WEINSTEIN, and R.H.HOLM, *J.Am.Chem.Soc.*, 1973, **95**, 613.

10.55 E.K.BAREFIELD, *Inorg.Chem.*, 1972, **11**, 2273.

10.56 V.L.GOEDKEN, J.MOLIN-CASE, and Y.WHANG, *J.Chem.Soc.,Chem.Commun.*,1973, 337.

10.57 N.R.de TACCONI, D.LEXA, and J.M.SAVEANT, *J.Am.Chem.Soc.*, 1979, **101**, 5780.

10.58 C.H.LANGFORD, and T.R.STENGLE, *Annu.Rev.Phys.Chem.*, 1968, **19**, 193.

10.59 B.P.HAY, and R.G.FINKE, *J.Am.Chem.Soc.*, 1987, **109**, 8013.

10.60 K.L.BROWN, and J.M.HAKIMI, *Inorg.Chem.*, 1984, **23**, 1756.

10.61 D.H.HAGUE, and J.HALPERN, *Inorg.Chem.*, 1967, **6**, 2059.

10.62 J.A.KERNOHAN, and J.F.ENDICOTT, *Inorg.Chem.*, 1970, **9**, 1504.

10.63 R.A.FIRTH, H.A.O.HILL, J.M.PRATT, R.J.P.WILLLIAMS, and W.R.JACKSON, *Biochemistry*, 1967, **6**, 2178.

10.64 H.A.O.HILL, J.M.PRATT, and R.J.P.WILLIAMS, *Chem.Brit.*, 1969, **5**, 156.

11 APPENDIX : SUPPLEMENTARY DATA FOR MAIN TEXT

11.1 SUPPLEMENTARY DATA FOR CHAPTER 3

Table 11.1.1 Absorbance of DAC/AHC at 344nm and 278nm at 35°C as a function of pH.

pH	A_{344nm}	A_{278nm}	pH	A_{344nm}	A_{278nm}
4.064	0.2727	0.6990	6.759	0.2507	0.6699
4.255	0.2730	0.7013	7.046	0.2486	0.6702
4.526	0.2711	0.6973	7.231	0.2459	0.6709
4.667	0.2701	0.7007	7.359	0.2437	0.6668
4.854	0.2681	0.6973	7.573	0.2410	0.6717
5.075	0.2672	0.6940	7.771	0.2381	0.6737
5.231	0.2649	0.6897	7.934	0.2364	0.6802
5.387	0.2632	0.6882	8.233	(0.1910)	0.6948
5.603	0.2610	0.6841	8.478	0.2287	0.7162
5.857	0.2576	0.6770	8.664	0.2227	0.7449
6.046	0.2555	0.6740	8.793	0.2226	0.7752
6.222	0.2530	0.6746	8.994	0.2238	0.8042
6.376	0.2517	0.6733	9.275	0.2217	0.8703
6.638	0.2510	0.6730	9.412	0.2216	0.9000

Table 11.1.2 Absorbance of DAC/AHC at 344nm and 278nm at 25°C as a function of pH.

pH	A_{344nm}	A_{278nm}	pH	A_{344nm}	A_{278nm}
2.820	0.4995	0.3776	7.319	0.4448	0.3022
3.064	0.5027	0.3795	7.505	0.4443	0.3055
3.208	0.5039	0.3800	7.690	0.4448	0.3104
3.385	0.5038	0.3787	7.849	0.4444	0.3167
3.755	0.5059	0.3778	8.076	0.4404	0.3299
3.856	0.5053	0.3777	8.161	0.4409	0.3380
4.008	0.5045	0.3779	8.422	0.4395	0.3625
4.287	0.5017	0.3738	8.606	0.4387	0.4007
4.447	0.5002	0.3724	8.790	[illegible]	.4560
4.635	0.5001	0.3712	9.061	[illegible]	.5096
4.899	0.4979	0.3670	9.143	0.4326	0.5704
5.030	0.4956	0.3653	9.384	0.4280	0.6611
5.175	0.4920	0.3610	9.718	0.4263	0.7791
5.355	0.4889	0.3567	9.909	0.4225	0.8451
5.690	0.4868	0.3511	10.042	0.4172	0.8760
5.781	0.4777	0.3406	10.208	0.4179	0.9298
5.954	0.4720	0.3323	10.374	0.4169	0.9517
6.184	0.4663	0.3233	10.590	0.4142	0.9671
6.513	0.4586	0.3117	10.763	0.4116	0.9892
6.820	0.4509	0.3048	11.054	0.4097	1.0033
6.854	0.4533	0.3052	11.240	0.4109	1.0073
7.025	0.4510	0.3020	11.396	0.4102	1.0080
7.109	0.4479	0.3025	11.589	0.4098	1.0102
7.168	0.4490	0.3026	11.745	0.4096	1.0095

Table 11.1.3 Absorbance of DAC/AHC at 344nm and 278nm at 15°C as a function of pH.

pH	A_{344nm}	pH	A_{278nm}
4.008	0.5370	7.839	0.7314
4.202	0.5384	7.958	0.7349
4.317	0.5387	8.133	0.7400
4.556	0.5368	8.305	0.7473
4.787	0.5378	8.554	0.7626
4.946	0.5366	8.788	0.7827
5.059	0.5337	9.084	0.8706
5.288	0.5289	9.287	0.9230
5.499	0.5257	9.463	0.9859
5.664	0.5187	9.678	1.0490
5.818	0.5144	9.886	1.1216
6.059	0.5078	10.043	1.1601
6.236	0.4978	10.336	1.2123
6.418	0.4919	10.435	1.2290
6.677	0.4861	10.619	1.2523
6.823	0.4826	10.791	1.2678
7.122	0.4782	11.013	1.2812
7.225	0.4762	11.215	1.2866
7.476	0.4741	11.376	1.2898
7.643	0.4722		
7.855	0.4705		
8.006	0.4669		
8.334	0.4655		
8.662	0.4646		
8.875	0.4656		

Table 11.1.4 Absorbance of DAC/AHC at 344nm and 278nm at 5°C as a function of pH.

pH	A_{344nm}	pH	A_{278nm}
3.533	1.6490	7.424	1.0902
3.753	1.6492	7.586	1.1021
3.995	1.6499	7.792	1.0888
4.098	1.6484	7.992	1.0947
4.366	1.6471	8.154	1.1029
4.576	1.6463	8.441	1.1096
4.772	1.6422	8.675	1.1198
4.881	1.6396	8.885	1.1331
4.961	1.6341	8.995	1.1474
5.254	1.6230	9.249	1.2037
5.398	1.6185	9.500	1.2626
5.489	1.6069	9.620	1.3066
5.717	1.5791	9.812	1.3868
6.104	1.5390	10.054	1.4840
6.368	1.5126	10.215	1.5674
6.549	1.4994	10.512	1.7030
6.713	1.4849	10.672	1.7663
7.056	1.4713	10.789	1.8061
7.254	1.4674	11.062	1.8648
7.426	1.4622	11.230	1.8868
7.682	1.4609	11.396	1.9126
7.847	1.4476	11.746	1.9290
8.188	1.4480	11.884	1.9366
8.399	1.4420	12.034	1.9416
8.648	1.4465	12.167	1.9444
8.826	1.4408	12.366	1.9418
		12.500	1.9395

11.2 SUPPLEMENTARY DATA FOR CHAPTER 4

Table 11.2.1 Absorbance at 348 nm versus amount of cyanide added for the titration of AHC (pH 12.0) with cyanide at 25°C.

$[CN^-]$ / mol dm^{-3}	A_{348}	A_{348}(corrected)
0	0.7558	0.7558
$4.17X10^{-6}$	0.7486	0.7490
$8.34X10^{-6}$	0.7404	0.7411
$1.25X10^{-5}$	0.7319	0.7330
$1.67X10^{-5}$	0.7173	0.7187
$2.09X10^{-5}$	0.7055	0.7073
$2.50X10^{-5}$	0.6925	0.6946
$2.92X10^{-5}$	0.6814	0.6838
$3.33X10^{-5}$	0.6690	0.6717
$3.74X10^{-5}$	0.6568	0.6598
$4.15X10^{-5}$	0.6454	0.6486
$4.57X10^{-5}$	0.6338	0.6373
$4.97X10^{-5}$	0.6219	0.6256
$5.42X10^{-5}$	0.6124	0.6164
$5.81X10^{-5}$	0.6008	0.6050
$6.20X10^{-5}$	0.5898	0.5942
$6.65X10^{-5}$	0.5810	0.5856
$7.04X10^{-5}$	0.5773	0.5822
$7.43X10^{-5}$	0.5770	0.5822
$7.88X10^{-5}$	0.5780	0.5835
$8.27X10^{-5}$	0.5762	0.5820
$1.03X10^{-4}$	0.5749	0.5821
$1.44X10^{-4}$	0.5724	0.5824

Table 11.2.2 Absorbance at 370 nm versus amount of azide added for the titration of AHC (pH 12.0) with azide at 25°C.

$[N_3^-]$ / mol dm^{-3}	A_{370}	A_{370}(corrected)
0	0.1662	0.1662
$1.22X10^{-3}$	0.1748	0.1750
$2.43X10^{-3}$	0.1851	0.1855
$3.64X10^{-3}$	0.1914	0.1920
$4.85X10^{-3}$	0.1982	0.1990
$6.06X10^{-3}$	0.2041	0.2051
$9.07X10^{-3}$	0.2147	0.2163
$1.21X10^{-2}$	0.2227	0.2249
$1.50X10^{-2}$	0.2287	0.2316
$2.10X10^{-2}$	0.2364	0.2405
$3.55X10^{-2}$	0.2481	0.2555
$4.69X10^{-2}$	0.2502	0.2602
$6.89X10^{-2}$	0.2536	0.2688
$1.21X10^{-1}$	0.2516	0.2793
$2.11X10^{-1}$	0.2419	0.2927
$3.06X10^{-1}$	0.2286	0.3052

Table 11.2.3 Absorbance at 368 nm versus amount of pyridine added for the titration of AHC (pH 12.0) with pyridine at 25°C.

[pyridine] / mol dm^{-3}	A_{368}	A_{368}(corrected)
0	0.2466	0.2466
$2.07X10^{-3}$	0.3081	0.3084
$4.13X10^{-3}$	0.3376	0.3383
$6.19X10^{-3}$	0.3550	0.3561
$8.25X10^{-3}$	0.3636	0.3651
$1.03X10^{-2}$	0.3747	0.3766
$1.23X10^{-2}$	0.3776	0.3799
$1.44X10^{-2}$	0.3800	0.3827
$1.64X10^{-2}$	0.3835	0.3866
$1.86X10^{-2}$	0.3863	0.3898
$2.15X10^{-2}$	0.3854	0.3893
$4.06X10^{-2}$	0.3957	0.4034
$6.03X10^{-2}$	0.3966	0.4083
$7.96X10^{-2}$	0.3937	0.4094
$9.95X10^{-2}$	0.3873	0.4069
$1.87X10^{-1}$	0.3740	0.4120

Table 1A.4 Absorbance at 365 nm versus amount of N-methylimidazole added for the titration of AHC (pH 12.0) with N-methylimidazole at 25°C.

[N-methylimidazole] / mol dm^{-3}	A_{365}	A_{365}(corrected)
0	0.5111	0.5111
$5.00X10^{-5}$	0.6384	0.6387
$1.00X10^{-4}$	0.6773	0.6780
$1.50X10^{-4}$	0.6929	0.6939
$2.49X10^{-4}$	0.7060	0.7078
$4.98X10^{-4}$	0.7171	0.7207
$9.90X10^{-4}$	0.7241	0.7313
$1.98X10^{-3}$	0.7343	0.7424
$4.44X10^{-3}$	0.7450	0.7551
$2.61X10^{-2}$	0.7259	0.7520

Table 11.2.5 Absorbance at 364 nm versus amount of 3-amino-1-propanol added for the titration of AHC (pH 12.0) with 3-amino-1-propanol at 25°C.

[3-amino-1-propanol] / mol dm^{-3}	A_{364}	A_{364}(corrected)
0	0.5867	0.5867
$2.63X10^{-4}$	0.6193	0.6196
$5.26X10^{-4}$	0.6466	0.6472
$7.88X10^{-4}$	0.6677	0.6687
$1.05X10^{-3}$	0.6946	0.6960
$1.31X10^{-3}$	0.7044	0.7062
$1.57X10^{-3}$	0.7081	0.7102
$2.10X10^{-3}$	0.7179	0.7208
$2.62X10^{-3}$	0.7270	0.7306
$3.92X10^{-3}$	0.7375	0.7430
$5.21X10^{-3}$	0.7464	0.7539
$7.78X10^{-3}$	0.7532	0.7645
$1.16X10^{-2}$	0.7570	0.7740
$1.78X10^{-2}$	0.7570	0.7835
$1.00X10^{-1}$	0.6515	0.8046

11.3 SUPPLEMENTARY DATA FOR CHAPTER 5

Table 11.3.1 (a) Pseudo first order rate constants, k'_{obs}, as a function of ligand concentration and pH at 25°C.

$[N_3^-]$ / mol dm^{-3}	k'_{obs} / s^{-1}				
	pH 11.5	pH 11.0	pH 10.5	pH 10.0	pH 9.5
0.0010	67(10)	83(2)	75(1)	68(1)	65(1)
0.0025	94(3)	118(2)	107(1)	122(1)	133(1)
0.0050	121(3)	132(1)	163(1)	232(1)	290(5)
0.010	137(2)	199(4)	311(3)	507(5)	698(12)
0.015	220(3)	243(3)	420(6)	760(7)	925(20)
0.020	234(3)	279(3)	610(7)	821(9)	{696(26)}

Table 11.3.1 (b) Pseudo first order rate constants, k'_{obs}, as a function of ligand concentration and pH at 25°C.

$[N_3^-]$ / mol dm^{-3}	k'_{obs} / s^{-1}				
	pH 9.0	pH 8.5	pH 8.0	pH 7.5	pH 7.0
0.0010	75(1)	67(1)	83(1)	116(1)	163(1)
0.0025	181(1)	180(1)	215(1)	326(3)	413(2)
0.0050	394(3)	492(3)	570(6)	693(7)	804(5)
0.010	769(9)	879(5)	1039(12)	1169(25)	1253(15)
0.015	1110(17)	1246(5)	1260(16)	1718(34)	1801( )
0.020	1314(24)	1473(11)	1662(43)	1692(41)	2215(36)

Table 11.3.1 (c) Pseudo first order rate constants, k'_{obs}, as a function of ligand concentration and pH at 25°C.

$[N_3^-]$ / mol dm^{-3}	k'_{obs} / s^{-1}			
	pH 6.5	pH 6.0	pH 5.5	pH 5.0
0.0004	87(1)	81(1)	77(1)	68(1)
0.0010	195(1)	206(1)	181(1)	135(1)
0.0020	378(2)	392(1)	315(3)	205(1)
0.0040	744(5)	735(4)	487(3)	319(2)
0.0060	1036(9)	991(5)	719(5)	{349(1)}
0.0080	1277(15)	1178(5)	857(8)	{376(2)}

Table 11.3.1 (d) Pseudo first order rate constants, k'_{obs}, as a function of ligand concentration and pH at 25°C.

$[N_3^-]$ / mol dm^{-3}	k'_{obs} / s^{-1}			
	pH 4.4	pH 4.0	pH 3.5	pH 3.0
0.0004	67(1)	66(2)	70(1)	86(1)
0.0010	120(2)	95(3)	103(2)	117(2)
0.0020	206(5)	166(2)	155(1)	152(3)
0.0040	290(5)	223(4)	{249(3)}	255(5)
0.0060	{291(3)}	{297(4)}	{261(2)}	{281(5)}
0.0080	492(10)	{296(4)}	{299(3)}	{274(5)}

11.4 SUPPLEMENTARY DATA FOR CHAPTER 6

Table 11.4.1 The dependence of the pH-dependent and pH-independent observed rate constants, in the main text k'_{obs} and k_{obs} respectively, measured at two different wavelengths, for the substitution of H_2O in aquocobalamin by pyridine at 35,0 °C and a pH of 6.48 on the ligand concentration.

[pyridine] / mol dm^{-3}	351 nm		362.5 nm			
			fast	fast	slow	slow
	k'_{obs} / s^{-1}	k_{obs} / s^{-1}	k'_{obs} / s^{-1}	k_{obs} / s^{-1}	k'_{obs} / s^{-1}	k_{obs} / s^{-1}
0.010	6.39	7.10				
0.012	6.91	7.53	7.7	8.5	7.52	8.19
0.017	7.76	8.46	8.1	8.8	7.60	8.29
0.025	7.96	8.67	16	17	7.71	8.40
0.050	8,65	9.43	12	13	7.94	8.65
0.099	9.98	10.9	15	17	9.08	9.89
0.199	12.7	13.8	18	20	10.9	11.9
0.298	14.7	16.0	21	23	12.0	13.1
0.398	16.8	18.3	23	25	12.6	13.7
0.497	18.2	19.8	26	28	13.7	14.9
0.597	18.6	20.2	26	29	14.8	16.1
0.696	19.0	20.7	25	27	15.7	17.1
0.795	19.3	21.0	27	30	15.6	17.0
0.895	19.6	21.2	27	30	15.5	16.7
0.994	19.6	21.4	27	29	15.1	16.5

Table 11.4.1 The dependence of the pH-dependent and pH-independent observed rate constants, in the main text k'_{obs} and k_{obs} respectively, measured at two different wavelengths, for the substitution of H_2O in aquocobalamin by pyridine at 25.0°C and a pH of 6.51 on the ligand concentration.

[pyridine] / mol dm^{-3}	351 nm		362.5 nm			
			fast	fast	slow	slow
	k'_{obs} / s^{-1}	k_{obs} / s^{-1}	k'_{obs} / s^{-1}	k_{obs} / s^{-1}	k'_{obs} / s^{-1}	k_{obs} / s^{-1}
0.010	1.99	2.21	1.8	2.0	2.09	2.33
0.012	2.09	2.26	5.2	5.7	2.24	2.42
0.017	2.10	2.27	3.9	4.2	2.19	2.37
0.025	2.23	2.41	2.5	2.8	2.36	2.55
0.050	2.53	2.74	6.4	7.0	2.57	2.79
0.099	3.05	3.30	5.1	5.6	3.04	3.30
0.199	3.93	4.26	12	13	3.92	4.25
0.298	4.54	4.94	13	14	4.57	4.96
0.398	5.15	5.57	13	14	5.39	5.84
0.497	5.66	6.12	14	15	5.78	6.24
0.597	5.82	6.28	13	14	5.97	6.45
0.696	6.03	6.50	14	15	6.20	6.69
0.795	6.14	6.62	13	14	6.28	6.77
0.895	6.37	6.87	13	14	6.39	6.89
0.994	6.39	6.88	13	14	6.42	6.91

Table 11.4.3 The dependence of the pH-dependent and pH-independent observed rate constants, in the main text k'_{obs} and k_{obs} respectively, measured at two different wavelengths, for the substitution of H_2O in aquocobalamin by pyridine at 15.0°C and a pH of 6.59 on the ligand concentration.

[pyridine] / mol dm^{-3}	351 nm		362.5 nm			
			fast	fast	slow	slow
	k'_{obs} / s^{-1}	k_{obs} / s^{-1}	k'_{obs} / s^{-1}	k_{obs} / s^{-1}	k'_{obs} / s^{-1}	k_{obs} / s^{-1}
0.010	0.540	0.594	0.68	0.74	0.434	0.477
0.012	0.549	0.604	0.68	0.75	0.456	0.501
0.017	0.551	0.606	0.72	0.80	0.422	0.465
0.025	0.583	0.641	2.2	2.4	0.613	0.674
0.050	0.667	0.734	1.8	2.0	0.697	0.766
0.099	0.825	0.908	1.7	1.9	0.851	0.936
0.199	1.09	1.20	3.3	3.7	1.25	1.37
0.298	1.31	1.45	3.8	4.2	1.49	1.64
0.398	1.50	1.63	4.0	4.4	1.67	1.82
0.497	1.68	1.84	4.2	4.7	1.82	1.99
0.597	1.76	1.92	3.8	4.2	1.85	2.01
0.696	1.85	2.00	4.1	4.5	1.93	2.09
0.795	1.91	2.06	4.8	5.2	2.04	2.23
0.895	1.91	2.06	6.0	6.6	2.13	2.32
0.994	1.94	2.09	6.4	7.0	2.14	2.34

Table I1.4.4 The dependence of the pH-dependent and pH-independent observed rate constants, in the main text k'_{obs} and k_{obs} respectively, measured at two different wavelengths, for the substitution of H_2O in aquocobalamin by pyridine at 5.0°C and a pH of 6.68 on the ligand concentration.

[pyridine] / mol dm^{-3}	351 nm		362.5 nm			
			fast	fast	slow	slow
	k'_{obs} / s^{-1}	k_{obs} / s^{-1}	k'_{obs} / s^{-1}	k_{obs} / s^{-1}	k'_{obs} / s^{-1}	k_{obs} / s^{-1}
0.010	0.117	0.129	3.7	4.1	0.110	0.122
0.012	0.129	0.143	0.41	0.46	0.116	0.129
0.017	0.128	0.142	0.39	0.43	0.119	0.132
0.025	0.137	0.152	0.21	0.23	0.136	0.151
0.050	0.159	0.176	0.50	0.55	0.156	0.173
0.099	0.204	0.226	0.60	0.67	0.200	0.222
0.199	0.275	0.305	1.1	1.2	0.308	0.342
0.298	0.336	0.369	0.85	0.93	0.345	0.379
0.398	0.387	0.426	0.79	0.87	0.377	0.415
0.497	0.435	0.474	0.93	1.0	0.428	0.467
0.597	0.443	0.483	2.0	2.2	0.531	0.579
0.696	0.469	0.506	2.3	2.5	0.569	0.614
0.795	0.487	0.526	1.6	1.7	0.561	0.606
0.895	0.492	0.528	2.4	2.6	0.588	0.635
0.994	0.496	0.536	2.6	2.8	0.624	0.674

11.5 SUPPLEMENTARY DATA FOR CHAPTER 7

11.5.1 Cyanide

Table 11.5.1.1 pH dependent (k'_{obs}) and pH independent (k_{obs}) rate constants for the substitution of H_2O in AHC (pH 11.89) by CN^- at 25°C as a function of ligand concentration.

$[CN^-]$ / mol dm^3	k'_{obs} / s^{-1}	k_{obs} / s^{-1}
0.002	4.560 (0.025)	137
0.005	8.745 (0.056)	263
0.010	17.59 (0.11)	529
0.015	23.31 (0.19)	701
0.020	28.24 (0.23)	849
0.040	50.86 (0.36)	$1.53X10^3$
0.060	64.02 (0.47)	$1.93X10^3$
0.080	81.52 (0.69)	$2.45X10^3$
0.120	105.9 (1.2)	$3.18X10^3$
0.150	125.7 (1.8)	$3.78X10^3$
0.200	137.7 (1.4)	$4.14X10^3$
0.299	153.1 (3.0)	$4.60X10^3$
0.499	170.1 (3.8)	$5.12X10^3$

Table 11.5.1.2 pH dependent (k'_{obs}) and pH independent (k_{obs}) rate constants for the substitution of H_2O in AHC (pH 12.04) by CN^- at 18°C as a function of ligand concentration.

$[CN^-]$ / mol dm^{-3}	k'_{obs} / s^{-1}	k_{obs} / s^{-1}
0.002	2.711 (0.032)	88.3
0.005	5.181 (0.058)	169
0.010	8.505 (0.078)	277
0.015	13.48 (0.10)	439
0.020	17.45 (0.16)	568
0.040	27.30 (0.38)	889
0.060	37.49 (0.38)	$1.22X10^3$
0.080	46.01 (0.38)	$1.50X10^3$
0.120	57.02 (0.85)	$1.86X10^3$
0.150	76.84 (1.74)	$2.59X10^3$
0.200	73.16 (0.80)	$2.38X10^3$
0.299	117.6 (1.9)	$3.83X10^3$
0.499	135.3 (3.8)	$4.41X10^3$

Table 11.5.1.3 pH dependent (k'_{obs}) and pH independent (k_{obs}) rate constants for the substitution of H_2O in AHC (pH 12.18) by CN^- at 12°C as a function of ligand concentration.

$[CN^-]$ / mol dm^{-3}	k'_{obs} / s^{-1}	k_{obs} / s^{-1}
0.002	0.4588 (0.0049)	16.3
0.005	2.434 (0.024)	86.4
0.010	5.335 (0.041)	189
0.015	7.255 (0.074)	258
0.020	8.696 (0.106)	309
0.040	15.89 (0.10)	564
0.060	18.96 (0.22)	673
0.080	25.30 (0.22)	898
0.120	31.67 (0.88)	$1.12X10^3$
0.150	38.31 (0.97)	$1.36X10^3$
0.200	43.34 (1.33)	$1.54X10^3$
0.299	57.50 (1.45)	$2.04X10^3$
0.499	56.58 (2.73)	$2.01X10^3$

Table 11.5.1.4 pH dependent (k'_{obs}) and pH independent (k_{obs}) rate constants for the substitution of H_2O in AHC (pH 12.33) by CN^- at 5°C as a function of ligand concentration.

$[CN^-]$ / mol dm^{-3}	k'_{obs} / s^{-1}	k_{obs} / s^{-1}
0.002	0.8858 (0.0169)	33.3
0.005	1.800 (0.016)	67.7
0.010	3.006 (0.034)	113
0.015	3.775 (0.040)	142
0.020	4.911 (0.059)	184
0.040	8.864 (0.086)	333
0.060	10.70 (0.09)	402
0.080	14.05 (0.10)	528
0.120	19.15 (0.32)	719
0.150	21.89 (0.41)	822
0.200	24.48 (0.80)	919
0.299	37.16 (2.03)	$1.40X10^3$
0.499	58.78 (7.09)	$2.21X10^3$

11.5.2 Azide

Table 11.5.2.1 pH dependent (k'_{obs}) and pH independent (k_{obs}) rate constants for the substitution of H_2O in AHC (pH 11.64) by N_3^- at 25°C as a function of ligand concentration.

$[N_3^-]$ / mol dm^{-3}	k'_{obs} / s^{-1}	k_{obs} / s^{-1}
0.010	104.7 (1.4)	$1.81X10^3$
0.015	132.6 (1.3)	$2.30X10^3$
0.020	138.6 (1.7)	$2.40X10^3$
0.025	143.8 (1.8)	$2.49X10^3$
0.050	168.6 (1.9)	$2.92X10^3$
0.100	301.1 (4.4)	$5.22X10^3$
0.200	427.7 (4.9)	$7.41X10^3$
0.299	543.9 (7.2)	$9.42X10^3$
0.400	649.4 (9.2)	$1.13X10^4$
0.500	673.2 (16.2)	$1.17X10^4$
0.600	690.6 (23.0)	$1.20X10^4$

Table 11.5.2.2 pH dependent (k'_{obs}) and pH independent (k_{obs}) rate constants for the substitution of H_2O in AHC (pH 11.80) by N_3^- at 18°C as a function of ligand concentration.

$[N_3^-]$ / mol dm^{-3}	k'_{obs} / s^{-1}	k_{obs} / s^{-1}
0.010	48.87 (0.93)	937
0.015	76.40 (1.09)	$1.46X10^3$
0.020	101.4 (1.7)	$1.94X10^3$
0.025	111.2 (1.6)	$2.13X10^3$
0.050	136.4 (1.8)	$2.62X10^3$
0.100	278.5 (4.3)	$5.34X10^3$
0.200	327.3 (4.7)	$6.27X10^3$
0.299	448.0 (10.2)	$8.59X10^3$
0.400	482.7 (10.2)	$9.25X10^3$
0.500	542.3 (17.9)	$1.04X10^4$

Table 11.5.2.3 pH dependent (k'_{obs}) and pH independent (k_{obs}) rate constants for the substitution of H_2O in AHC (pH 11.84) by N_3^- at 12°C as a function of ligand concentration.

$[N_3^-]$ / mol dm^{-3}	k'_{obs} / s^{-1}	k_{obs} / s^{-1}
0.010	28.86 (0.40)	484
0.015	42.51 (0.54)	713
0.020	62.11 (1.13)	$1.04X10^3$
0.025	64.79 (0.80)	$1.09X10^3$
0.050	89.52 (0.84)	$1.50X10^3$
0.100	162.5 (2.0)	$2.73X10^3$
0.200	206.2 (2.6)	$3.46X10^3$
0.299	254.1 (4.9)	$4.26X10^3$

Table 11.5.2.4 pH dependent (k'_{obs}) and pH independent (k_{obs}) rate constants for the substitution of H_2O in AHC (pH 12.00) by N_3^- at 5°C as a function of ligand concentration.

$[N_3^-]$ / mol dm^{-3}	k'_{obs} / s^{-1}	k_{obs} / s^{-1}
0.010	18.64 (0.17)	337
0.015	22.17 (0.30)	401
0.020	29.15 (0.20)	528
0.025	30.32 (0.27)	549
0.050	42.81 (0.56)	775
0.100	82.27 (0.69)	1.49×10^3
0.200	131.7 (1.2)	2.38×10^3
0.299	167.7 (1.4)	3.04×10^3
0.400	211.5 (2.6)	3.83×10^3
0.500	243.3 (2.8)	4.40×10^3
0.600	288.3 (8.9)	5.22×10^3

11.5.3 Pyridine

Table 11.5.3.1 pH dependent (k'_{obs}) and pH independent (k_{obs}) rate constants for the substitution of H_2O in AHC (pH 11.96) by pyridine at 25°C as a function of ligand concentration.

[pyridine] / mol dm^{-3}	k'_{obs} / s^{-1}	k_{obs} / s^{-1}
0.010	16.49 (0.04)	579
0.012	16.50 (0.04)	579
0.016	22.28 (0.03)	782
0.025	32.61 (0.03)	$1.14X10^3$
0.050	46.15 (0.07)	$1.62X10^3$
0.100	98.27 (0.26)	$3.45X10^3$
0.200	152.2 (0.7)	$5.34X10^3$
0.300	169.1 (0.8)	$5.94X10^3$
0.400	207.5 (1.6)	$7.29X10^3$

Table 11.5.3.2 pH dependent (k'_{obs}) and pH independent (k_{obs}) rate constants for the substitution of H_2O in AHC (pH 12.04) by pyridine at 18°C as a function of ligand concentration.

[pyridine] / mol dm^{-3}	k'_{obs} / s^{-1}	k_{obs} / s^{-1}
0.010	8.654 (0.007)	273
0.012	13.58 (0.01)	429
0.016	11.61 (0.01)	367
0.025	17.75 (0.01)	561
0.050	23.35 (0.02)	737
0.100	51.99 (0.05)	$1.64X10^3$
0.200	86.39 (0.14)	$2.73X10^3$
0.300	97.85 (0.22)	$3.09X10^3$
0.400	133.7 (0.5)	$4.22X10^3$

Table 11.5.3.3 pH dependent (k'_{obs}) and pH independent (k_{obs}) rate constants for the substitution of H_2O in AHC (pH 12.26) by pyridine at 12°C as a function of ligand concentration.

[pyridine] / mol dm^{-3}	k'_{obs} / s^{-1}	k_{obs} / s^{-1}
0.010	4.646 (0.005)	197
0.012	7.323 (0.006)	311
0.016	6.338 (0.005)	269
0.025	9.725 (0.010)	413
0.050	12.86 (0.009)	546
0.100	29.46 (0.03)	$1.25X10^3$
0.200	48.65 (0.04)	$2.07X10^3$
0.300	57.31 (0.09)	$2.44X10^3$
0.400	75.65 (0.1)	$3.21X10^3$

Table 11.5.3.4 pH dependent (k'_{obs}) and pH independent (k_{obs}) rate constants for the substitution of H_2O in AHC (pH 12.34) by pyridine at 5°C as a function of ligand concentration.

[pyridine] / mol dm^{-3}	k'_{obs} / s^{-1}	k_{obs} / s^{-1}
0.010	2.317 (0.009)	86.7
0.012	3.559 (0.009)	133
0.016	3.053 (0.008)	114
0.025	5.195 (0.014)	194
0.050	6.570 (0.012)	246
0.100	14.77 (0.05)	553
0.200	24.09 (0.08)	901
0.300	27.28 (0.16)	$1.02X10^3$
0.400	33.30 (0.37)	$1.25X10^3$

11.5.4 N-methylimidazole

Table 11.5.4.1 pH dependent (k'_{obs}) and pH independent (k_{obs}) rate constants for the substitution of H_2O in AHC (pH 12.03) by N-methylimidazole at 25°C as a function of ligand concentration.

[N-methylimidazole] / mol dm^{-3}	k'_{obs} / s^{-1}	k_{obs} / s^{-1}
0.010	8.378 (0.032)	344
0.013	12.40 (0.05)	509
0.017	27.99 (0.14)	($1.15X10^3$)
0.025	21.57 (0.08)	886
0.050	37.96 (0.17)	$1.56X10^3$
0.100	77.97 (1.99)	$3.20X10^3$
0.200	124.3 (2.2)	$5.11X10^3$

Table 11.5.4.2 pH dependent (k'_{obs}) and pH independent (k_{obs}) rate constants for the substitution of H_2O in AHC (pH 12.18) by N-methylimidazole at 18°C as a function of ligand concentration.

[N-methylimidazole] / mol dm^{-3}	k'_{obs} / s^{-1}	k_{obs} / s^{-1}
0.010	4.763 (0.053)	212
0.013	6.682 (0.035)	298
0.017	13.54 (0.06)	(604)
0.025	12.59 (0.10)	561
0.050	22.14 (0.20)	987
0.100	43.06 (0.38)	$1.92X10^3$
0.200	80.07 (0.97)	$3.57X10^3$

Table 11.5.4.3 pH dependent (k'_{obs}) and pH independent (k_{obs}) rate constants for the substitution of H_2O in AHC (pH 12.23) by N-methylimidazole at 12°C as a function of ligand concentration.

[N-methylimidazole] / mol dm^{-3}	k'_{obs} / s^{-1}	k_{obs} / s^{-1}
0.010	2.679 (0.021)	106
0.013	3.726 (0.027)	148
0.017	7.757 (0.045)	(308)
0.025	7.146 (0.046)	284
0.050	13.32 (0.12)	529
0.100	22.37 (0.23)	(889)

Table 11.5.4.4 pH dependent (k'_{obs}) and pH independent (k_{obs}) rate constants for the substitution of H_2O in AHC (pH 12.45) by N-methylimidazole at 5°C as a function of ligand concentration.

[N-methylimidazole] / mol dm^{-3}	k'_{obs} / s^{-1}	k_{obs} / s^{-1}
0.010	1.254 (0.019)	61.7
0.013	1.840 (0.014)	90.5
0.017	3.769 (0.027)	(185)
0.025	3.594 (0.031)	177
0.050	6.624 (0.065)	326
0.100	12.79 (0.09)	629
0.200	21.26 (0.21)	$1.05X10^3$

11.5.5 3-amino-1-propanol

Table 11.5.5.1 pH dependent (k'_{obs}) and pH independent (k_{obs}) rate constants for the substitution of H_2O in AHC (pH 11.97) by 3-amino-1-propanol at 25°C as a function of ligand concentration.

[3-amino-1-propanol] / mol dm^{-3}	k'_{obs} / s^{-1}	k_{obs} / s^{-1}
0.0097	0.5126	18.4
0.014	0.6516	23.4
0.018	0.7067	25.4
0.025	0.8812	31.6
0.050	1.360	48.8
0.10	2.578	92.6
0.20	4.661	167
0.30	7.745	278
0.41	8.833	317
0.51	11.85	425
0.58	14.58	523
0.70	17.52	629
0.80	18.61	668
0.89	20.26	727
0.97	24.49	879

Table 11.5.5.2 pH dependent (k'_{obs}) and pH independent (k_{obs}) rate constants for the substitution of H_2O in AHC (pH 12.17) by 3-amino-1-propanol at 18°C as a function of ligand concentration.

[3-amino-1-propanol] / mol dm^{-3}	k'_{obs} / s^{-1}	k_{obs} / s^{-1}
0.0097	0.1742	7.59
0.014	0.2231	9.73
0.018	0.2488	10.8
0.025	0.3753	16.4
0.050	0.6079	26.5
0.10	1.114	48.6
0.20	2.061	89.9
0.30	3.251	142
0.41	4.235	185
0.51	5.490	239
0.58	6.988	305
0.70	8.233	359
0.80	9.039	394
0.89	9.781	426
0.97	11.60	506

Table 11.5.5.3 pH dependent (k'_{obs}) and pH independent (k_{obs}) rate constants for the substitution of H_2O in AHC (pH 12.32) by 3-amino-1-propanol at 12°C as a function of ligand concentration.

[3-amino-1-propanol] / mol dm^{-3}	k'_{obs} / s^{-1}	k_{obs} / s^{-1}
0.0097	0.08984	4.37
0.014	0.09631	4.68
0.018	0.1123	5.46
0.025	0.1622	7.89
0.050	0.2734	13.3
0.10	0.4926	24.0
0.20	0.9572	46.6
0.30	1.569	76.3
0.41	2.080	101
0.51	3.076	150
0.58	3.529	172
0.70	4.191	204
0.80	4.550	221
0.89	5.332	259
0.97	7.000	340

Table 11.5.5.4 pH dependent (k'_{obs}) and pH independent (k_{obs}) rate constants for the substitution of H_2O in AHC (pH 12.47) by 3-amino-1-propanol at 5°C as a function of ligand concentration.

[3-amino-1-propanol] / mol dm^{-3}	k'_{obs} / s^{-1}	k_{obs} / s^{-1}
0.0097	0.06306	3.25
0.014	0.05345	2.75
0.018	0.06251	3.22
0.025	0.08776	4.52
0.050	0.1615	8.31
0.10	0.3091	15.9
0.20	0.5722	29.4
0.30	0.7731	39.8
0.41	0.9777	50.3
0.51	1.523	78.4
0.58	1.795	92.4
0.70	2.573	132
0.80	2.608	134
0.89	2.860	147
0.97	3.342	172

11.6 SUPPLEMENTARY DATA FOR CHAPTER 8

Figure 11.6.1 Proton NMR spectrum of 4-phenyl-1,2-dithiole-3-thione in deuterated acetone at 25°C using a 200 MHz spectrometer.

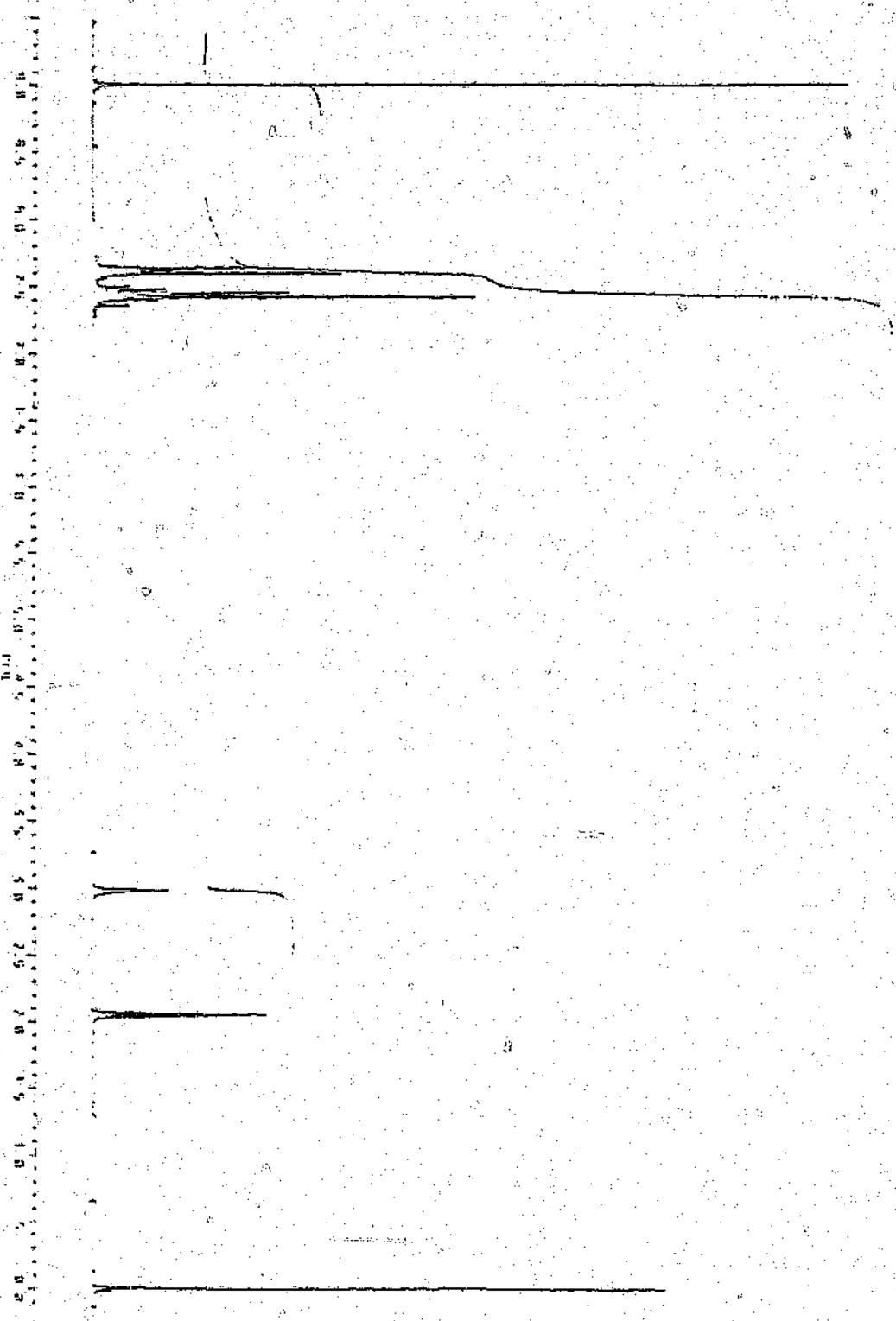


Figure 11.6.2 Proton NMR spectrum of 4-phenyl-1,2-dithiolium perchlorate in D_2O at 25°C using a 200 MHz spectrometer.

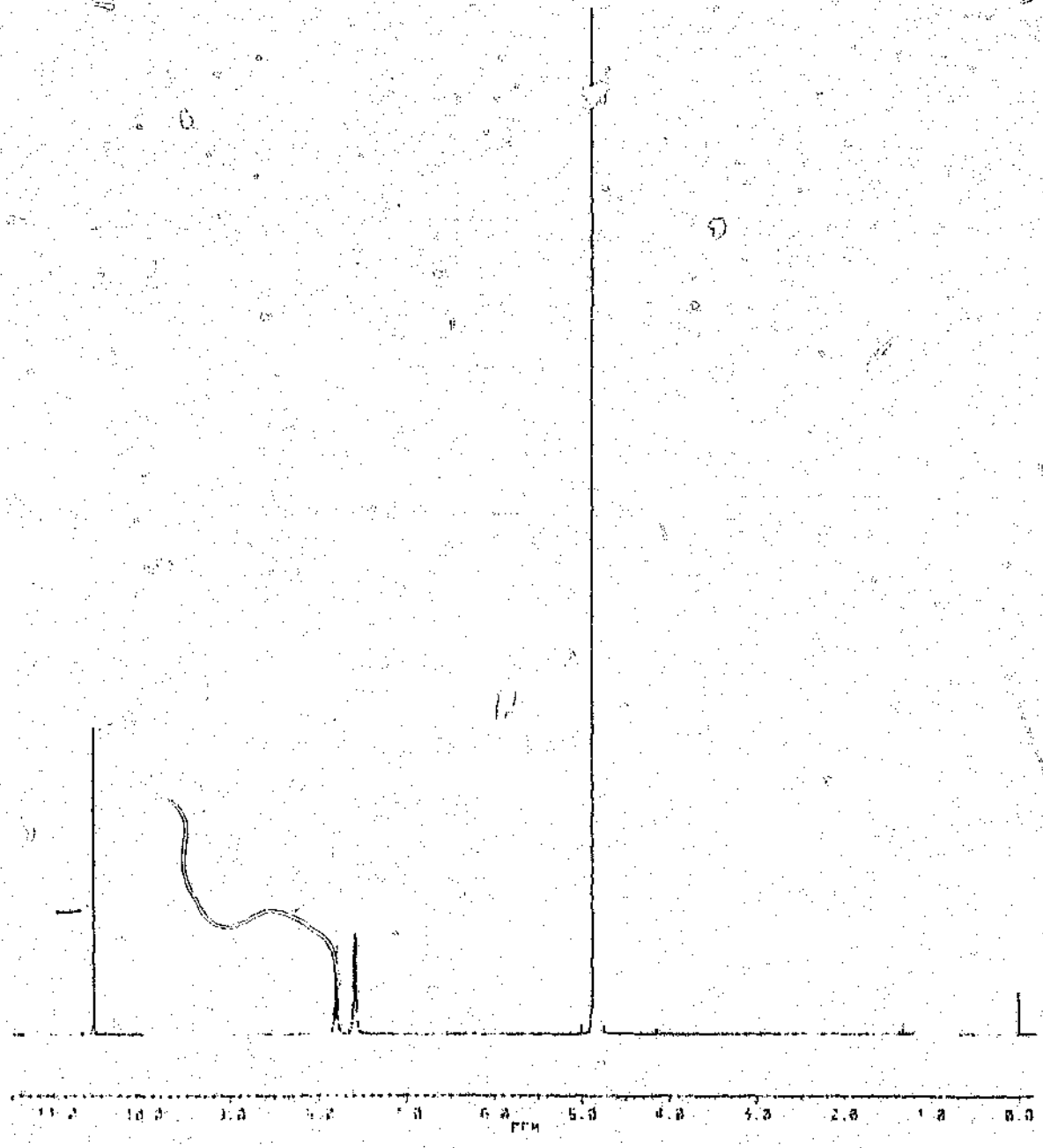


Figure 11.6.3 Proton NMR spectrum of N,N'-bis(2-thioformyl-2-phenylvinyl)trimethylenediamine in deuterated acetone at 25°C using a 200 MHz spectrometer.

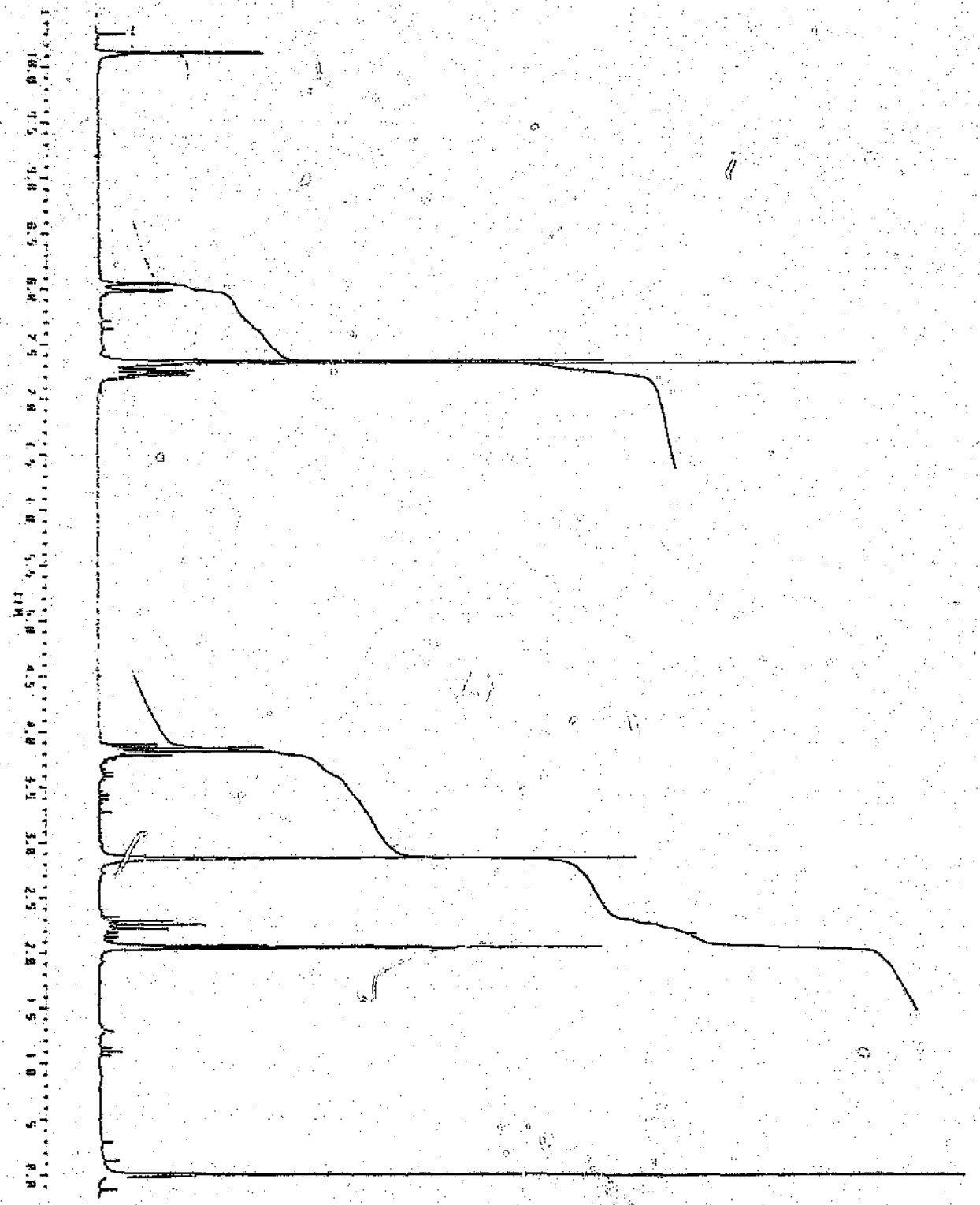
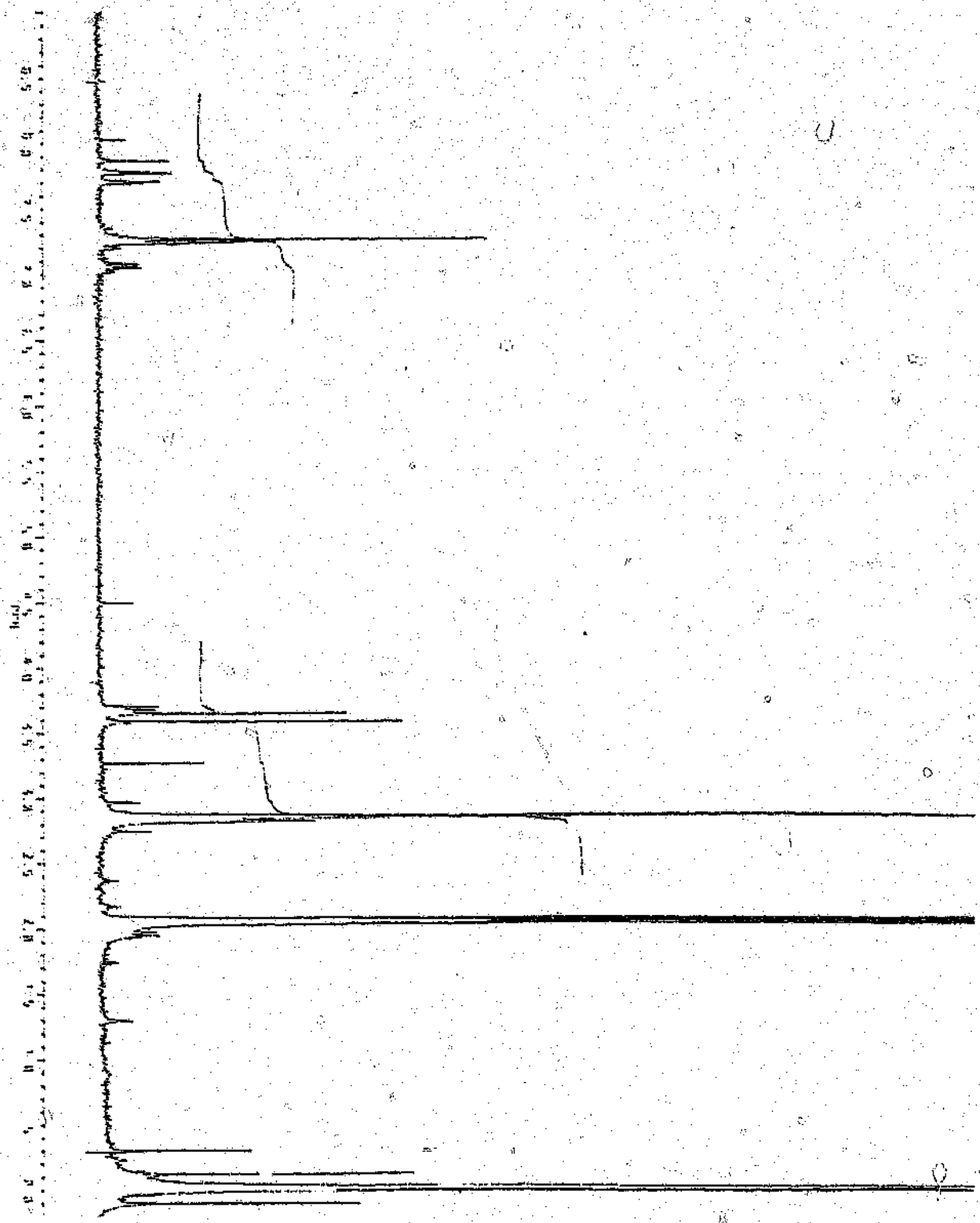


Figure 11.6.4 Proton NMR spectrum of 6,14-diphenyl-1,4,8,12-tetraazacyclopentadeca-4,4,12,14-tetraene in deuterated acetone at 25°C using a 200 MHz spectrometer.



12 APPENDIX : DERIVATIONS OF EQUATIONS USED IN MAIN TEXT

12.1 CHAPTER 3

Derivation of equations 3.3.1 and 3.3.2

The two reactions of interest are,

$$DAC \rightleftharpoons AHC + H^+ \qquad (K_{a1})$$
$$AHC \rightleftharpoons DHC + H^+ \qquad (K_{a2})$$

Then, $K_{a1} = \dfrac{[H^+]_{eq}[AHC]_{eq}}{[DAC]_{eq}}$ and, $K_{a2} = \dfrac{[H^+]_{eq}[DHC]_{eq}}{[AHC]_{eq}}$

Considering only the first equilibrium and using Beer's law, the absorbance measured when only DAC is present, A_o, is described by,

$$A_o = \varepsilon_{DAC} b [DAC]_o$$

where b is the cell path length

If 100% conversion of DAC to AHC occurs, then the absorbance at the same wavelength, due only to the AHC, A_1, is described by,

$$A_1 = \varepsilon_{AHC} b [AHC]_o$$

At any time during the equilibrium titration, the absorbance measured, A, is given by,

$$A = \varepsilon_{DAC} b [DAC]_{eq} + \varepsilon_{AHC} b [AHC]_{eq}$$

now, $[AHC]_o = [DAC]_{eq} + [AHC]_{eq}$

then, $A = \varepsilon_{DAC^b}[DAC]_{eq} + \varepsilon_{AHC^b}([AHC]_o - [AHC]_{eq})$

$= \varepsilon_{AHC^b}[AHC]_o + [DAC]_{eq}(\varepsilon_{DAC^b} - \varepsilon_{AHC^b})$

$= A_1 + [DAC]_{eq}(\varepsilon_{DAC^b} - \varepsilon_{AHC^b})$

$$\text{thus } [DAC]_{eq} = \frac{A - A_1}{\varepsilon_{DAC^b} - \varepsilon_{AHC^b}}$$

similarly, $A = A_o + [AHC]_{eq}(\varepsilon_{AHC^b} - \varepsilon_{DAC^b})$

$$\text{thus } [AHC]_{eq} = \frac{A - A_b}{\varepsilon_{AHC^b} - \varepsilon_{DAC^b}}$$

$$= \frac{A_o - A}{\varepsilon_{DAC^b} - \varepsilon_{DAHC^b}}$$

$$\text{hence, } K_{a1} = \frac{A_o - A}{\varepsilon_{DAC^b} - \varepsilon_{AHC^b}} \times \frac{\varepsilon_{DAC^b} - \varepsilon_{AHC^b}}{A - A_1} \times [H^+]_{eq}$$

$$= \frac{A_o - A}{A - A_1} \times [H^+]_{eq} \qquad \text{(equation 3.3.1)}$$

Similarly, considering only the second equilibrium: if 100% conversion of AHC to DHC occurs, then the absorbance at the same wavelength, due only to the DHC is A_2.

$$\text{Then, } K_{a2} = \frac{A_1 - A}{A - A_2} \times [H^+]_{eq} \qquad \text{(equation 3.3.2)}$$

Derivation of Equations 3.3.3, 3.3.4, and 3.3.5.

Let the fraction of cobinamide present as DHC be f_{DHC}, the fraction present as AHC be f_{AHC}, and the fraction present as DAC be f_{DAC}.

Then $[\text{cobinamide}]_{total} = [DAC]_{eq} + [AHC]_{eq} + [DHC]_{eq}$

and $A_{total} = f_{DAC}A_{DAC} + f_{AHC}A_{AHC} + f_{DHC}A_{DHC}$

Now, reading all concentrations as equilibrium concentrations,

$$f_{DAC} = \frac{[DAC]}{[DHC] + [AHC] + [DAC]}$$

$$= \frac{[DAC]}{K_{a2}[AHC]/[H^+] + [AHC] + [DAC]}$$

$$= \frac{[DAC]}{K_{a1}K_{a2}[DAC]/[H^+]^2 + [DAC]K_{a1}/[H^+] + [DAC]}$$

$$= \frac{[H^+]^2}{K_{a1}K_{a2} + K_{a1}[H^+] + [H^+]^2}$$

$$\text{and, } f_{AHC} = \frac{[AHC]}{[DHC] + [AHC] + [DAC]}$$

$$= \frac{[AHC]}{K_{a2}[AHC]/[H^+] + [AHC] + [H^+][AHC]/K_{a1}}$$

$$= \frac{K_{a1}}{K_{a1}K_{a2}/[H^+] + K_{a1} + [H^+]}$$

and, $$f_{DHC} = \frac{[DHC]}{[DHC] + [AHC] + [DAC]}$$

$$= \frac{[DHC]}{[DHC] + [H^+][DHC]/K_{a2} + [H^+]^2[DHC]/K_{a1}K_{a2}}$$

$$= \frac{K_{a1}K_{a2}}{K_{a1}K_{a2} + K_{a1}[H^+] + [H^+]^2}$$

then $$A_{total} = \frac{A_{DAC}[H^+]^2}{K_{a1}K_{a2} + K_{a1}[H^+] + [H^+]^2} + \frac{A_{AHC}K_{a1}}{K_{a1}K_{a2}/[H^+] + K_{a1} + [H^+]} + \frac{A_{DHC}K_{a1}K_{a2}}{K_{a1}K_{a2} + K_{a1}[H^+] + [H^+]^2}$$ (equation 3.3.3)

When a titration to determine a single deprotonation equilibrium constant was performed, data was fitted by one of two simplified forms of equation 3.3.1,

$$\text{then, } A_{total} = \frac{A_{AHC}}{1 + [H^+]/K_{a1}} + \frac{A_{DAC}}{1 + K_{a1}/[H^+]} \quad \text{(equation 3.3.5)}$$

$$\text{then, } A_{total} = \frac{A_{DHC}}{1 + [H^+]/K_{a2}} + \frac{A_{AHC}}{1 + K_{a2}/[H^+]} \quad \text{(equation 3.3.6)}$$

12.2 CHAPTER 4

Derivation of Equation 4.3.1

For the reaction, AHC + L ⇌ HC-L

$$\text{then, } K_{eq} = \frac{[HC\text{-}L]}{[AHC][L]}$$

since, $[AHC]_{total} = [AHC] + [HC\text{-}L]$

$$K_{eq}\{[AHC]_{total} - [HC\text{-}L]\} = \frac{[HC\text{-}L]}{[L]}$$

$$K_{eq}[AHC]_{total}[L] - K_{eq}[HC\text{-}L][L] = [HC\text{-}L]$$

$$[HC\text{-}L] = \frac{K_{eq}[AHC]_{total}[L]}{1 + K_{eq}[L]}$$

Let the fraction of cobinamide present as AHC be f_{AHC}, the fraction present as HC-L be $f_{HC\text{-}L}$, and the fraction present as L-Co-L be $f_{L\text{-}Co\text{-}L}$,

$$\text{now, } A = f_{AHC}A_{AHC} + f_{HC\text{-}L}A_{HC\text{-}L}$$

$$= \frac{[AHC]A_{AHC}}{[AHC]_{total}} + \frac{[HC\text{-}L]A_{HC\text{-}L}}{[AHC]_{total}}$$

$$= \frac{[HC\text{-}L]A_{AHC}}{K_{eq}[L][AHC]_{total}} + \frac{[HC\text{-}L]A_{HC\text{-}L}}{[AHC]_{total}}$$

$$= \frac{[HC\text{-}L]}{[AHC]_{total}} \times \left(A_{AHC}/K_{eq}[L] + A_{HC\text{-}L} \right)$$

$$= \frac{K_{eq}[AHC][L]}{[AHC] + [HC\text{-}L]} \times \left(A_{AHC}/K_{eq}[L] + A_{HC\text{-}L} \right)$$

$$= \frac{K_{eq}[L]}{1 + K_{eq}[L]} \times \left(A_{AHC}/K_{eq}[L] + A_{HC\text{-}L} \right)$$

$$= \frac{A_{AHC} + A_{HC\text{-}L}K_{eq}[L]}{1 + K_{eq}[L]} \qquad (4.3.1)$$

Derivation of Equation 4.3.2

For the simultaneous addition model, the reaction under consideration is,

$$AHC + 2L \rightleftarrows L\text{-}Co\text{-}L$$

then,
$$K_{eq} = \frac{[L\text{-}Co\text{-}L]}{[AHC][L]^2}$$

now $A = A_{AHC}f_{AHC} + A_{L\text{-}Co\text{-}L}f_{L\text{-}Co\text{-}L}$

$$f_{AHC} = \frac{[AHC]}{[AHC] + [L\text{-}Co\text{-}L]}$$

$$= \frac{[AHC]}{[AHC] + K_{eq}[AHC][L]^2}$$

$$= \frac{1}{1 + K_{eq}[L]^2}$$

$$f_{L\text{-}Co\text{-}L} = \frac{[L\text{-}Co\text{-}L]}{[AHC] + [L\text{-}Co\text{-}L]}$$

$$= \frac{[L\text{-}Co\text{-}L]}{[L\text{-}Co\text{-}L]/K_{eq}[L]^2 + [L\text{-}Co\text{-}L]}$$

$$= \frac{1}{1 + 1/K_{eq}[L]^2}$$

$$\text{thus, } A = \frac{A_{AHC}}{1 + K_{eq}[L]^2} + \frac{A_{L\text{-}Co\text{-}L}}{1 + 1/K_{eq}[L]^2} \quad (4.3.2)$$

However, the assumption that $[L] \sim [L]_{total}$ is no longer necessarily valid since a high binding equilibrium constant means that saturation is reached with very low concentrations of ligand. An equation was derived to describe [L] and the solutions to this equation were then substituted into equation 4.3.2.

now, $[L]_{total} = [L] + 2[L\text{-}Co\text{-}L]$

$$[L] = [L]_{total} - 2[L\text{-}Co\text{-}L]$$

$$= [L]_{total} - 2[AHC]_{total} f_{L\text{-}Co\text{-}L}$$

$$= [L]_{total} - 2[AHC]_{total} \times \frac{[L\text{-}Co\text{-}L]}{[AHC] + [L\text{-}Co\text{-}L]}$$

$$= [L]_{total} - \frac{2[AHC]_{total}K_{eq}[L]^2}{K_{eq}[L]^2 + 1}$$

then, $K_{eq}[L]^3 + [L] = K_{eq}[L]^2[L]_{total} + [L]_{total} - 2[AHC]_{total}K_{eq}[L]^2$

$$K_{eq}[L]^3 + [L]^2(2[AHC]_{total}K_{eq} - [L]_{total}K_{eq}) + [L] - [L]_{total} = 0$$

Derivation of Equation 4.3.3

For the sequential addition model, the reactions under consideration are,

$$AHC + L \rightleftharpoons HC\text{-}L$$
$$HC\text{-}L + L \rightleftharpoons L\text{-}Co\text{-}L$$

then,
$$K_1 = \frac{[HC\text{-}L]}{[AHC][L]}$$

$$K_2 = \frac{[L\text{-}Co\text{-}L]}{[HC\text{-}L][L]}$$

This situation is analogous to the deprotonation of DAC, dealt with in chapter 3 (equation 3.3.1),

thus,

$$A = \frac{A_{AHC}}{1 + K_1[L] + K_1K_2[L]^2} \quad \frac{A_{HC-L}}{1 + K_2[L] + 1/K_1[L]} + \frac{A_{L-Co-L}}{1 + 1/K_2[L] + 1/K_1K_2[L]^2} \qquad (4.3.3)$$

Again, the assumption that $[L] - [L]_{total}$ is no longer necessarily valid. An equation was derived to describe [L], and the solutions to this equation were then substituted into equation 4.3.3.

now, $[L]_{total} = [L] + [HC\text{-}L] + 2[L\text{-}Co\text{-}L]$

$$[L] = [L]_{total} - [HC\text{-}L] - 2[L\text{-}Co\text{-}L]$$

$$= [L]_{total} - [AHC]_{total}(f_{HC-L} + 2f_{L-Co-L})$$

$$f_{HC-L} + 2f_{L-Co-L} = \frac{K_1[L]}{1 + K_1[L] + K_1K_2[L]^2} + \frac{2K_1K_2[L]^2}{1 + K_1[L] + K_1K_2[L]^2}$$

$$= \frac{K_1[L] + 2K_1K_2[L]^2}{1 + K_1[L] + K_1K_2[L]^2}$$

then,

$$[L] = [L]_{total} + \frac{-[AHC]_{total}K_1[L] - [AHC]_{total}2K_1K_2[L]^2}{1 + K_1[L] + K_1K_2[L]^2}$$

$$[L] + K_1[L]^2 + K_1K_2[L]^3 = [L]_{total} + K_1[L]_{total}[L] + [L]_{total}K_1K_2[L]^2 - [AHC]_{total}2K_1K_2[L]^2 - [AHC]_{total}K_1[L]$$

$$[L]^3K_1K_2 + [L]^2(K_1 - [L]_{total}K_1K_2 - [AHC]_{total}{}^2K_1K_2) + [L](1 - [L]_{total}K_1 + [AHC]_{total}K_1) - [L]_{total} = 0$$

Derivation of Equation 4.3.4

At any pH, the experimental binding constant for the reaction,

corrin + L ⇌ Co-L

$$\text{is, } K_{exp} = \frac{[\text{Co-L}]}{[L]_{total}[\text{corrin}]_{total}}$$

The reaction of interest however is,

AHC + L ⇌ Co-L

$$\text{for which, } K = \frac{[\text{Co-L}]}{[L][AHC]} \text{ at high pH}$$

$$\text{since, } K_{a2} = \frac{[DHC][H^+]}{[AHC]}$$

$$\text{and, } [\text{corrin}]_{total} = [DHC] + [AHC]$$

$$= \frac{K_{a2}[AHC]}{[H^+]} + [AHC]$$

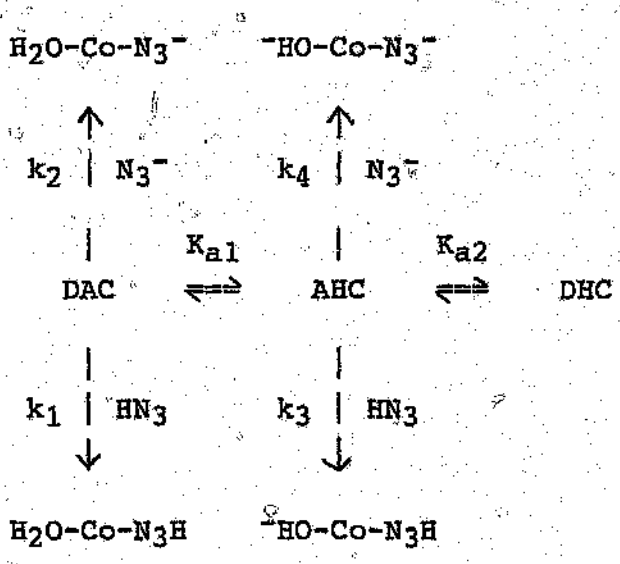
$$= [AHC](1 + K_{a2}/[H^+])$$

$$\text{Thus, } K = \frac{K_{exp}([H^+] + K_{a2})}{[H^+]} \qquad (4.3.4)$$

12.3 CHAPTER 5

Derivation of Equation 5.2.1.

The reaction scheme below indicates all the possible forward reactions that can contribute to the value of k'_{obs}, and hence k_{II}^{obs}. Reverse reactions have been ignored for simplicity. Both DAC and AHC react with azide, though in the case of DAC a second substitution reaction is possible. However, since the first substitution reaction is rate determining, a second substitution will not contribute to the magnitude of k'_{obs}, and hence this possibility is ignored in the reaction scheme. Both N_3^- and HN_3 can coordinate to DAC/AHC.[11]



Now, $$\frac{d[Co\text{-}L]}{dt} = k'_{obs}[Co]_{total}[L]_{total}$$

and, $$\frac{d[Co\text{-}L]}{dt} = k_1[DAC][HN_3] + k_2[DAC][N_3^-] + k_3[AHC][HN_3] + k_4[AHC][N_3^-]$$

Considering first the cobinamides, and reading all concentrations as equilibrium concentrations,

$$K_{a1} = \frac{[AHC][H^+]}{[DAC]} \quad \text{and} \quad K_{a2} = \frac{[DHC][H^+]}{[AHC]}$$

since, $[Co]_{total} = [DAC] + [AHC] + [DHC]$

$$= [DAC] + K_{a1}[DAC]/[H^+] + K_{a1}K_{a2}[DAC]/[H^+]^2$$

$$= [DAC](1 + K_{a1}/[H^+] + K_{a1}K_{a2}/[H^+]^2)$$

thus,

$$[DAC] = \frac{[H^+]^2[Co]_{total}}{K_{a1}K_{a2} + K_{a1}[H^+] + [H^+]^2}$$

similarly,

$$[AHC] = \frac{K_{a1}[H^+][Co]_{total}}{K_{a1}K_{a2} + K_{a1}[H^+] + [H^+]^2}$$

and,

$$[DHC] = \frac{K_{a1}K_{a2}[Co]_{total}}{K_{a1}K_{a2} + K_{a1}[H^+] + [H^+]^2}$$

Considering the ligand now,

$$K_L = \frac{[N_3^-][H^+]}{[HN_3]}$$

since, $[L]_{total} = [N_3^-] + [HN_3]$

$$= [N_3^-][H^+]/K_L + [N_3^-]$$

$$= [N_3^-](1 + [H^+]/K_L)$$

thus,
$$[N_3^-] = \frac{[L]_{total}}{1 + [H^+]/K_L}$$

similarly,
$$[HN_3] = \frac{[L]_{total}}{1 + K_L/[H^+]}$$

$$k'_{obs}[Co]_{total}[L]_{total} = \frac{k_1[H^+]^2[Co]_{total}}{K_{a1}K_{a2} + K_{a1}[H^+] + [H^+]^2} \times \frac{[L]_{total}}{1 + K_L/[H^+]}$$

$$+ \frac{k_3K_{a1}[H^+][Co]_{total}}{K_{a1}K_{a2} + K_{a1}[H^+] + [H^+]^2} \times \frac{[L]_{total}}{1 + K_L/[H^+]}$$

$$+ \frac{k_2[H^+]^2[Co]_{total}}{K_{a1}K_{a2} + K_{a1}[H^+] + [H^+]^2} \times \frac{[L]_{total}}{1 + [H^+]/K_L}$$

$$+ \frac{k_4K_{a1}[H^+][Co]_{total}}{K_{a1}K_{a2} + K_{a1}[H^+] + [H^+]^2} \times \frac{[L]_{total}}{1 + [H^+]/K_L}$$

thus,
$$k'_{obs} = \frac{k_1[H^+]^2}{(K_{a1}K_{a2} + K_{a1}[H^+] + [H^+]^2)(1 + K_L/[H^+])}$$

$$+ \frac{k_2[H^+]^2}{(K_{a1}K_{a2} + K_{a1}[H^+] + [H^+]^2)(1 + [H^+]/K_L)}$$

$$+ \frac{k_3K_{a1}[H^+]}{(K_{a1}K_{a2} + K_{a1}[H^+] + [H^+]^2)(1 + K_L/[H^+])}$$

$$+ \frac{k_4 K_{a1}[H^+]}{(K_{a1}K_{a2} + K_{a1}[H^+] + [H^+]^2)(1 + [H^+]/K_L)}$$

$$k'_{obs} = \frac{k_1[H^+]^3 + k_2[H^+]^2 K_L + k_3 K_{a1}[H^+]^2 + k_4 K_{a1}[H^+]K_L}{(K_{a1}K_{a2} + K_{a1}[H^+] + [H^+]^2)(K_L + [H^+])}$$

(5.3.1)

12.4 CHAPTERS 6 AND 7

Derivation of Equation 6.3

For a D mechanism, equations 6.1 and 6.2 apply. If k_{-2} is significant, then the observed rate constant, k_{obs}, is related to the microscopic rate constants by equation 6.3.

$$M\text{-}H_2O \underset{k_{-1}}{\overset{k_1}{\rightleftharpoons}} M + H_2O \qquad (6.1)$$

$$M + L \underset{k_{-2}}{\overset{k_2}{\rightleftharpoons}} M\text{-}L \qquad (6.2)$$

then, $$\frac{d[M\text{-}L]}{dt} = k_2[M][L] - k_{-2}[M\text{-}L]$$

Applying the steady state approximation with respect to [M], then, $$\frac{d[M]}{dt} = 0$$

and, $$k_1[M\text{-}H_2O] + k_{-2}[M\text{-}L] = k_{-1}[M] + k_2[M][L]$$

then, $$[M] = \frac{k_1[M\text{-}H_2O] + k_{-2}[M\text{-}L]}{k_{-1} + k_2[L]}$$

and, $$\frac{d[M\text{-}L]}{dt} = \frac{k_2k_1[M\text{-}H_2O][L] + k_2k_{-2}[M\text{-}L][L]}{k_{-1} + k_2[L]} - k_{-2}[M\text{-}L]$$

$$= \frac{k_2k_1[M\text{-}H_2O][L] + k_2k_{-2}[M\text{-}L][L]}{k_{-1} + k_2[L]}$$

$$\frac{- k_{-2}k_{-1}[M\text{-}L] - k_2k_{-2}[M\text{-}L][L]}{k_{-1} + k_2[L]}$$

$$= \frac{k_2k_1[M\text{-}H_2O][L] - k_{-1}k_{-2}[M\text{-}L]}{k_{-1} + k_2[L]}$$

Since there is no spectroscopic evidence for the existence of free metal ions,

then, $[M]_T \sim [M\text{-}H_2O] + [M\text{-}L]$

and, $[M\text{-}L] = [M\text{-}H_2O]_o - [M\text{-}H_2O]$

where $[M\text{-}H_2O]_o$ is the total corrinoid concentration before addition of any ligand,

$$\text{thus, } \frac{d[M\text{-}L]}{dt} = \frac{k_2k_1[M\text{-}H_2O][L] - k_{-1}k_{-2}[M\text{-}H_2O]_o + k_{-1}k_{-2}[M\text{-}H_2O]}{k_{-1} + k_2[L]}$$

Under pseudo first order conditions it follows that $[L]_T \sim [L]_o$

where the subscripts have the same meaning as above.

let $k_2' = k_2[L]$

$$\text{thus, } \frac{d[M\text{-}L]}{dt} = \frac{k_2'k_1[M\text{-}H_2O] - k_{-1}k_{-2}[M\text{-}H_2O]_o + k_{-1}k_{-2}[M\text{-}H_2O]}{k_{-1} + k_2'}$$

$$= \frac{(k_2'k_1 + k_{-1}k_{-2})[M\text{-}H_2O] - k_{-1}k_{-2}[M\text{-}H_2O]_o}{k_{-1} + k_2'}$$

since, $[M] \sim 0$

then, $\frac{d[M\text{-}L]}{dt} = \frac{-d[M\text{-}H_2O]}{dt}$

thus, $-\frac{d[M\text{-}H_2O]}{dt} = \frac{(k_2'k_1 + k_{-1}k_{-2})[M\text{-}H_2O] - k_{-1}k_{-2}[M\text{-}H_2O]_o}{k_{-1} + k_2'}$

and, $$-\int_{[M\text{-}H_2O]_o}^{[M\text{-}H_2O]} \frac{d[M\text{-}H_2O]}{\left(\frac{(k_2'k_1 + k_{-1}k_{-2})}{(k_{-1} + k_2')}\right)[M\text{-}H_2O] - \left(\frac{(k_{-1}k_{-2})}{(k_{-1} + k_2')}\right)[M\text{-}H_2O]_o} = \int_0^t dt$$

now, $\frac{dx}{ax + b} = a^{-1}\ln(ax + b) + c$

$$t\Big|_0^t = -\frac{k_{-1} + k_2'}{k_2'k_1 + k_{-1}k_{-2}} X$$

$$\ln\left(\frac{k_2'k_1 + k_{-1}k_{-2}}{k_{-1} + k_2'}[M\text{-}H_2O] - \frac{k_{-1}k_{-2}}{k_{-1} + k_2'}[M\text{-}H_2O]_o\right)\Bigg|_{[M\text{-}F_2O]_o}^{[M\text{-}H_2O]}$$

At equilibrium, $k_2k_1[M\text{-}H_2O]_e[L] = k_{-1}k_{-2}[M\text{-}L]_e$

so, $k_2'k_1[M\text{-}H_2O]_e = k_{-1}k_{-2}[M\text{-}H_2O]_o - k_{-1}k_{-2}[M\text{-}H_2O]_e$

$k_{-1}k_{-2}[M\text{-}H_2O]_o = k_2'k_1[M\text{-}H_2O]_e + k_{-1}k_{-2}[M\text{-}H_2O]_e$

$= (k_2'k_1 + k_{-1}k_{-2})[M\text{-}H_2O]_e$

$$\ln \left(\frac{(k_2'k_1 + k_{-1}k_{-2})[M\text{-}H_2O] - (k_2'k_1 + k_{-1}k_{-2})[M\text{-}H_2O]_e}{k_{-1} + k_2'} \right) \Bigg|_{[M\text{-}H_2O]_o}^{[M\text{-}H_2O]}$$

$$= - \frac{(k_2'k_1 + k_{-1}k_{-2})}{(k_{-1} + k_2')} \times t \Bigg|_0^t$$

thus,

$$\ln \left(\frac{(k_2'k_1 + k_{-1}k_{-2})}{(k_{-1} + k_2')} ([M\text{-}H_2O] - [M\text{-}H_2O]_e) \right) \Bigg|_{[M\text{-}H_2O]_o}^{[M\text{-}H_2O]}$$

$$= - \frac{(k_2'k_1 + k_{-1}k_{-2})}{(k_{-1} + k_2')} \times t \Bigg|_0^t$$

and,

$$\ln \frac{\dfrac{(k_2'k_1 + k_{-1}k_{-2})}{(k_{-1} + k_2')} ([M\text{-}H_2O] - [M\text{-}H_2O]_e)}{\dfrac{(k_2'k_1 + k_{-1}k_{-2})}{(k_{-1} + k_2')} ([M\text{-}H_2O]_o - [M\text{-}H_2O]_e)}$$

$$= - \frac{(k_2'k_1 + k_{-1}k_{-2})}{(k_{-1} + k_2')} \times t$$

thus, $$\ln\left\{\frac{[M\text{-}H_2O] - [M\text{-}H_2O]_e}{[M\text{-}H_2O]_o - [M\text{-}H_2O]_e}\right\} = - \frac{(k_2'k_1 + k_{-1}k_{-2})}{(k_{-1} + k_2')} \times t$$

since A $[M\text{-}H_2O]$

A_1 $[M\text{-}H_2O]_e$

A_o $[M\text{-}H_2O]_o$

$$\ln \frac{(A - A_1)}{(A_o - A_1)} = - \frac{(k_2'k_1 + k_{-1}k_{-2})}{(k_{-1} + k_2')} \times t$$

or, $$\frac{(A - A_1)}{(A_o - A_1)} = \exp\left\{- \frac{(k_2'k_1 + k_{-1}k_{-2})}{(k_{-1} + k_2')} \times t\right\}$$

which is the equation for a first order process,

so, $$k_{obs} = \frac{k_1k_2' + k_{-1}k_{-2}}{k_{-1} + k_2'}$$

$$k_{obs} = \frac{k_1k_2[L] + k_{-1}k_{-2}}{k_{-1} + k_2[L]} \qquad (6.3)$$

Derivation of Equation 6.4

For a D mechanism, equations 6.1 and 6.2 apply. If k_{-2} is not significant, then the observed rate constant, k_{obs}, is related to the microscopic rate constants by equation 6.4.

$$M\text{-}H_2O \underset{k_{-1}}{\overset{k_1}{\rightleftharpoons}} M + H_2O \qquad (6.1)$$

$$M + L \underset{k_{-2}}{\overset{k_2}{\rightleftharpoons}} M\text{-}L \qquad (6.2)$$

now, $\dfrac{d[M\text{-}L]}{dt} = k_2[M][L]$

Applying the steady state approximation with respect to [M], then $\dfrac{d[M]}{dt} = 0$

and, $k_1[M\text{-}H_2O] = k_{-1}[M] + k_2[M][L]$

then, $[M] = \dfrac{k_1[M\text{-}H_2O]}{k_{-1} + k_2[L]}$

thus, $\dfrac{d[M\text{-}L]}{dt} = \dfrac{k_1k_2[M\text{-}H_2O][L]}{k_{-1} + k_2[L]}$

Under pseudo first order conditions,

$$\frac{d[M\text{-}L]}{dt} = k_{obs}[M\text{-}H_2O]$$

thus,

$$k_{obs} = \frac{k_1 k_2[L]}{k_{-1} + k_2[L]} \qquad (6.4)$$

Derivation of Equation 6.7

In the case of an I_D mechanism (equations 6.5 - 6.6), the observed rate constant is given by equation 6.7 if k_{-4} is significant.

$$M\text{-}H_2O + L \underset{}{\overset{K}{\rightleftharpoons}} \{ H_2O...M...L \} \qquad (6.5)$$

$$\{ H_2O...M...L \} \underset{k_{-4}}{\overset{k_4}{\rightleftharpoons}} M\text{-}L + H_2O \qquad (6.6)$$

now,

$$K = \frac{[M\text{-}H_2O,L]}{[M\text{-}H_2O][L]}$$

Let $[M\text{-}H_2O]_T = [M\text{-}H_2O] + [M\text{-}H_2O,L]$

$$= \frac{[M\text{-}H_2O,L]}{[L]K} + [M\text{-}H_2O,L]$$

$$= [M\text{-}H_2O,L] \times \frac{1 + K[L]}{K[L]}$$

thus,

$$[M\text{-}H_2O,L] = \frac{K[L][M\text{-}H_2O]_T}{1 + K[L]}$$

now, $\frac{d[M\text{-}L]}{dt} = k_4[M\text{-}H_2O,L] - k_{-4}[M\text{-}L]$

$$= \frac{Kk_4[M\text{-}H_2O]_T[L]}{1 + K[L]} - k_{-4}[M\text{-}L]$$

Since there is no spectroscopic evidence for the existence of free metal ions,

then, $[M]_T \sim [M\text{-}H_2O] + [M\text{-}L]$

and, $[M\text{-}L] = [M\text{-}H_2O]_o - [M\text{-}H_2O]_T$

where $[M\text{-}H_2O]_o$ is the total corrinoid concentration before addition of any ligand,

so, $\frac{d[M\text{-}L]}{dt} = \frac{Kk_4[M\text{-}H_2O]_T[L]}{1 + K[L]} - k_4[M\text{-}H_2O]_o + k_{-4}[M\text{-}H_2O]_T$

$$= \frac{(Kk_4[L] + k_{-4} + k_{-4}[L]K)[M\text{-}H_2O]_T}{1 + K[L]} - k_{-4}[M\text{-}H_2O]_o$$

but, $\frac{d[M\text{-}L]}{dt} = -\frac{d[M\text{-}H_2O]_T}{dt}$

$$-\int_{[M\text{-}H_2O]_o}^{[M\text{-}H_2O]_T} \frac{d[M\text{-}H_2O]_T}{\left\{\frac{(Kk_4[L] + k_{-4} + k_{-4}[L]K)}{(1 + K[L])}\right\}[M\text{-}H_2O]_T - k_{-4}[M\text{-}H_2O]_o} = \int_0^t dt$$

now, $\dfrac{dx}{ax + b} = a^{-1}\ln(ax + b) + c$

so, $t\Big|_0^t = -\dfrac{(1 + K[L])}{(Kk_4[L] + k_{-4} + k_{-4}[L]K)} X$

$$\ln\left(\frac{(Kk_4[L] + k_{-4} + k_{-4}[L]K)[M\text{-}H_2O]_T}{(1 + K[L])} - k_4[M\text{-}H_2O]_o\right)\Bigg|_{[M\text{-}H_2O]_o}^{[M\text{-}H_2O]_T}$$

then, $-\dfrac{(Kk_4[L] + k_{-4} + k_{-4}[L]K)}{(1 + K[L])} X\, t\Big|_0^t$

$$= \ln\left(\frac{(Kk_4[L] + k_{-4} + k_{-4}[L]K)[M\text{-}H_2O]_T}{(1 + K[L])} - k_4[M\text{-}H_2O]_o\right)\Bigg|_{[M\text{-}H_2O]_o}^{[M\text{-}H_2O]_T}$$

At equilibrium $\dfrac{k_4K[L][M\text{-}H_2O]_e}{1 + K[L]} = k_{-4}[M\text{-}L]$

thus, $\dfrac{k_4K[L][M\text{-}H_2O]_e}{1 + K[L]} = k_{-4}[M\text{-}H_2O]_o - k_{-4}[M\text{-}H_2O]_e$

$$(k_4K[L] + k_{-4} + Kk_{-4}[L])[M\text{-}H_2O]_e = (k_{-4} + Kk_{-4}[L])[M\text{-}H_2O]_o$$

then, $$-\frac{(k_4 + k_{-4})K[L] + k_{-4}}{(1 + K[L])} \times t$$

$$= \ln\left[\frac{(k_4K[L] + k_{-4} + k_{-4}[L])([M\text{-}H_2O]_T - [M\text{-}H_2O]_e)}{1 + K[L]}\right]\Bigg|_{[M\text{-}H_2O]_o}^{[M\text{-}H_2O]_T}$$

$$-\frac{(k_4 + k_{-4})K[L] + k_{-4}}{(1 + K[L])} \times t = \ln\left[\frac{[M\text{-}H_2O]_T - [M\text{-}H_2O]_e}{[M\text{-}H_2O]_o - [M\text{-}H_2O]_e}\right]$$

since $A \propto [M\text{-}H_2O]$

$A_1 \propto [M\text{-}H_2O]_e$

$A_o \propto [M\text{-}H_2O]_o$

$$\ln\frac{A - A_1}{A_o - A_1} = -\frac{(k_4 + k_{-4})K[L] + k_{-4}}{(1 + K[L])} \times t$$

Since the reaction is under pseudo first order conditions, it appears to be a simple exponential process which is the equation for a first order process.

so, $$\frac{A - A_1}{A_o - A_1} = \exp\left[-\frac{(k_4 + k_{-4})K[L] + k_{-4}}{(1 + K[L])} \times t\right]$$

thus, $$k_{obs} = \frac{(k_4 + k_{-4})K[L] + k_{-4}}{(1 + K[L])}$$

or, $$k_{obs} = \frac{k_4K[L]}{1 + K[L]} + k_{-4} \qquad (6.7)$$

Derivation of Equation 6.8

In the case of an I_D mechanism (equations 6.5 - 6.6), the observed rate constant is given by equation 6.8 if k_{-4} is insignificant.

$$M\text{-}H_2O + L \underset{}{\overset{K}{\rightleftharpoons}} \{ H_2O...M...L \} \qquad (6.5)$$

$$\{ H_2O...M...L \} \underset{k_{-4}}{\overset{k_4}{\rightleftharpoons}} M\text{-}L + H_2O \qquad (6.6)$$

now,
$$K = \frac{[M\text{-}H_2O,L]}{[M\text{-}H_2O][L]}$$

and,
$$[M\text{-}H_2O]_T = [M\text{-}H_2O] + [M\text{-}H_2O,L]$$
$$= [M\text{-}H_2O] + K[M\text{-}H_2O][L]$$
$$= [M\text{-}H_2O](1 + K[L])$$

then,
$$[M\text{-}H_2O] = \frac{[M\text{-}H_2O]_T}{1 + K[L]}$$

and,
$$\frac{d[M\text{-}L]}{dt} = k_4[M\text{-}H_2O,L]$$
$$= Kk_4[M\text{-}H_2O,L][L]$$
$$= \frac{Kk_4[M\text{-}H_2O]_T[L]}{1 + K[L]}$$

Under pseudo first-order conditions,

$$\frac{d[M\text{-}L]}{dt} = k_{obs}[M\text{-}H_2O]_T$$

$$k_{obs} = \frac{k_4K[L]}{1 + K[L]} \qquad (6.8)$$

Derivation of Equations 6.2.2

Rearranging and inverting equation 6.7 gives,

$$\frac{1}{k_{obs} - k_{-4}} = \frac{1}{k_4K[L]} + \frac{K[L]}{k_4K[L]}$$

$$\frac{1}{k_{obs} - k_{-4}} = \frac{1}{k_4K[L]} + \frac{1}{k_4} \qquad (6.2.2)$$

Derivation of Equations 6.2.3

Similarly, inverting equation 6.8 gives,

$$\frac{1}{k_{obs}} = \frac{1}{k_4K[L]} + \frac{K[L]}{k_4K[L]}$$

$$\frac{1}{k_{obs}} = \frac{1}{k_4K[L]} + \frac{1}{k_4} \qquad (6.2.3)$$

Derivation of Equations 6.2.4

Multiplying out equation 6.7 gives,

$$k_{obs} + k_{obs}K[L] = k_4K[L] + k_{-4} + k_{-4}K[L]$$

$$k_{obs} - k_{-4} = K[L](-k_{obs} + k_4 + k_{-4})$$

$$\frac{k_{obs} - k_{-4}}{[L]} = -k_{obs}K + (k_4 + k_{-4})K \qquad (6.2.4)$$

Derivation of Equations 6.2.5

Multiplying out equation 6.8 gives,

$$k_{obs} + k_{obs}K[L] = k_4K[L]$$

$$k_{obs} = K[L](-k_{obs} + k_4)$$

$$\frac{k_{obs}}{[L]} = -k_{obs}K + k_4K \qquad (6.2.5)$$

13 APPENDIX : DETAILS ON EXPERIMENTAL MEASUREMENTS

13.1 pH DETERMINATION

The pH of solutions was measured with a Metrohm 605 ion/pH meter and a Metrohm 6.0210.100 micro combination glass electrode with NaCl internal solution (to prevent precipitation of $KClO_4$ in the porous junction) calibrated against standard buffers, all maintained at the appropriate temperature with a circulating water bath.

13.2 UV/VIS SPECTROPHOTOMETER

A Cary 2300 or a Cary 219 spectrophotometer with a thermostatted cell holder (± 0.1°C) was used for spectrophotometric work.

13.3 HIGH PERFORMANCE LIQUID CHROMATOGRAPHY

High performance liquid chromatography was performed on a SpectraPhysics SP8800 ternary gradient system coupled to a Linear 2000 variable wavelength spectrophotometric detector and a Varian 4290 integrator. Analytical work was performed using a Brownlee Laboratories 5 µm C18 10 cm X 4.6 mm column. Semi-preparative work was performed using a Brownlee Laboratories 20 µm C18 Aquapore 25 cm X 10 mm column.

13.4 STOPPED FLOW SPECTROPHOTOMETRY

Stopped flow spectrophotometry was carried out using a Hi-Tech Scientific SF-51 stopped flow spectrometer (cell pathlength 1.00 cm) interfaced through a DAS-50 A/D board with an IBM-type PC. The temperature of the system was maintaine (± 0.1°C) with a circulating water bath.

Author: Bradley, J. C.
Name of thesis: Kinetics of the ligand substitution reactions of Co(iii) corrinoids and model macrocyclic compounds.

PUBLISHER:
University of the Witwatersrand, Johannesburg
©2015

LEGALNOTICES:

Copyright Notice: All materials on the University of the Witwatersrand, Johannesburg Library website are protected by South African copyright law and may not be distributed, transmitted, displayed or otherwise published in any format, without the prior written permission of the copyright owner.

Disclaimer and Terms of Use: Provided that you maintain all copyright and other notices contained therein, you may download material (one machine readable copy and one print copy per page)for your personal and/or educational non-commercial use only.

The University of the Witwatersrand, Johannesburg, is not responsible for any errors or omissions and excludes any and all liability for any errors in or omissions from the information on the Library website.